

A CALCIUM OXALATE PHASE STABILITY AND DISSOLUTION STUDY

By

NAUF SALEH AI-JUHANI

A thesis submitted to the

Graduate School-Camden

Rutgers, The State University of New Jersey

In partial fulfillment of the requirements

For the degree of Master of Science

Graduate Program in Chemistry

Written under the direction of

Dr. George Kumi

and approved by

Dr. George Kumi

Dr. Georgia Arbuckle-Keil

Dr. Hao Zhu

Camden, New Jersey

May 2017

THESIS ABSTRACT

A calcium oxalate phase stability and dissolution study

By

NAUF SALEH AL-JUHANI

Thesis Director:
Dr. George Kumi

The presence of calcium oxalate (CaOx) hydrate crystals, which have low solubility in water, is widespread in nature. These crystals cause undesirable effects in certain aspects of human life, and many of these problems are still unsolved due to the lack of necessary information about the crystallization and dissolution mechanisms of these crystals. To obtain more insight into the thermal stability of CaOx crystals, a comparative study of calcium oxalate monohydrate (COM) dendritic and calcium oxalate dihydrate (COD) bipyramidal crystals has been undertaken using a combination of Raman microscopy and thermal stage. Crystal structure transformations in these crystals with respect to various temperatures were determined. Experimental results indicate that COM is stable up to ~ 110 °C, and above this temperature the anhydrous calcium oxalate (COA) forms. This transformation is reversible since the COA crystals created convert back to the COM phase upon cooling to temperatures below this transition temperature. In contrast, the COD phase is stable up to ~ 120 °C, and above this temperature COD dehydrates and transforms to COA. This is an irreversible transformation because dehydrated crystals converted to COM upon cooling. The dehydration process for COD alters the overall

crystal habit, resulting in cracks and crystal splintering. To further an understanding about CaOx dissolution, an experimental protocol was also developed to study CaOx crystal dissolution using a microfluidic device. CaOx dissolution was investigated in the presence of various carboxylate-ion-bearing species at different solution pH values to demonstrate the capabilities of this device. In the pH range studied (4 – 10), solutions with molecular species containing multiple (more than three) carboxylate ions have a noticeably higher CaOx dissolution ability than molecular species with only a few (two or less) carboxylate ions.

Dedication

I would like to dedicate this thesis, first, to my mother Fawziah and my father Saleh who always prayed for my safety in the lab and for the success of every experiment I performed. I really appreciate your prayers. I know that in every part of the research process, I am guided by God because of your prayers.

I would also like to dedicate this thesis to my lovely husband Meshal for his undying support and understanding as I labored through countless experiments and required forms. I can't imagine how I would finish this thesis had you not taken most of the responsibilities at home in order to give me more time to work on my thesis. You have also showered me with encouragements that pushed me through the tiring days and sleepless nights. Thank you, dear, for everything. Also, I would also like to dedicate this thesis to my children, for being a source of joy and inspiration. I also felt so much support coming from you. Your hugs and kisses have been a really great energy booster.

To my uncle Abdulraheem who has given a lot of material and financial support, this thesis is also for you. You are the first one to offer help when I need anything. Thank you for always coming to my aid. Throughout my journey as a student, your support was indispensable. I am so blessed to have you. I also dedicate my thesis to my brothers and sister, especially Ohood, who have continuously supported me throughout these years.

Lastly, I dedicate this work to anyone who might read and find my research helpful. It has always been my dream to be able to contribute something to the scientific world. I am glad that I accomplished this one. It has been a rocky road for me, but it was all worth it.

Acknowledgements

I would like to express my sincere gratitude to my advisor Dr. Kumi for his inspiring guidance, generous advice and encouragement throughout my research project. He always welcomes new ideas and assists in solving the problems. His valuable knowledge, expertise, constant support, valuable feedback and patience made me able to complete my research work. I am highly indebted to him for his time, energy and unconditional support. He provided me assistance at each and every step. His encouragement and motivation has made me able to make this formidable task, attainable.

Words will never be enough to express my gratitude to my committee member, Dr. Arbuckle. She is an incredible lady and the best female professor I have ever had the pleasure of working with. Her friendly behavior, constant effort and hard work made me able to learn things very fast. I always enjoy her classes because she motivates every student to learn as much as possible. I can never forget our well-informed conversations. She always believed in my skills and her motivational talks made me more confident. Whenever, a negative situation occurs, she is the one who inspired me with her positive attitude. Her supervision made me able to explore my creative side.

Last but not the least; I owe a deep sense of gratitude to my committee member Dr. Zhu for his sincere teachings and assistance. He is the one who provided valuable information and advised me to think deeply.

Table of Contents

Thesis Abstract.....	ii
Dedication.....	iv
Acknowledgements.....	v
Table of Contents.....	vi
List of Figures.....	viii
List of Tables.....	xiii
Chapter 1 Introduction.....	1
1.1 Calcium oxalate (CaOx): discovery, importance and challenges.....	1
1.2 Crystal terminology.....	4
1.3 CaOx forms and structure.....	10
1.4 Crystal characterization methods.....	16
1.5 CaOx phase stability and phase transformations.....	17
1.6 CaOx dissolution.....	19
1.7 Research goals and objectives.....	20
1.8 Thesis outline.....	21
Chapter 2 Experimental Methods and Procedures.....	22
2.1 Materials.....	22
2.2 Methods.....	22
2.2.1 Preparatory procedures.....	22
2.2.2 Microfluidic crystallization device fabrication and properties.....	23
2.2.3 CaOx crystal synthesis in the microfluidic crystallization device.....	25
2.2.4 Microfluidic dissolution device fabrication.....	27

2.3. Characterization techniques	29
2.3.1 Raman Spectroscopy.....	29
2.3.2 Scanning Electron Microscopy (SEM)	30
2.4. CaOx phase transformation.....	31
2.4.1 Experimental details and procedures	31
2.5 CaOx dissolution experiments	32
2.5.1 Experimental details and procedures	32
Chapter 3 Results and Discussions	34
3.1 CaOx Raman spectroscopy using a thermal stage	34
3.1.1 COM phase transitions – dendritic	34
3.1.2 COD phase transition	46
Summary	59
3.2 Dissolution results and discussion	59
3.2.1 5 mM Experiments (varying pH).....	62
3.2.2 5 mM experiment with constant pH.....	66
Chapter 4 Future Directions.....	71
References.....	74

List of Figures

Figure 1-1. Crystal systems, the 14 Bravais Lattices. I= Body-Centered, F= Face-Centered, and C= Side-Centered	5
Figure 1-2. (a) Sodium as an example of a monatomic lattice and (b) sodium chloride as an example of a polyatomic lattice	7
Figure 1-3. The (100) surface of a primitive cubic crystal	10
Figure 1-4. (a) Square antiprisms and (b) distorted square antiprisms	11
Figure 1-5. The COM crystal structure showing: (a) the Ca coordination polyhedron, (b and c) the bidentate and unidentate ligands, (d) the three edges shared between each Ca coordination polyhedron, (e) the Ca layers that are parallel to the (100) plane (4 unit cells shown), (f and g) the hexagons formed by the Ca ion, (h) the two types of oxalate ions in COM, and (i) the oxalate ions between the ‘Ca-oxalate’ layers that alternate with water (water molecules also form a ribbon-like pattern – shown by dashed blue line)	12
Figure 1-6. The COD crystal structure showing: (a) the Ca coordination polyhedron, (b) the four-fold symmetry of the Ca polyhedra arrangement, (c) the bidentate and unidentate ligands, (d) two (of the four) different rows of Ca polyhedra in a unit cell; polyhedra in each row are connected, and (e) each polyhedra shares two different edges with adjacent polyhedra.....	14
Figure 2-1. The UV photolithography process to obtain a master structure all slides were exposed to UV radiation through a mask.....	25
Figure 2-2. The crystallization experiment set-up	26
Figure 2-3. An optical image of the crystal line in the center of middle stream.....	27

Figure 2-4. (a) A schematic of the the microfluidic dissolution device fabrication from the top, (b) a schematic of the microfluidic dissolution device master structure, and (c) an optical image microfluidic device.....	28
Figure 2-5. The phase transformation set-up	31
Figure 2-6. The dissolution experiment set up.....	32
Figure 2-7. An optical image of dissolution experiment set-up.....	33
Figure 3-1-1. (a) SEM and (b) optical images of COM dendrites. Scale bar in SEM images is 5 μm , and in optical images is 20 μm . Dendrites encircled in Panel A tended to form significant amounts under our synthesis conditions.....	35
Figure 3-1-2. Raman spectrum of a COM crystal between 25 $^{\circ}\text{C}$	35
Figure 3-1-3. Raman spectrum of a COM crystal between 75-175 $^{\circ}\text{C}$	38
Figure 3-1-4. Raman spectrum of a COM crystal between 100-125 $^{\circ}\text{C}$	38
Figure 3-1-5. Raman spectrum of a COM crystal at 25 $^{\circ}\text{C}$ after 5, 20, 60 and 120 minutes.....	39
Figure 3-1-6. Raman spectrum of a COM crystal from 75-175 $^{\circ}\text{C}$	40
Figure 3-1-7. Raman spectrum of a COM crystal between 100-125 $^{\circ}\text{C}$	41
Figure 3-1-8. Raman spectrum of a COM crystal at 25 $^{\circ}\text{C}$ after 5, 20, 60 and 120 minutes.....	41
Figure 3-1-9. Raman spectrum of a COM crystal at 25 $^{\circ}\text{C}$	42

Figure 3-1-10. Raman spectrum of a COM crystal between 75-175 °C.....	43
Figure 3-1-11. Raman spectrum of a COM crystal between 100 -125 °C. The broad peak at ~960 cm ⁻¹ is from the Si substrate.	44
Figure 3-1-12. Raman spectrum of a COM crystal at 25 °C after 5, 20, 60 and 120 minutes.....	44
Figure 3-1-13. A COM crystal unheated and after being heated. The broad peak at ~960 cm ⁻¹ is from the Si substrate	45
Figure 3-1-14. (a) SEM and (b) optical images of COD biyramids. Scale bar in SEM images is 5 µm, and scale bar in optical image is 20 µm.....	46
Figure 3-1-15. Raman spectrum of a COD crystal at 25 °C	47
Figure 3-1-16. Raman spectrum of a COD crystal between 75-150 °C	48
Figure 3-1-17. Raman spectrum of a COD crystal between 100-125 °C	49
Figure 3-1-18. Raman spectrum of a COD crystal at 25 °C after 5, 15, 60, 120 and 180 minutes.....	50
Figure 3-1-19. Raman spectrum of a COD crystal between 75-150 °C	51
Figure 3-1-20. Raman spectrum of a COD crystal between 100-125 °C	52
Figure 3-1-21. Raman spectrum of a COD crystal at 25 °C after 5,15, 60, 120 and 180 minutes.....	52
Figure 3-1-22. Raman spectrum of a COD crystal at 25 °C	53

Figure 3-1-23. Raman spectrum of a COD crystal between 75-150 °C	54
Figure 3-1-24. Raman spectrum of a COD crystal between 100-125 °C	55
Figure 3-1-25. Raman spectrum of a COD crystal at 25 °C after 5, 15, 60, 120 and 180 minute	55
Figure 3-1-26. Different COD crystals after being heated.....	58
Figure 3-1-27. SEM images of CaOx crystals after being heated to 125°C. Prior to heating, the phase for these various crystals was (a) COD (i.e., COD bipyramids) and (b) COM (i.e., COM dendrites); the only bipyramid in panel (b) is encircled. SEM images were taken at room temperature (i.e., after cooling samples and then sputter-coating with a metal film). Scale bar in SEM images is 5 µm	58
Figure 3-1-28. Different COM crystals after being heated.....	59
Figure 3-2-1. (a, b) SEM images of COM crystals (prismatic and dendritic) and (c) optical images of COM crystals (prismatic and dendritic). Scale bar of a = 1 µm, b = 5 µm, and c = 20 µm	61
Figure 3-2-2. Illustration of different size of crystals due to the different velocity in the middle stream (the square travels faster)	61
Figure 3-2-3. (a) Optical images of the dissolution action of EDTA and (b) optical images of the dissolution action of citrate. The scale bar is 20 µm	63
Figure 3-2-4. (a) Optical images of the dissolution action of malonate and (b) optical images of the dissolution action of acetate. The scale bar is 20 µm. The encircled object is most likely a piece of silicon.....	64

Figure 3-2-5. (a) Optical images of EDTA dissolution action at pH \approx 10 and (b) optical images of dissolution action of citrate at pH \approx 10. The scale bar is 20 μ m67

Figure 3-2-6. (a) Optical images of the dissolution action of malonate at pH \approx 10 and (b) optical images of dissolution action of acetate at pH \approx 10, the scale bar, the scale bar is 20 μ m68

List of Tables

Table 1.1. Several types of kidney stones; their chemical formula and occurrence	3
Table 3-1-1. Raman bands for COM, COD, and COA in the specified regions obtained from published data ^{34, 42, 61, 65, 67, 68}	34
Chart 3-1-1. Comparing ten COD crystals with temperature.....	57
Table 3-2-1. Illustration the fully deprotonated structures of acetate, malonate, citrate, and EDTA ions.....	60
Table 3-2-2. Illustration of 5 mM Experiments of EDTA, citrate, malonate and acetate ions (varying pH). pKa values obtained from Quantitative Chemical Analysis. ⁸³	65
Table 3-2-3. Illustration of 5 mM Experiments of EDTA, citrate, malonate and acetate (constant pH). pKa values obtained from Quantitative Chemical Analysis. ⁸³	69

Chapter 1: Introduction

1.1 Calcium oxalate (CaOx): discovery, importance and challenges

CaOx is ubiquitous in nature and industry. For example, it is found in a large number of plant species¹ and in kidney stones.² CaOx needs to be separated from living tissue because it is toxic,³ and the low solubility of CaOx allows it to be isolated within biological systems. Apparently, it is for these reasons that CaOx is biomineralized in areas where it cannot contaminate the rest of the organism, such as in raphides (plant crystal) or kidney stones.⁴ CaOx raphides in plants are believed to be a calcium reservoir, and these raphides are also believed to deter animals from grazing on them.¹

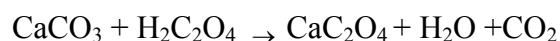
CaOx crystals were first isolated by M.A. Donn  from urine in 1838.⁵ Determination of the composition of this crystal was achieved several decades later. Initial report describe CaOx precipitating from solution as a finely divided crystalline precipitate resembling an amorphous sediment.⁵

CaOx affects certain aspects of human life, such as human health. Kidney stones, also known as renal calculi, are the most widely recognized malady of the urinary tract influencing around 10% of the worldwide populace.⁶ In industrialized populations, the number of people who suffer from kidney stone disease has increased over the past 30 years. Gender, race, and ethnicity influence who may get kidney stones. For example, men get kidney stones more regularly than women. However, a recent investigation shows that the number of women getting kidney stones is rising, and a high percentage of kidney stones are made of CaOx crystalline aggregates.⁷ These crystals form, by the combination of calcium with oxalic acid, if there is a high amount of calcium in the urine. This undesirable mineral agglomeration can lead to sickness, and it may prompt high

blood pressure and promote diabetes mellitus.^{8,9} In addition, there are different types of kidney stones such as uric acid, struvite and CaOx; CaOx is the most common type (Table 1.1).

Currently, kidney stone disease can be treated according to the type of stone by different methods including medication, lithotripsy, ureteroscopy and tunnel surgery. However, the significant issue in CaOx-related kidney stone disease is the high recurrence rate after stone removal.¹⁰ Up to now, the exact mechanisms for stone pathophysiology and the formation of kidney stones disease are not known.¹¹ In particular, the mechanism by which CaOx monohydrate (COM) crystals grow into pathological stones is still ambiguous.¹² Understanding the properties of CaOx isolated crystals and agglomerations may provide a route to alternative non-invasive surgical treatments and may lead to methods of preventing kidney stone nucleation and growth (or at least their recurrence).

CaOx is also found in patinas that exist widely in nature. A patina is a thin surface layer that forms on artifacts, marble monuments, and limestone of different historical periods at various locations. Studies show that the formation of CaOx can be ascribed basically to the activity of oxalic acid secreted by lichens (or more rarely by other microorganisms such as blue algae and fungi) which live and multiply on such surfaces. The calcium carbonate of the stone surface reacts with oxalic acid giving rise to the precipitation of calcium oxalate by the following equation:¹³



In addition, in many cane sugar mills, CaOx causes a huge problem by reducing the transfer coefficient of the evaporator station. This reduction results from deposition of

CaOx on the Calandra tubes of evaporators, and therefore CaOx formation affects the production efficiency of the machinery.¹⁴

Type	Calcium Oxalate	Uric Acid	Struvite	Cystine	Brushite
Occurrence%	70%	5-10%	10%	1%	1%>
Chemical formula	$\text{CaC}_2\text{O}_4 \cdot \text{H}_2\text{O}$ $\text{CaC}_2\text{O}_4 \cdot 2\text{H}_2\text{O}$	$\text{C}_5\text{H}_4\text{N}_4\text{O}_3$	$(\text{NH}_4)\text{MgO}_4 \cdot 6(\text{H}_2\text{O})$	$(\text{SCH}_2\text{CH}(\text{NH}_2)_2\text{CO}_2\text{H})_2$	$\text{CaHPO}_4 \cdot 2\text{H}_2\text{O}$

Table 1.1 Several types of kidney stones, their chemical formula and occurrence. The information obtained from UW Health website.¹⁵

The study of the hydrates of CaOx has posed several challenges. For many years, kidney stones were believed to be the trihydrate form of CaOx. They are actually a mixture of monohydrate and dihydrate CaOx crystals.² The Gibbs phase rule was invoked to show that there is only one thermodynamically stable phase,¹⁶ and the monohydrate is the thermodynamically stable solid phase. The dihydrate and the trihydrate are metastable products formed during the precipitation process. The structural similarities between the monohydrate and the trihydrate are believed to enable the trihydrate to easily dehydrate to the monohydrate.¹⁷ It has been reported that the trihydrate transforms to the monohydrate under thermal action,¹⁸ while the transformation of the dihydrate to the monohydrate is reportedly not a direct crystal transformation. This transformation involves a solvent-mediated step.¹⁸ This is due to the fact that the dihydrate and monohydrate have vastly different crystal structures.

Computational simulations of CaOx formation are complicated because there is only one thermodynamically stable crystal phase: the monohydrate. Hence, any computation in which the molecules are provided with flexibility will naturally optimize to the monohydrate structure. It is for this reason that existing computations generally only

consider the monohydrate.¹⁹ Other challenges are that (1) it is hard to synthesize large (more than 30 μm) CaOx crystals and (2) it is hard to synthesize only one specific phase in whatever size. For example, COT crystal formation is difficult under normal conditions because it is a kinetically stable product, and conditions that favor the formation of an energetically unstable crystal must be created in order for it to form. Moreover, oftentimes more than one phase of CaOx forms simultaneously, so it can be difficult to isolate one form from other forms.

1.2 Crystal terminology

As with many crystals, CaOx has several forms. It is helpful to use crystal terminology to describe these various CaOx forms. Thus, a brief description of crystal terminology is presented in the following paragraphs.

All constituents of a solid can be classified into two classes, namely crystalline or amorphous. The key difference between a crystalline and an amorphous solid is the nature of their atomic-scale structure. In amorphous materials, such as plastic or glass, the atoms and molecules are not organized in a definite lattice pattern. Also, amorphous solids have curved or irregular surfaces, and melt over a wide range of temperatures. There is no long-range order in amorphous substances.²⁰ On the other hand, any crystal consists of basic building blocks, each of which contains all the structural features and symmetry elements of the crystal. These basic building blocks are repeated regularly in three-dimensional space, and each of these blocks is termed a unit cell. Each unit cell has at least one atom or molecule.²⁰ Crystalline solids have sharp, well-defined melting points. The location of an atom in a crystal shows a feature called long-range order or translation periodicity, and atomic positions repeat in space in a regular array. The

identification marker for any solid compound is its crystal structure, and the arrangement of atoms in the crystal are specific and directly related to the natural properties of the crystal. The patterns of arrangement of each atom in a crystal is called the crystal lattice. In other words, a crystal lattice is a set of infinitely arranged points related to each other by transitional symmetry. The external appearance of a crystal is related to the symmetry properties of the lattice, and all lattices are described by one of the fourteen Bravais lattices (Figure 1-1) that each belong to one of the seven crystal systems.²¹

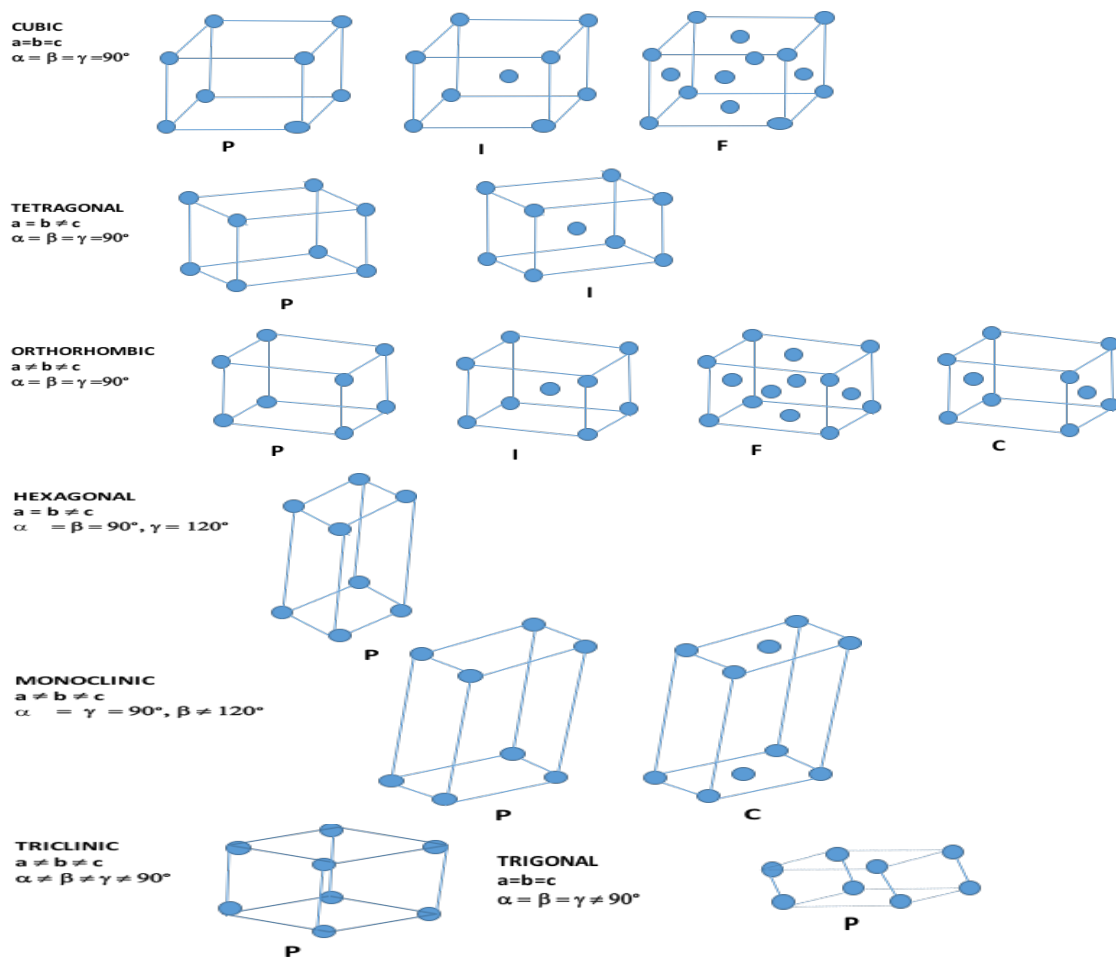


Figure 1-1. Crystal systems, the 14 Bravais Lattices. I= Body-Centered, F= Face-Centered, and C= Side-Centered.

Crystal systems can be defined by the relationship between the individual dimensions

(**a**, **b**, and **c**) and the angles (**α** , **β** and **γ**) of the unit cell.²² Indeed, any unit cell, is described by a system of coordinates, i.e., 3 axes (*a*, *b*, *c*), and by the angles formed between these axes. The angle **α** is between the *b* and *c* axis, **β** is the angle between *a* and *c*, and **γ** is the angle between *a* and *b*. These systems are the triclinic, monoclinic, hexagonal, orthorhombic, tetragonal, trigonal, and cubic systems. Generally, triclinic crystals are not symmetrical which can lead to some fairly strange shapes. In the monoclinic system, all three unit cell axes are unequal in length, with two axes perpendicular to each other, like skewed tetragonal crystals. Monoclinic crystals usually form prisms and double pyramids. The monoclinic unit cell is distinguished by a single 2-fold rotation axis called an axis of 2-fold symmetry, about which the cell can be rotated by 180° without changing its configuration, and/or a single mirror plane. In the orthorhombic system, all three axes are unequal in length, but they all are perpendicular to one another. Crystals of this system form rhombic prisms or double pyramids (two pyramids stuck together).

In crystals of the tetragonal system, two of the three axes are equal in length, and all three axes are perpendicular to one another. Minerals of this system all possess a single 4-fold symmetry axis. Tetragonal crystals commonly form double pyramids and prisms. The trigonal unit cell possesses a single 3-fold axis of rotation. In contrast, minerals of the hexagonal system possess four unique axes, three of which are (1) equal length, (2) separated by equal angles, and (3) lie in the same plane. The fourth is perpendicular to the plane of the other three. However, the unit cell for this class can also be represented by three axes. The cubic class is also known as the isometric class. In this class, all three axes are of equal length and intersect at right angles. All axes are perpendicular to one another.

All the lattices of the systems described above can be primitive (only one lattice point

per unit cell) or non-primitive (more than one lattice point per unit cell). The fourteen Bravais lattices are produced from the combination of the seven crystal systems with these two lattice types.²³ Furthermore, a crystal lattice can be categorized as either monatomic or polyatomic (Figure 1-2). In a monatomic lattice only one type of atom is present to make a face within the lattice structure. However, a polyatomic crystal lattice contains more than one type of atom per crystal face.

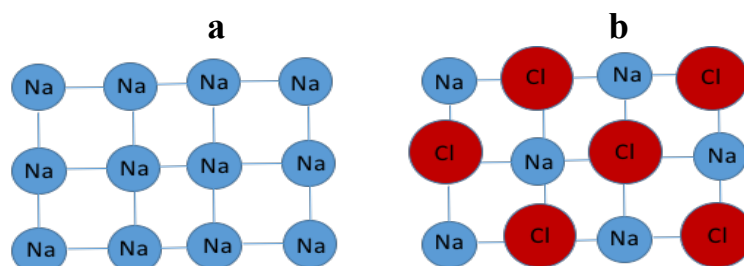


Figure 1-2. (a) Sodium as an example of a monatomic lattice and (b) sodium chloride as an example of a polyatomic lattice.

On the other hand, knowing the type of atoms and the arrangement of bonds predicts what type of crystal will form. There are four main types of crystals, as grouped by their chemical and physical properties: covalent, ionic, metallic, and molecular. Each crystal type has a different bond connection between its atoms. Various types of crystals are formed based on the arrangement of bonds between atoms. Covalent crystals are solid substances in which atoms are covalently bonded with their neighbors thereby creating very stable crystals. A known example of a covalent crystal is a diamond, which is one of the hardest materials on earth. Ionic crystals, e.g., sodium chloride, are solids that contain ionic bonds in their structure, and the atoms are arranged in a pattern based on charge. Some examples of a metallic crystal, include iron, silver, and sodium. In molecular crystals, atoms are held together by weak van der Waal forces or hydrogen bonds. A familiar example is ice (solid H_2O).

The term space group is used to describe the unique arrangement of points within the

lattice. In three dimensions, there are 219 distinct types, or 230 if chiral copies are considered distinct.²⁰ Recently, a commission of the International Union of Crystallography (IUCr) proposed a sufficiently broad definition of a 'crystal'. The definition "went beyond three-dimensional periodicity to include quasicrystals and other unexpected structures that might be discovered". According to the commission, "a crystal is defined as any solid with an 'essentially discrete diffraction diagram'." ²⁴

There can be more than one form of crystal for any material. Each of these forms can be classified as a polymorph, solvate, hydrate, or desolvated solvate. Polymorphism is defined as the ability of a chemical compound to exist in two or more crystalline structures. Polymorphs have different chemical and physical properties (e.g., melting points, chemical reactivity, different dissolution rates and bioavailability) due to their different crystal structures. Polymorphs can be classified as either enantiotropic or monotropic, based on whether or not one form can transform reversibly to another.²⁰ Solvates or (pseudo polymorphs) are crystalline solid adducts containing either stoichiometric or nonstoichiometric amounts of a solvent incorporated within the crystal structure. If the incorporated solvent is water, a solvate is termed a hydrate.²⁵ Thus, a hydrated crystal is a crystal that contains water as part of its chemical formula and structure.²⁵ Desolvated solvates are formed when (1) a solvate is removed and (2) the crystal retains the structure of the solvate.

Polymorphs and solvates of a particular molecule show different physical properties due to the relationship between structure and property. For example, diamond and graphite are polymorphs. Both of them are composed of pure carbon. However, they have different structures and different properties. For instance, diamond is the hardest substance known

in nature, while graphite is soft and slippery to touch. Diamond is a poor conductor of electricity, but is a good conductor of heat. However, graphite is a good conductor of heat and electricity. Diamond and graphite are also known as allotropes because they are composed of the same element that exist in more than one structural form. Water is another substance that has polymorphs. Each one of the fifteen known crystalline solid phases is called ice. On earth, the most abundant of these phases is hexagonal crystalline ice Ih. The most common phase transition to hexagonal ice occurs when liquid water is cooled below 0 °C (273.15 K, 32 °F) at standard atmospheric pressure. On earth, ice can be found as hexagonal ice in different substances such as hail and glaciers. Amorphous ice appears more in outer space (whereas hexagonal crystalline ice is extremely rare in outer space).²⁶

In summary, planes, axes, and angles are used to describe the unit cell of a crystal. According to Steno's law, even though a crystal may be broken or distorted, the angles between the faces and sides of the crystal are constant. This fundamental law was a major development in crystallography.

In a crystal, it is important to be able to specify a plane or a set of planes, and this is usually done using Miller indices. Within a crystal lattice, Miller indices are used to define directional and planar orientation. These planes have different arrangements and density of atoms. Indices may be used to indicate a particular crystal face, a set of faces, a direction or a set of directions. The Miller indices family of lattice planes is determined by three integers h , k , and l . For example, to determine the Miller index of the (100) plane in a simple cubic unit cell, the intercept of the plane with three axes should be found. Then, the reciprocals are taken. Finally, by multiplying each intercept value by the least

common multiple number, to make each an integer, the Miller indices (h , k , l) are obtained (Figure 1-3).

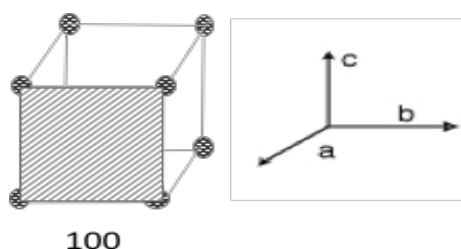


Figure 1-3. The (100) surface of a primitive cubic crystal.

1.3 CaOx forms and structure

CaOx can exist in three different hydrates forms, and each of these hydrates have different overall shapes. The three different hydrates are called calcium oxalate monohydrate (COM), calcium oxalate dihydrate (COD) and calcium oxalate trihydrate (COT).

COM ($\text{CaOx} \cdot \text{H}_2\text{O}$) is known as whewellite. Whewellite is a monoclinic crystal that belongs to the space group $P2/c$ with eight formula units in each unit cell.²⁷ As previously mentioned, crystals in this system have a unit cell with three unequal axis lengths (Figure 1-1). Two of these axes intersect each other at an oblique angle while the third axis is perpendicular to the plane of the other two. A monoclinic unit cell has a specific symmetry feature which is a single axis, called an axis of 2-fold symmetry. It is a proper axis of rotation, and is denoted by the symbol C_n , where n is termed the order of the axis. The cell can be rotated through an angle of $360/n$ about this axis to produce an equivalent configuration. In the $P2/c$ space group, the P refers to lattice type, which is a primitive unit cell (one lattice point per unit). The number 2 refers to a 2-fold screw axis along b (the unique axis). A two-fold screw axis, 2_1 , refers to a rotation of 180° , combined with a

translation of along the screw axis. The c refers to a glide plane (specifically a glide plane along c axis) that involves a reflection in the ac plane, followed by a translation along the c axis. The operation of a glide plane is a reflection and a translation of a specific length parallel to the plane.

For COM, the lattice parameters for length and angles are $a=6.250$ Å, $b=14.471$ Å, $c=10.114$ Å, and $\beta=109.978$.²⁸ In COM, the Ca coordination polyhedra are distorted square antiprisms (Figure 1-4). At each vertex of these polyhedra, there are oxygen atoms; seven oxygens from neighboring oxalate groups and one oxygen from a water molecule (Figure 1-5). Four of the seven ‘oxalate oxygens’ are from bidentate oxalate ions and the other three are from unidentate oxalate ions. Three edges are shared between each Ca coordination polyhedron, i.e., each polyhedron is connected to three other polyhedra. The polyhedral layers are formed parallel to the (100) plane.

Within these layers, Ca atoms exist at the vertices of hexagons with one of the two types of oxalate ions at the center of the hexagon. The molecular plane for one group of oxalate ions is aligned along the (100) plane (i.e., the plane containing the Ca ions) forming a layer of Ca and oxalate ions, while the other type of oxalate ions exist in between these layers or sheets. The oxalate ions between these ‘Ca-oxalate’ layers alternate with water molecules to form a ribbon-like pattern (water molecules also form a ribbon-like pattern).²⁷

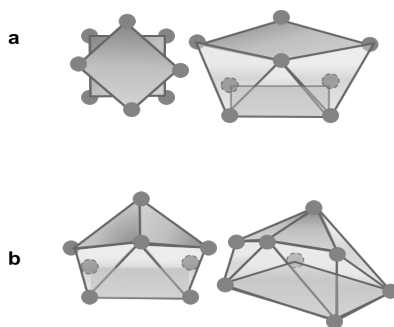


Figure 1-4. (a) Square antiprisms and (b) distorted square antiprisms.

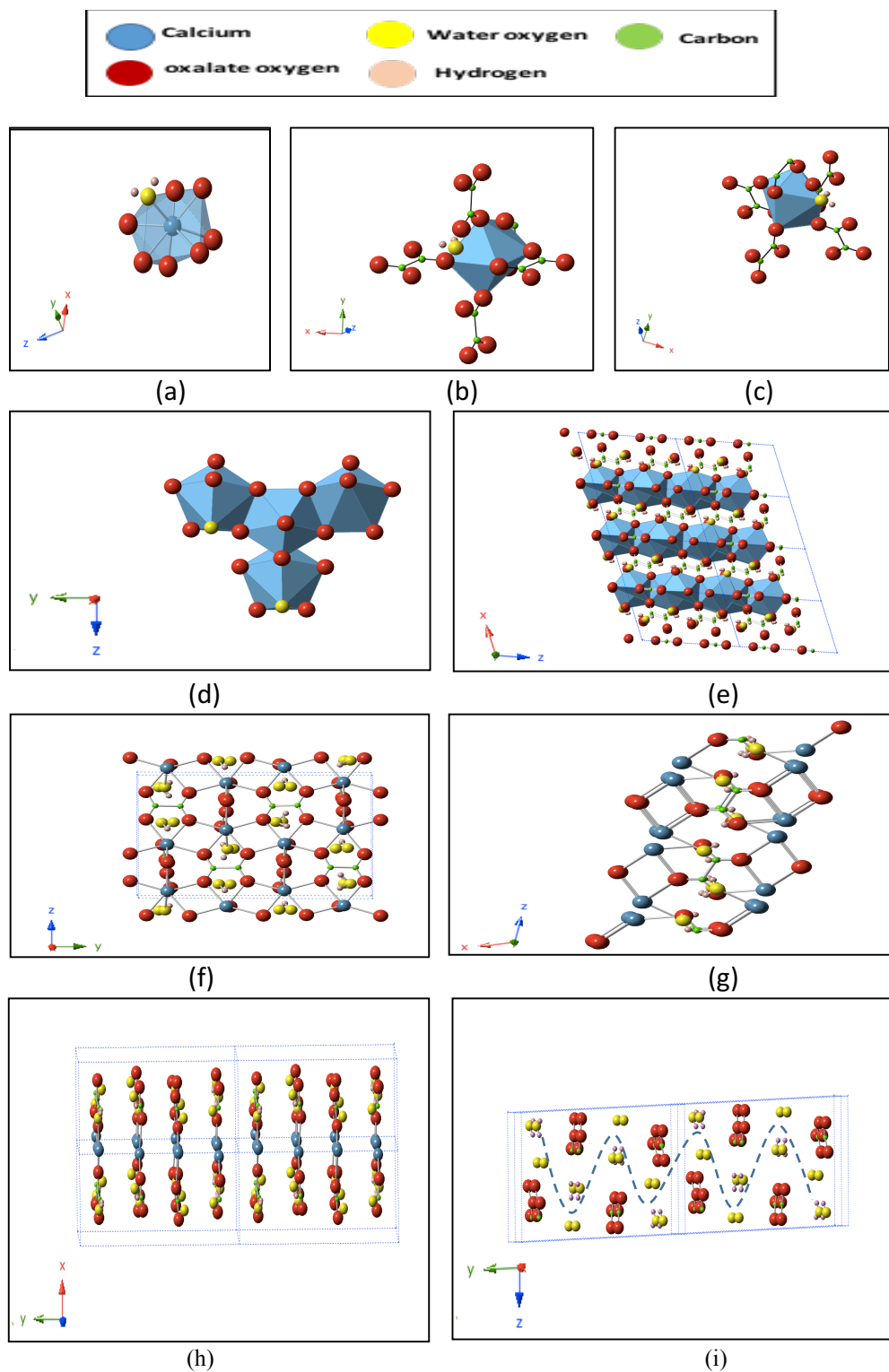


Figure 1-5. The COM crystal structure showing: (a) the Ca coordination polyhedron, (b and c) the bidentate and unidentate ligands, (d) the three edges shared between each Ca coordination polyhedron, (e) the Ca layers that are parallel to the (100) plane (4 unit cells shown), (f and g) the hexagons formed by the Ca ion, (h) the two types of oxalate ions in COM, and (i) the oxalate ions between the 'Ca-oxalate' layers that alternate with water (water molecules also form a ribbon-like pattern – shown by dashed blue line). Images created by using Crystal Maker version 9.2.9.

CaOx dihydrate ($\text{CaOx} \cdot 2\text{H}_2\text{O}$) is known as weddellite. Weddellite is so-named because it was first isolated from deposits in the Weddell sea.²⁹ Weddellite crystallizes in the $I4/m$ space group to form a tetragonal crystal.²⁷ I refers to lattice type, which is a body centered lattice cell. The number 4 implies a 4-fold symmetry axis ($360/4$), while the letter m refers to oblique glide planes. In this crystal system $a = b \neq c$ and $\alpha = \beta = \gamma = 90^\circ$. The lattice type is body-centered (I) which means lattice points at the corners and the body center. The lattice parameters for weddellite are $a = 12.371 \text{ \AA}$, $b = 12.371 \text{ \AA}$, and $c = 7.357 \text{ \AA}$.³⁰

The Ca coordination polyhedron in weddellite is a distorted square antiprism. In this structure, six of the eight oxygens belong to four oxalate groups and the remaining two oxygens belong to water molecules (Figure 1-6). Four of the six ‘oxalate oxygens’ are from bidentate oxalate ions and the other two are from unidentate oxalate ions. In contrast to whewellite, calcium is coordinated to one more water molecule and one less oxalic group.²⁷ Each Ca polyhedron is linked to two different adjacent polyhedra. Thus, the Ca ion coordination polyhedra form rows that run along the c direction. The four-fold symmetry of the arrangement of these polyhedra generates a channel where zeolitic water can reside.²⁷ With respect to the whewellite structure, the sheet structure with oxalate chains does not appear in weddellite.²⁸ This channel that has water molecules is a major characteristic feature of weddellite, and this feature distinguishes weddellite from those of whewellite and caoxite (which both have the sheet structure).²⁸

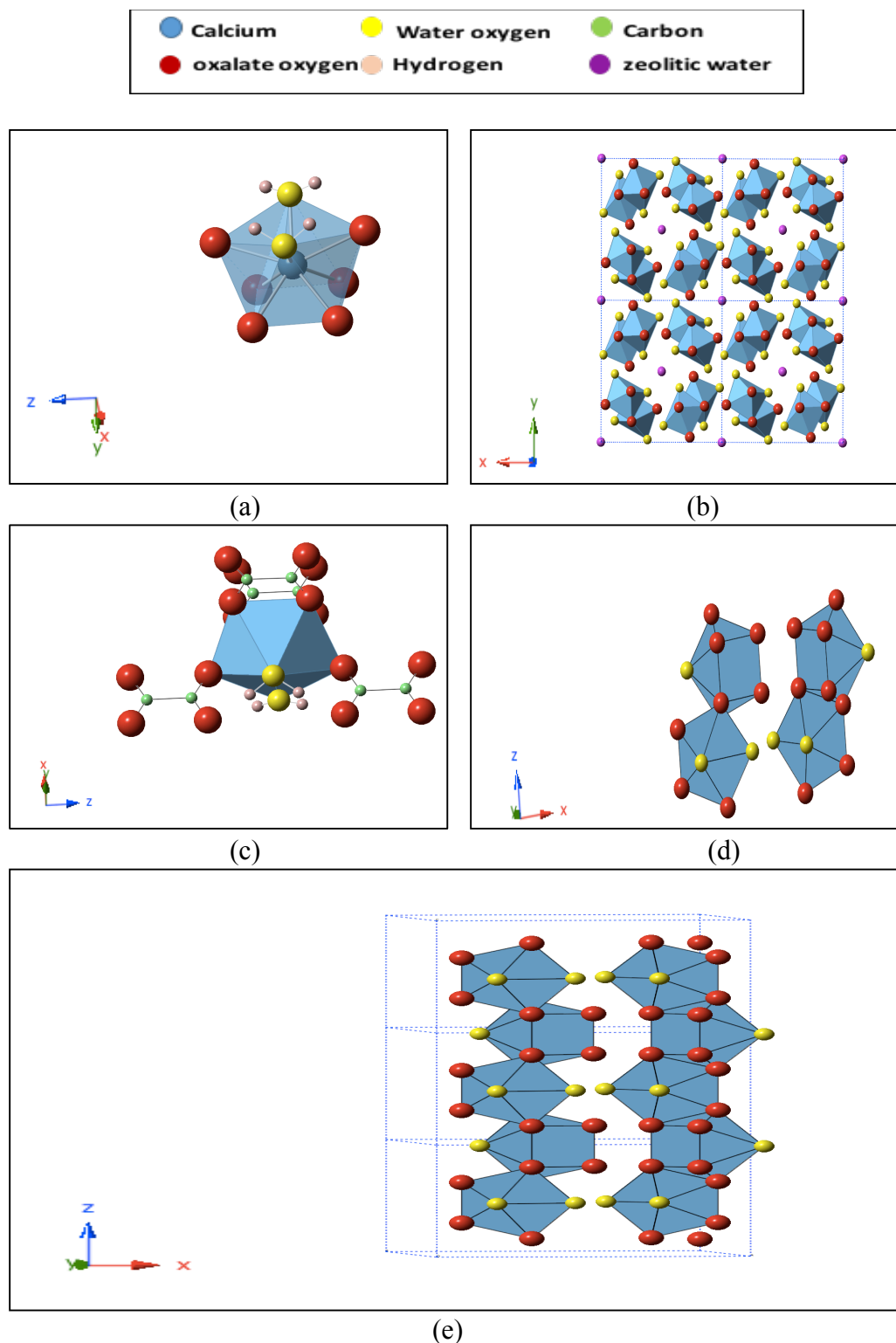
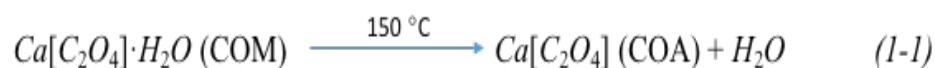


Figure 1-6. The COD crystal structure showing: (a) the Ca coordination polyhedron, (b) the four-fold symmetry of the Ca polyhedra arrangement, (c) the bidentate and unidentate ligands, (d) two (of the four) different rows of Ca polyhedra in a unit cell; polyhedra in each row are connected, and (e) each polyhedra shares two different edges with adjacent polyhedra. Images created by using Crystal Maker version 9.2.9.

Calcium oxalate trihydrate (COT), known as caoxite, is a form of CaOx that is rarely found and hard to synthesize. To produce this trihydrate phase, low temperatures (10-37 °C) are required.³¹ CaOx trihydrate crystallizes into the *P1* space group with two formula units in the unit cell. The calcium polyhedron is a distorted antiprism with three water oxygens and five oxalate oxygens (from three oxalate groups); two oxalate ions coordinate in a bidentate fashion while one is a unidentate ligand. Adjacent polyhedra share an edge, so COT crystals contain a chain of alternating polyhedra and oxalate ions.¹⁸

An anhydrous crystal for CaOx has also been reported.³² An anhydrous crystal is one that has had all of the water molecules removed from it, usually by heating the hydrated crystal to a constant mass. The complete dehydration of COM, COD and COT will produce anhydrous CaOx (COA). As shown in equations (1-1) and (1-2), the complete dehydration of COM and COD proceed in a one-step reaction.



However, the complete dehydration of COT takes place in two steps. According to equation (1-3), COT first converts to COM, followed by a second step to form COA as shown in equation (1-1).³³



However, there is at least one study that suggests the temperature range for COM dehydration is between 158.1 – 161.1 °C, which is a different temperature than the 150 °C also reported.^{33, 34}

COA is monoclinic (Figure 1), belonging to the space group is $P2/m$. The lattice parameters are $a=6.247$ Å, $b=7.515$ Å, and $c=9.653$ Å, while $\beta=90.21^\circ$.³³ The crystal structures of COA and COM are closely related. They each have layers consisting of Ca together with layers of oxalate, which are stacked along the a axis. The oxalate ions (Ox1 and Ox2) are in two various structural conditions: Ox1 is in a planar coordination with six calcium ions and Ox2 is surrounded by four calcium ions.^{24, 33}

1.4 Crystal characterization methods

Analyzing chemical substances and confirming their identities is an important part of chemistry. Modern laboratories provide a wide range of analytical techniques. To characterize a crystal structure, having the pure form of the crystal is beneficial. There are three main techniques that can be used, namely single-crystal X-ray diffractometry (SCXRD), computational techniques and Powder X-ray diffractometry (PXRD). In order to determine crystal structure by conventional single-crystal X-ray diffractometry (SCXRD), a satisfactory size (generally, the minimum dimension along each axis of the crystal should exceed 0.05 mm) and a good (defect free) quality of crystal is required.²⁰ In fact, structure solution by SCXRD is the most reliable technique for crystal structure determination.²⁰ It provides detailed crystal structure information, including unit cell dimensions, bond-lengths, and bond-angles.

If the determination of crystal structure using SCXRD is not possible because of the difficulty in obtaining suitable single crystals, computational techniques can be applied to predict crystal structures. Nowadays, there are various predictive techniques have been developed, and these methods are being refined to produce more accurate results.^{20, 35, 36} The accuracy of a determined structure can be initially estimated by comparison with an

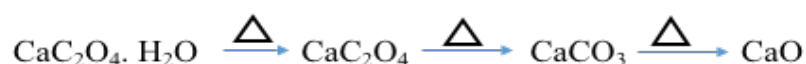
experimentally predicted structure.²⁰

Moreover, the determination of crystal structure can be attempted using a powder X-ray diffraction pattern when the sample is available in powder form. PXRD gives a "unique feature" of the solid phase which can sometimes be utilized to define crystal structure.²⁵ PXRD is a powerful tool for distinguishing between different phases of the same compound.³⁷ The main advantages of PXRD are (1) it is considered a powerful and rapid technique for identification of unknown mineral, (2) it offers an unambiguous material identification, and (3) it requires minimal sample preparation. On the other hand, this technique has some limitations. For example, homogeneous and single phase substances are best for identification of an unknown. Also, the unit cell prediction and indexing of patterns for a non-isometric crystal are complex.³⁸

1.5 CaOx phase stability and phase transformations

Solid state chemistry utilizes thermal analysis for studying reactions in the solid state, phase transitions, phase diagrams, and thermal degradation reactions. Thermal analysis provides information about changes in material properties as a function of temperature. Several techniques are commonly used. These are distinguished from each other by the property which is measured. Thermogravimetric analysis (TGA), thermovolumetry and differential thermal analysis, are being utilized increasingly in the examination of chemical reactions in the liquid and solid states at increased temperatures. These strategies include the continuous measurement of a variation in a physical property, for example (volume, weight, heat capacity) as the sample temperature is raised, ordinarily at a predetermined rate.³⁹

COM is often used as a standard material to demonstrate TGA performance.⁴⁰ COM exhibits three weight losses with temperature in an inert atmosphere (e.g. N₂). The monohydrate is the commonly described phase, and as such it is usually used in thermogravimetry (TG) to find both the reasonable temperature regions in which decomposition happens and also to determine the accuracy of the mass losses taking place in the different stages. The following sequence is commonly reported for COM,⁴¹



The thermal treatment studies of some oxalate materials such as ferrous oxalate, copper oxalate, and magnesium oxalate started in the 1960s, and these studies were related to the progress in thermal analysis technology at the time.^{42, 43, 44} In fact, thermal analysis has been applied to study the kinetics of formation of COD to mimic what is happening in renal stones.⁴⁵ Lozano and coworkers also determined the kinetics of the thermal decomposition of COM.⁴⁶ A (TGA) study in 1997 suggested COD transforms to COM by 100 °C.⁴¹ A 2003 study by Frost and Weier indicated that there are two processes taking place, and they reported the existence of two different water molecule environments in the crystal structure.⁴² They used Raman and infrared emission spectroscopy combined with a thermal stage to analyze the decomposition of a naturally occurring sample of COD. Their results indicate a weight loss step associated with water loss (which was confirmed by mass spectrometry) over the 100-114 °C temperature range. At 114 °C, a phase change reportedly occurred, producing COA. Surprisingly, the authors of this report also state that COD transforms to COM at around 97 °C. The changes in molecular structure during the phase changes were determined from shifts in the Raman vibrational band positions of the symmetric stretching mode (500-3500 cm⁻¹). In 2004, Frost and Weier also reported the

thermal decomposition of COM using similar techniques. That study suggests COM is stable to 161 °C after which it transforms to COA.³⁴ The results of these studies are confusing because they do not (1) clearly explain if COD converts directly to COA or if it converts to COM then dehydrates to form COM and (2) clarify whether the COM to COA transition occurs at 114 °C or 161 °C.

1.6 CaOx dissolution

Dissolution treatment has been broadly accepted as successful therapy for uric acid stones,⁴⁷ and it has also been investigated for other stone types such as cysteine,⁴⁸ and calcium phosphate.⁴⁹ A dissolution agent would be an ideal strategy to dissolve kidney stones. In addition, this strategy would also be ideal to prevent recurrent stones.⁴⁷ Crowell is believed to have reported the first case of stone dissolution; he was successfully able to dissolve a cystine stone within 10 months.⁵⁰ In 1939, Albright and coworkers reported that human calcium phosphate bladder stones were dissolved by using isotonic citrate solutions (pH = 4.0).⁵¹ Multi carboxylic acids, such as citric acid, have been shown to be effective substances in the treatment of uroliths.^{52, 53} More recently, Bouropoulos and coworkers, proposed that maleic acid copolymers are potent inhibitors for crystal growth of COM.⁵⁴

Tartaric acid also has been recently studied as a CaOx dissolution agent. The proportion of COM crystals in the CaOx precipitation reduced, and the percentage of COD or/and COT increased, when the concentration of tartrates was increased. This demonstrated the ability of tartrates to inhibit COM formation and to promote COD or COT growth. The decrease of the percentage of COM crystals and the percentage increase of the COD or COT crystals was linear with respect to the logarithm of the concentration of the tartrates.⁵⁵ In clinical studies, the citrus extract from lemon juice has been shown to decrease urine

acidity, thus reducing kidney stone incidence.^{56, 57, 58}

In 2012, Chutipongtanate and coworkers suggested that citrate, not phosphate, had an important dissolution effect on COM crystals as shown by reduction of crystal size (~37% decrease), crystal number (~53% decrease) and total mass (~72% decrease). These results were relative to a blank and negative control (deionized water). Citrate could remove (dissolve or dislodge) up to 85% of the adherent COM crystals from a renal tubular cell surface.⁵⁹

Even though *in vitro* experiments have demonstrated the inhibition of carboxylic acids on the crystallization of CaOx, the inhibitory mechanisms of various carboxylic acids on urolithiasis remain ambiguous. So far, a dissolution therapy approach has not been achieved for COM-related kidney stone disease, and there is a lack of characterizations of COM dissolution agents.

1.7 Research goals and objectives

One of the goals of this research was to determine the phase transition characteristics of COD by answering specific questions. What is the lowest temperature at which a thermally-induced COD transformation can take place? Is this a reversible transition? What does COD transform to; anhydrous CaOx or COM? With respect to the overall crystal shape, what happens during a COD transition? The answers to these questions will establish an upper limit for the drying of COD crystals, thereby assisting research exploring the properties of COD crystals. To accomplish this goal requires (1) synthesis of COD crystals and (2) use of a Raman microscope to monitor any CaOx phase transformation.

Another goal of this investigation was to explore calcium oxalate dissolution using different carboxylic acid solutions to obtain preliminary results on developing a system to

study more about CaOx dissolution. To achieve this objective, a protocol using a microfluidic dissolution device has been developed to compare the dissolution ability of various solutions.

1.8 Thesis outline

Chapter 1 provides the motivation for the fundamental research described in this thesis, it also presents some background information and a literature review of current knowledge about CaOx phase transformation and dissolution. The key objectives of this thesis and the main questions that this research intends to answer are also outlined. Chapter 2 details the CaOx synthesis process that was used in this work. Also, the details of how any CaOx phase transformation was monitored will be provided. Chapter 3 presents the experimental results and analysis, and Chapter 4 provides suggestions for future research.

Chapter 2: Experimental Methods and Procedures

2.1 Materials

The oligomers that were used to make the resin were dipentaerythritol pentaacrylate (Sartomer SR 399), and tris (2-hydroxy ethyl) isocyanurate triacrylate (Sartomer SR 368). The photoinitiator for this resin was ethyl (2,4,6-trimethylbenzoyl) phenylphosphinate (Lucirin TPO-L, BASF). Materials purchased from Sigma Aldrich were used as received, and these materials were ethanol (99.5 assay %), 2-propanol (99.5 assay %), acetone (99.5 assay %), calcium chloride (CaCl_2 , $\geq 93\%$), potassium oxalate monohydrate ($\text{K}_2\text{C}_2\text{O}_4 \cdot \text{H}_2\text{O}$, 99.5-101.0 %), and sodium malonate (disodium propanedioate $\text{Na}_2\text{C}_3\text{H}_2\text{O}_4$). Calcium oxalate monohydrate was purchased from Alfa Aesar. Acryloxypropyl trimethoxysilane (95 %) and tridecafluoro-1,1,2,2-tetrahydrooctyl dimethylchlorosilane (TFD) were acquired from Gelest. Silicon substrates ($\sim 25 \text{ mm}^2$) were cut from a silicon wafer purchased from Ted Pella (Type P/100). Polytetrafluoroethylene (0.022" ID \times 0.042" OD, Cole Parmer) tubes were used for all devices. Ammonia-based buffer solutions were made using ammonium chloride and sodium hydroxide solution. Food coloring was used to make the dye solutions. To fabricate a device, a polydimethylsiloxane (PDMS) elastomeric kit (Sylgard, DowChemical) was used. Sodium citrate (trisodium 2-hydroxypropane-1,2,3-tricarboxylate $\text{Na}_3\text{C}_6\text{H}_5\text{O}_7$), disodium Ethylenediamine tetraacetate $\text{Na}_2\text{C}_{10}\text{H}_{14}\text{O}_8\text{N}_2$, ammonium chloride, and sodium hydroxide were purchased from Fisher Scientific, while sodium acetate $\text{NaC}_2\text{H}_3\text{O}_2$ was acquired from EM Science.

2.2 Methods

2.2.1 Preparatory procedures

Preparatory procedures were conducted prior to fabricating any of the microfluidic

devices used in this study. These microfluidic devices were made by the commonly used soft lithography method. The necessary preparations steps are described briefly below.

Preparation of the acrylate-functionalized glass was done by placing microscope slides in three different solutions (~30 secs each). These solutions were propanol, acetone, and distilled water. Then, the clean slides were dried in an oven (~1 hour, ~100 °C). After obtaining a hydrophilic surface on the glass slides by using an oxygen-plasma cleaner (Harrick Plasma, PDC-32G), the slides were put in an acrylate solution (~15 hours). The acrylate solution consisted of 3-acryloxypropyl trimethoxysilane (2 vol%), deionized water (5 vol%), and ethanol (93 vol%). Next, the slides were put in ethanol (~1 hour) to remove any excess of 3-acryloxypropyl trimethoxysilane. Finally, all slides were placed in an oven (~1 hour, 100 °C).

Fluorocarbon-coated slides were prepared by placing microscope slides into a desiccator that had a watch glass with a small amount (1-2 drops) of TFD. To make the TFD vapor deposit onto the slide, the desiccator was evacuated and closed (i.e., the outlet valve of the desiccator was closed). Slides were left in this closed environment for about an hour.

The photoresist was important for making the acrylate polymer master microstructure. SR368 (43 wt %), SR399 (54 wt %), and Lucirin TPO-L (3 wt %) were mixed (~18 hours) to produce a homogenous composition. Polydimethylsiloxane (PDMS) was prepared by using a 1:11 wt % ratio of the curing agent-to-base from PDMS. The PDMS mixture was degassed after being well stirred.

2.2.2 Microfluidic crystallization device fabrication and properties

UV photolithography. To produce an acrylate polymer structure, a fluorocarbon-

functionalized slide and an acrylated slide were needed. Five layers of scotch tape were positioned as spacers on two sides of a fluorocarbon-functionalized slide to define the film height. Next, some photoresist (~5 drops) was placed in the middle of the fluorocarbon-functionalized slide. This photoresist was then covered by an acrylated slide. Then, a transparent mask with the wanted design was placed above the acrylated slide (Figure 2-1). All slides were exposed (~220 sec) to UV light (Black-Ray B-100A, UVP). After exposure, the mask was removed, and the two slides were separated carefully. The acrylated slide, which contained the master structure, was then washed twice with acetone (~1 min for each wash) to remove any unexposed resin. After this washing step, the master structure was heated (~4 hours at ~75 °C) to ensure there was no photoresist within the master structure. This heating step was needed because without it the PDMS in contact with the surface of master structure did not crosslink.

Soft lithography. To mold the master structure, an acrylated slide was placed inside an open box made of aluminum foil. This box was then filled with PDMS to cover the master structure. The filled box was heated (~5 hours at ~75 °C), and then the crosslinked PDMS was removed from the slide. After removing this PDMS mold, 3 inputs and 3 outputs were bored into the mold (Harris Unicore, 1.20 mm). Tubes were inserted in each of the holes. Another flat PDMS piece, made by the same method, was then adhered to this PDMS mold from the same master structure (PDMS master). Before attaching these two PDMS pieces, both PDMS structures were oxygen plasma-cleaned (~30 sec, ~600 mTorr O₂).

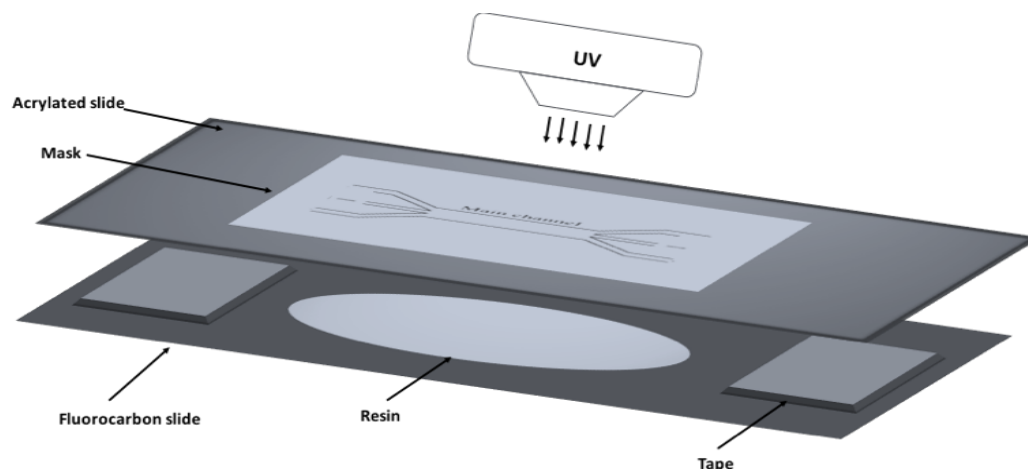


Figure 2-1. The UV photolithography process to obtain a master structure; all slides were exposed to UV radiation through a mask.

2.2.3 CaOx crystal synthesis in the microfluidic crystallization device

Synthesis Method 1. The main goal in the Synthesis Method 1 was to produce a significant amount of COD crystals, so as to be able to study the phase transformation of such crystals. To form these COD crystals, the same reusable microfluidic device was used in all experiments. The first step in the synthesis process was to inhibit bubble formation inside the tubes and the device by placing the device in an ethanol bath. This ethanol bath was placed in a desiccator and then vacuum-treated for ~30 minutes. After this vacuum treatment, three ethanol syringes were attached to the three input tubes of the device. Each syringe was placed in individual pumps (two pumps were from New Era, NE-1000, and one was from Kent Scientific Genie Plus). The three output tubes were attached to needles that funneled the solution into three separate beakers. The middle beaker contained the collection slide, which was either a glass or a silicon slide. A stereomicroscope (Stereo Zoom 4, Bausch and Lomb) was used to optically monitor the microchannel stream throughout the experiment (Figure 2-2). The first solution, ethanol, was passed through the device at a high rate (100 $\mu\text{L}/\text{min}$) for 3-5 minutes, while the three output syringes were in

three ethanol beakers. Starting with an ethanol solution removes any bubbles that may cause rapid and undesired crystallization that clogs the device and disrupts the desired flow pattern.

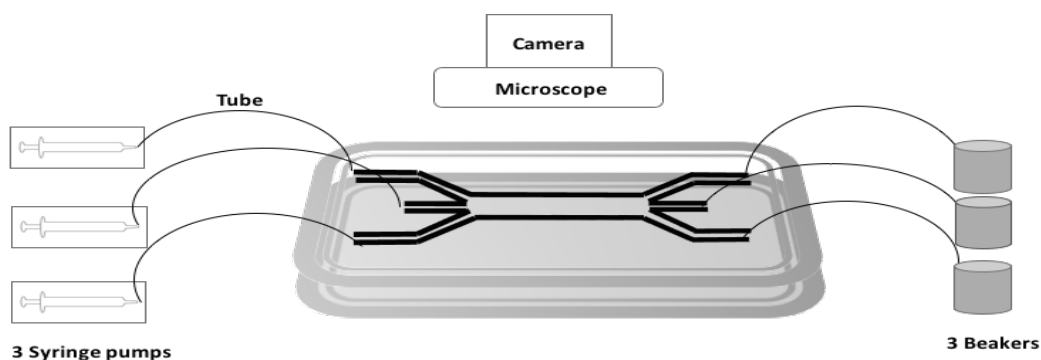


Figure 2-2. The crystallization experiment set-up.

Next, the input tubes were switched to NaCit (0.01 mM) and dye solutions while submerged in a distilled water bath. This switching while submerged is necessary to avoid introducing any bubbles into the device. NaCit (0.01 mM) was passed through the middle input, while the other inputs were switched to dye solutions. Passing dye solutions through the channels was used to visually ensure the desired flow pattern was being obtained. The three output tubes were then removed from the three ethanol beakers and placed in beakers filled with distilled water. A flow rate of 20 $\mu\text{L}/\text{min}$ was used for each of the two side streams, while the middle stream was set to 60 $\mu\text{L}/\text{min}$. After 5 minutes, the two side input tubes were switched (while submerged) to distilled water, and this distilled water was passed through the two side streams to remove all of the dye solution. The two distilled water syringes were exchanged with a solution of 200 mM $\text{K}_2\text{C}_2\text{O}_4 \cdot \text{H}_2\text{O}$ and 40 mM CaCl_2 , which are the solutions with crystal components.

To prevent the dissolution of the CaOx crystals on the collection slide in the collection beaker, the distilled water in the middle beaker was replaced with a beaker containing a

supersaturated solution of CaOx. The channel stream was carefully monitored for detection of the line of crystal (in the center of main channel). Once the crystal line was detected, the experiment was run for an additional ~30 minutes (Figure 2-3). After this 30-minute run time, the collection slide was removed from the middle beaker, and this slide was left to dry at room temperature. To clean the device, any adhered CaOx crystals were removed from the channel by passing 2 M HCl through the tubes and channel of the device. The channels and tubes were then rinsed by flowing distilled water through them.



Figure 2-3. An optical image of the crystal line in the center of middle stream.

Synthesis Method 2. The goal in Synthesis Method 2 was to produce a significant amount of COM crystals, so as to be able to study the dissolution of COM crystals. COM has different habits such as dendritic, X-shaped, and prismatic. To form COM crystals, equimolar side stream input concentrations (80 mM) were used. Distilled water was introduced as the middle stream to allow COM crystals to form. Other than these changes, the same procedures used in Synthesis Method 1 were applied to synthesize COM crystals.

2.2.4 Microfluidic dissolution device fabrication

To make the microfluidic dissolution device, a microscope slide and a silicon wafer were used to make a particular structure with specific dimensions. Three layers of small (1.5×0.5 cm) glass squares, cut from a microscope slide, were adhered to both ends of a

piece of silicon (4×1.5 cm) which was placed on the center of microscope slide (Figure 2-4 a and b). The entire assembly was put inside a box made of aluminum foil. Then, the aluminum foil container was filled with PDMS (see Section 2.2.1) and heated for ~30 minutes. Next, the PDMS mold was separated from the microscope slide. An input and an output access hole were bored into the mold (Harris Unicore, 1.20 mm), and tubes were inserted into the access holes. To produce an enclosed channel, a glass cover slide was attached to the PDMS mold (by tape) on the upper part of the microfluidic device (Figure 2-4c).

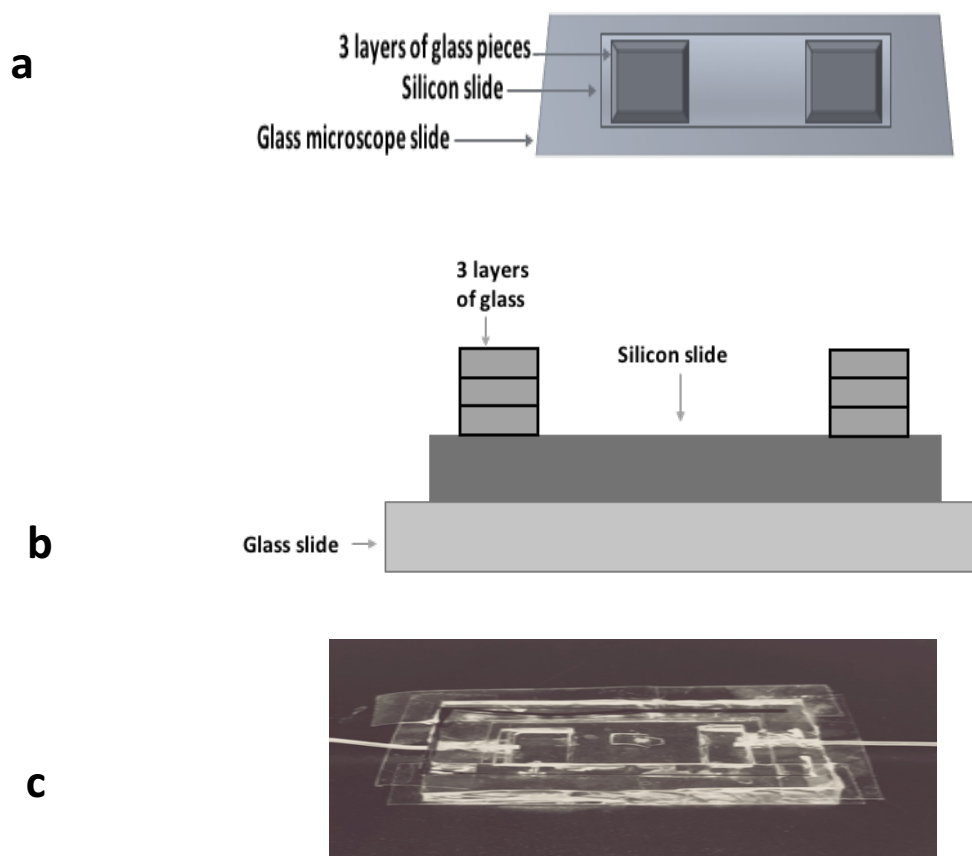


Figure 2-4. (a) A schematic of the microfluidic dissolution device fabrication from the top, (b) the microfluidic dissolution device master structure, and (c) an optical image microfluidic device.

2.3. Characterization techniques

2.3.1 Raman Spectroscopy

Raman spectroscopy is a method that is dependent on the scattering of light, and it is used to observe a wide range of frequency modes in molecules, such as vibrational and rotational modes.⁶⁰ When light interacts with matter, energy can be exchanged through absorption, simulated emission, Raman scattering, or spontaneous emission. In Raman spectroscopy, laser light is directed onto a sample and the scattered light, which radiates in all directions, is analyzed. This scattered light consists of radiation (1) that has the same frequency as the frequency of the laser light and (2) that has different frequencies than the laser light. The frequencies of the Raman scattered light, which are different from the laser light frequency, depend upon the vibrational energies of the molecular species in the sample. Compared to the intensity of the laser light, the intensity of the Raman scattered light is small (less than 0.1%). Most of the scattered light usually has the same frequency as the laser light, and this type of scattering is known as Rayleigh scattering. The laser light in a Raman instrument is usually in the visible region of the electromagnetic spectrum. Raman spectroscopy is a method which collects the chemical fingerprints that are associated with molecules.

In Raman microscopy, the excitation laser light is focused to a small (few μm) spot by a microscope, so as to limit excitation to a selected region of the sample; the size of the excitation area depends upon the objective lens used. By positioning a sample on a stage, it is possible to obtain the Raman spectrum from different areas of a sample. Confocal Raman microscopy/spectroscopy brings together Raman spectroscopy and confocal imaging, which produces high-resolution images and characterizes specimens and

materials based on chemical composition.

Hot stage Raman spectroscopy (HSRS) is a useful method to study a mineral's thermal stability when an extremely small quantity of mineral is available. In HSRS, the Raman spectra collected is a function of temperature and is obtained using a thermal stage.^{34, 42, 61} Any changes observed in the spectra are associated with changes in the molecular structure.⁶² In this work the thermal stability of CaOx is studied using HSRS.

2.3.2 Scanning Electron Microscopy (SEM)

Scanning electron microscopy (SEM) makes use of electrons to form a high magnification image (e.g., 40,000×). The advantages of SEM when compared to traditional microscopes include huge field depth, high resolution, and clear images. An electron gun at the top of the electron microscope produces a beam of electrons. The beam travels vertically through a vacuum. The beam is focused directed to the sample by lenses and electromagnetic waves. The sample releases X-rays and electrons when the beam strikes it. The X-rays and electrons are collected by detectors and they are converted into signals. The signals are displayed as an image on a monitor. SEM uses a vacuum and electrons to produce the image. Hence, the sample is treated before it is used. Water is removed from samples and non-metallic samples are made conductive. Metallic samples require no prior preparation before they are used. There are concerns regarding radiation safety because backscattered electrons and X-rays are produced during the operation of SEM. The images that are produced by SEM provide information regarding surface morphology. Thus, it is widely used in scientific research and industry. The applications of SEM include examination of surface contamination, detection and analysis of surface fractures,

identification of crystalline structures, micro-structure analysis, qualitative analyses of chemical compositions, and detection of spatial variations in chemicals.^{63, 64}

2.4. CaOx phase transformation

2.4.1 Experimental details and procedures

CaOx crystals were generated by flowing specific concentrations of $\text{K}_2\text{C}_2\text{O}_4 \cdot \text{H}_2\text{O}$ (200 mM) and CaCl_2 (40 mM) through the two outermost input tubes of the crystallization microfluidic crystallization device (see Synthesis Method 1). The solution flowing through the middle tube was NaCit (0.01 mM). The substrate containing the synthesized CaOx crystals was placed inside of an aluminum foil sleeve that had two holes which allowed attachment of this foil to the temperature-controlled stage. The sample was covered and placed under an objective of a Raman microscope (Figure 2-5). The instrument was calibrated with a silicon wafer (520-nm line) by using a 532-nm excitation laser (6.25 W) and a 100 \times objective. Each sample spectrum was recorded as an average of 4 scan collections that were acquired with a 5-second acquisition time, using a 50 \times objective and a 1200 gr/mm grating. Spectra were collected at various temperature intervals. The Raman spectrum for any crystal examined was recorded at 25 °C to confirm its crystal phase before heating the sample. Also, an optical image was collected before any heating. The temperature was increased (~ 5 °C /min) until the desired temperature was obtained. Once this desired temperature was reached, an image and the spectrum were recorded.

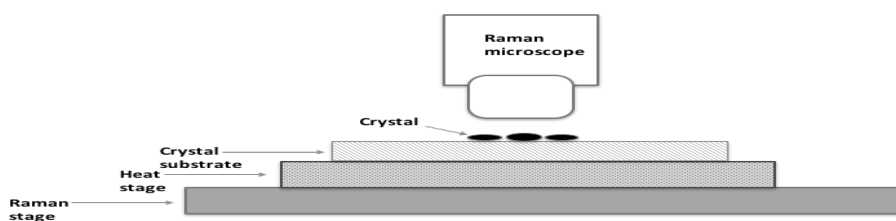


Figure 2-5. The phase transformation set-up.

2.5 CaOx dissolution experiments

2.5.1 Experimental details and procedures

CaOx crystals were generated by flowing specific concentrations of $\text{K}_2\text{C}_2\text{O}_4 \cdot \text{H}_2\text{O}$ (80 mM) and CaCl_2 (80 mM) through the microfluidic crystallization device (see Synthesis Method 2). These CaOx crystals were collected on various substrates (silicon and glass). The slide containing the CaOx crystals was placed inside of the microfluidic dissolution device, and covered by a cover slide. The dissolution device was placed under a microscope objective, and images were taken as the experiment progressed. A syringe containing the dissolving solution being studied was inserted into the input tube placed on the syringe pump (see Section 3.2). The output tube was attached to an empty syringe which was also placed on a syringe pump (Figures 2-6 and 2-7). A flow rate of 200 $\mu\text{L}/\text{min}$ was set for both pumps (“flow in” for the input pump and “withdraw” for the outlet pump). Images were collected every 5 minutes for ~ 1 hour unless crystals dissolved in a shorter amount of time. In this case images were collected up until all crystals had dissolved.

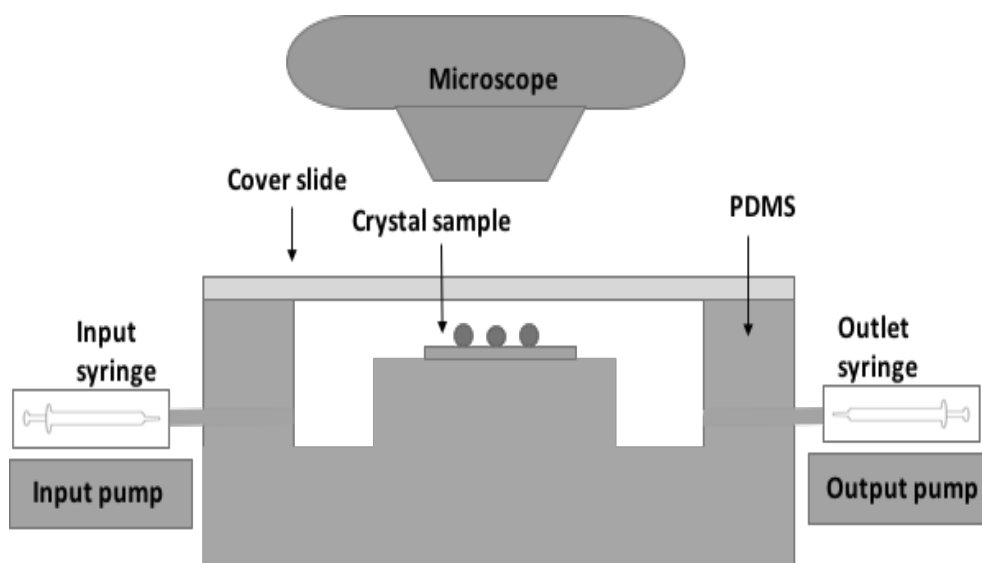


Figure 2-6. The dissolution experiment set up.

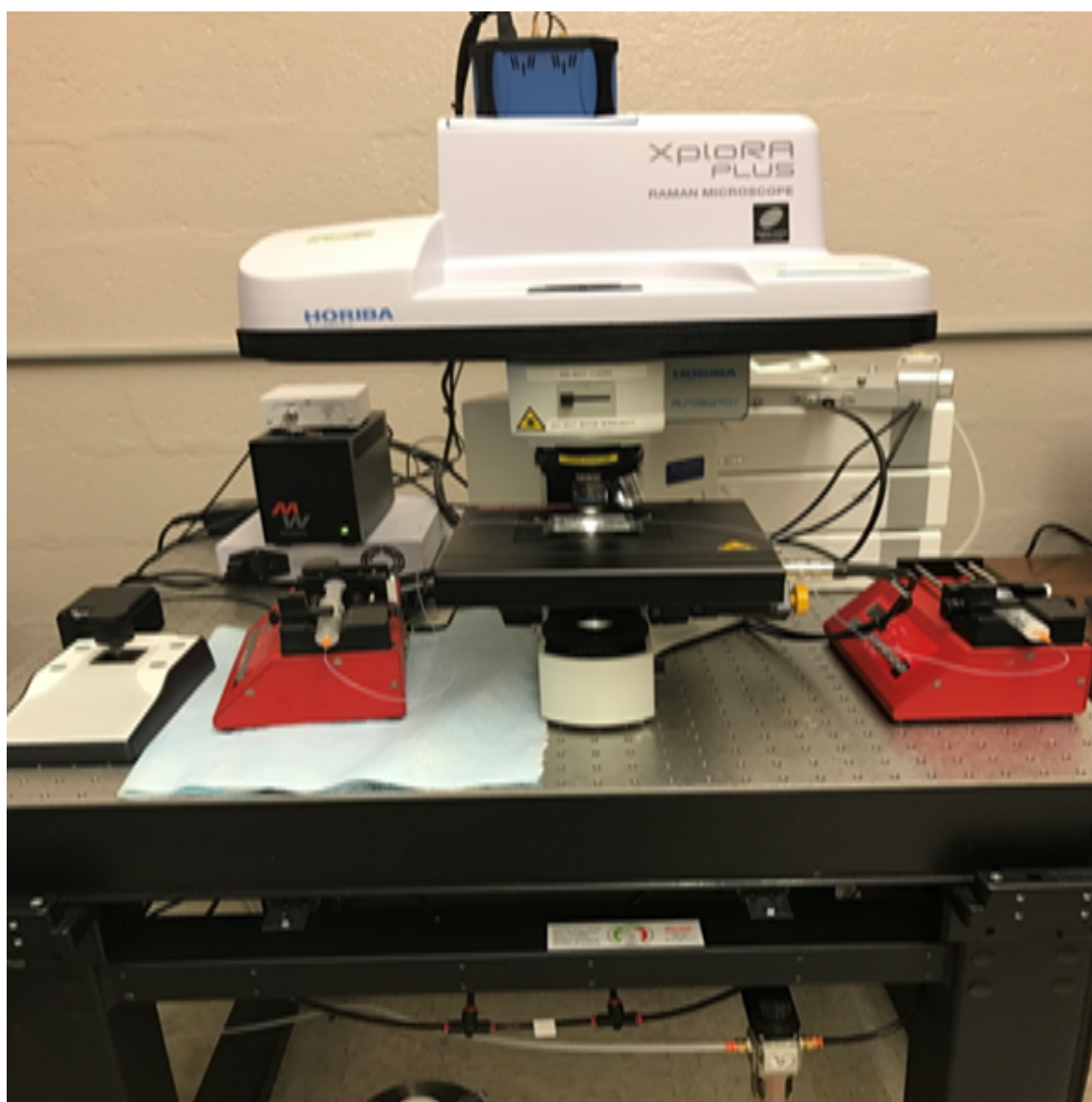


Figure 2-7. An optical image of dissolution experiment set-up.

Chapter 3: Results and Discussions

3.1 CaOx Raman spectroscopy using a thermal stage

The Raman band location and assignment obtained for COM, COD, and COA in the regions of 1400-1550 cm^{-1} , 1600-1700 cm^{-1} , and 800-950 cm^{-1} from other studies are listed in Table 3-1-1. The COM and COD data presented in this table were measured at room temperature (20-25 $^{\circ}\text{C}$).^{34, 42, 61, 65, 66, 67, 68} Our experiments were performed using single isolated crystals that, according to our optical and vibrational characterizations, were morphologically pure. Also, for the most part, crystals characterized in this study were not agglomerated. Therefore, our results are free of any possible agglomeration-like or ensemble- effects (e.g., from having a mixture of different forms).

Crystal phase	Wavenumber region (cm^{-1})			Reference number
	1400–1500	1600–1700	800–950	
COM	1464, 1490	1630	896	42
	1464, 1992	1631	896	34
	1463, 1491	1630	895	66
	1462, 1489	1632	896	67
COD	1475	1628	909	65
	1476	1631	911	68
	1476	1637	911	61
COA	1466, 1478	1647	904	42
	1466, 1478	1646	904	34
	1467, 1480	1648	901	66
	1467, 1479	1644	904	67

Table 3-1-1 Raman bands region for COM, COD, and COA obtained from published data 34, 42, 61, 65, 66, 67, and 68.

3.1.1 COM phase transitions – dendritic

The COM solid phase has different habits, and they are usually named based on their shapes.^{69, 70} It is difficult to control crystallization conditions such that only one habit forms, and therefore there are usually several COM habit forms that crystallize during COD formation. A particular form of COM dendrites tends to be more prevalent (than other

dendritic forms) during CaOx synthesis in which Na-Cit is an additive (Figure 3-1-1). Because the presence of Na-Cit favors the formation of COD crystals,^{71, 72} our synthesis using NaCit as an additive yielded significant amount of COD bipyramids and these COM dendrites. To allow comparison with COD phase transitions, this research focused on determining the phase transformation of these COM dendrites. Figure 3-1-1 shows the COM crystal habits that were acquired in this study.

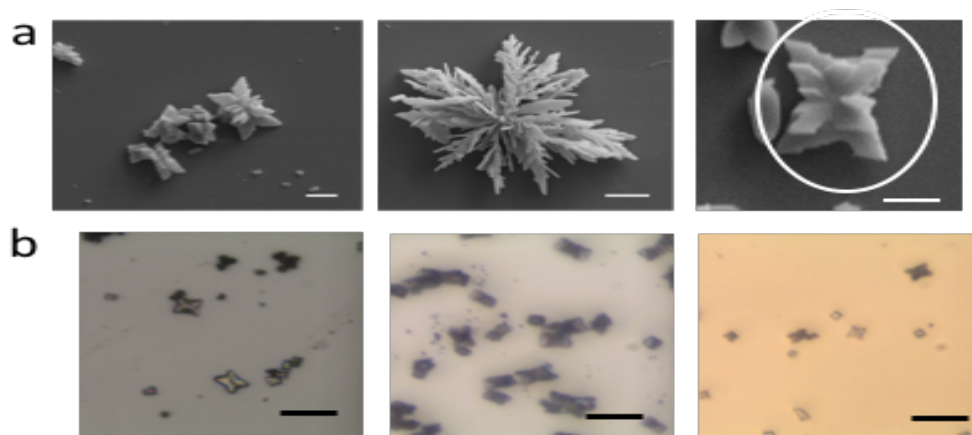


Figure 3-1-1. (a) SEM and (b) optical images of COM dendrites. Scale bar in SEM images is 5 μm , and in optical images is 20 μm . Dendrites encircled in Panel A tended to form in significant amounts under our synthesis conditions.

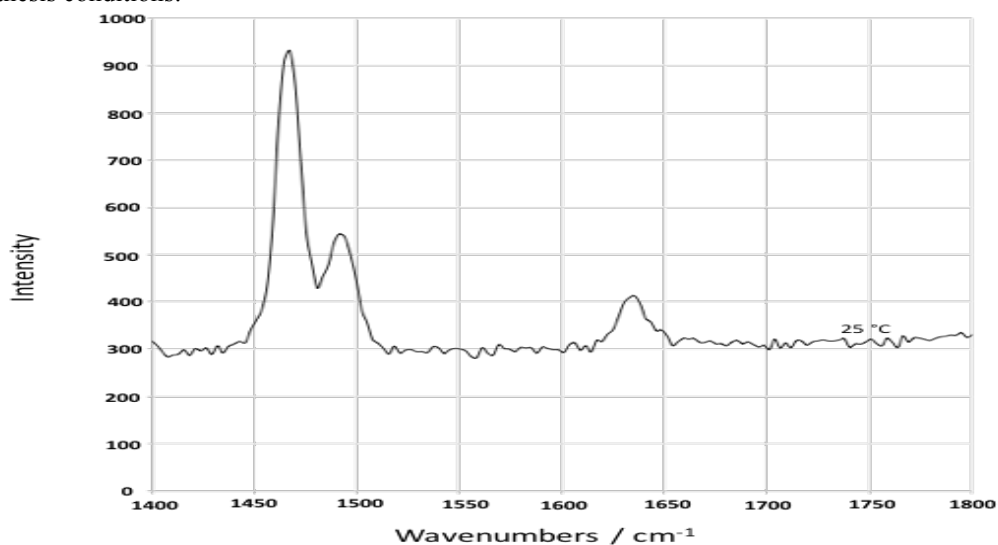


Figure 3-1-2. Raman spectrum of a COM crystal at 25 °C.

3.1.1.1 COM dendrites Raman spectra in 1400-1550 cm^{-1} region

COM crystal vibration studies using Raman spectroscopy have been undertaken for some time. Many studies have investigated the vibrational spectra of COM crystals at room temperature in the 400 - 4000 cm^{-1} region.^{34, 66, 67} Often, two peaks of relatively high intensity (C-O vibrations of the oxalate group) in the 1400-1800 cm^{-1} region confirmed the COM phase. These peaks are located at 1466 and 1490 cm^{-1} . Spectra (peak positions, intensities) of our single COM dendrites crystal exhibited identical peaks in the same region. For instance, at 25 °C, the C-O stretching vibration was observed at 1464 and 1491 cm^{-1} for a dendrite COM crystal (Figure 3-1-2). This band position indicates the COM structure, and this spectrum is in agreement with other previously published data.^{34, 66, 67} However, it is expected to have differences in the Raman intensity for the same crystal due to changes in crystal orientation.⁷³

The Raman spectrum for a single COM dendrites crystal at various temperatures is shown in Figure 3-1-3. Clear changes in the Raman spectra were observed in the 1400-1550 cm^{-1} region between 75 °C and 175 °C. At 75 °C, the Raman spectrum showed the same band positions as was obtained for this crystal at 25 °C (i.e., 1464 and 1491 cm^{-1}). This data suggests that up to 75 °C, COM was not converted to any other phase. However, in this experiment, when the temperature was increased to 125 °C, the Raman spectrum showed a significant shift in these band positions. These two bands were observed around 1467 cm^{-1} and 1477 cm^{-1} , and these bands correspond to COA stretching modes. These changes in peak position and intensity indicated that the COM crystal had dehydrated, and these structural changes occurred as the temperature increased. These thermally-induced spectral changes that occurred by 125 °C were observed in at least fifteen other isolated COM dendrites. No more than six crystals were examined per substrate (either glass or

silicon), and thus these crystals were distributed across at least three different substrates. Therefore, more than three separate crystallization experiments were used to obtain these crystal-containing substrates. The inferred structural changes for these crystals are not in agreement with a 2004 study which indicated that the COM phase was stable, based on Raman spectra, up to 150 °C and stable up to 161 °C according to the TGA.³⁴ However, TGA does not accurately determine the specific temperature at which a phase transformation occurs. These differences may be due to differences in the crystal properties (e.g., aggregation, mixture of habit, or crystal size) between our crystals and those used in that study. As the temperature is increased to 175 °C, the band shifts remain constant. This observation suggests that the crystal remained in the COA phase up to 175 °C.

In order to identify the precise temperature at which the phase change occurred, the temperature of the sample was heated in smaller increments of 5 °C beginning at 100 °C (Figure 3-1-4). At 110 °C, the spectrum changed to a broad peak around 1479 cm^{-1} with a small shoulder at 1466 cm^{-1} , indicating that the phase change happened by 110 °C for this specific crystal. For dendrites crystals, the Raman spectral changes with temperature (in the three wavenumber regions specified in Table 3-1-1) for five different crystals on the same substrate were characterized. The spectrum for each crystal was taken one after another, 5 minutes after the appropriate temperature had been attained. While there were slight differences in the temperature of the phase transition to COA, all crystals showed the described thermally-induced spectral change (i.e. spectral shift to 1466 and 1479 cm^{-1}) within the temperature range of 100-115 °C.

The spectral features of COA and COM are expected to be different, (i.e., have some differences) because of their differing unit cell structure. Considering two factors, we conclude that our COM crystals convert to COA by 125 °C. First, by all accounts COM crystals become COA by 175 °C (i.e., even though there are wide differences in reported COM to COA transition temperatures, there are no reports claiming CaOx remains hydrated at this temperature). Second, our Raman spectra at 125 °C and 175 °C for our heated COM samples are identical.

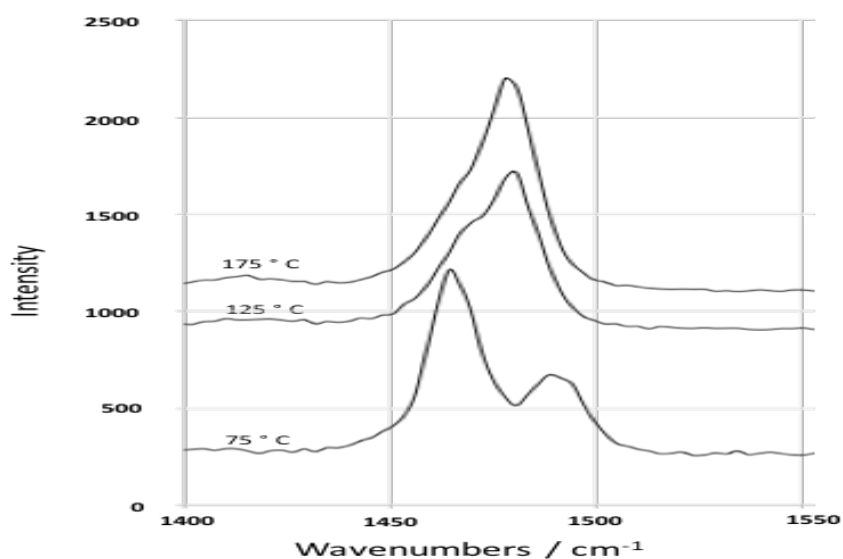


Figure 3-1-3. Raman spectrum of a COM crystal between 75-175 °C.

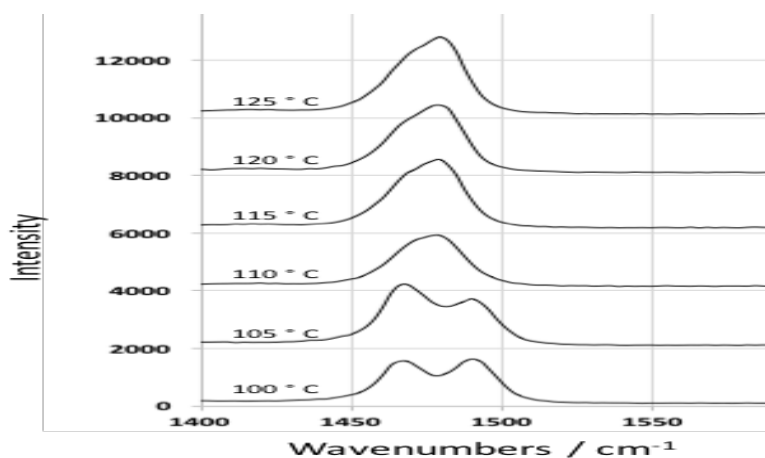


Figure 3-1-4. Raman spectrum of a COM crystal between 100-125 °C.

Unlike previous studies, our crystals were cooled down to 25 °C in order to observe the temperature impact on phase stability. Interestingly, a phase change was observed again when the sample was cooled from 125 °C to 25 °C (Figure 3-1-5). Specifically, when a COM crystal that had been heated to 125 °C was cooled back to 25 °C, the Raman spectrum showed shifts (within 5 minutes) in band positions and relative intensities (1464 and 1490 cm^{-1}) of the two peaks in this region. These bands positions agree with COM stretching vibrations.

Since cooling down our heated COM samples results in the recovery of the original spectrum, we conclude that the COA to COM transition is reversible and relatively fast (within 5 minutes) at 25 °C. We also note that the COM to COA transition is fast (~5 minutes) at 110 °C (Figure 3-1-4). This observation is probably due to the similarity in COM and COA structure.³³

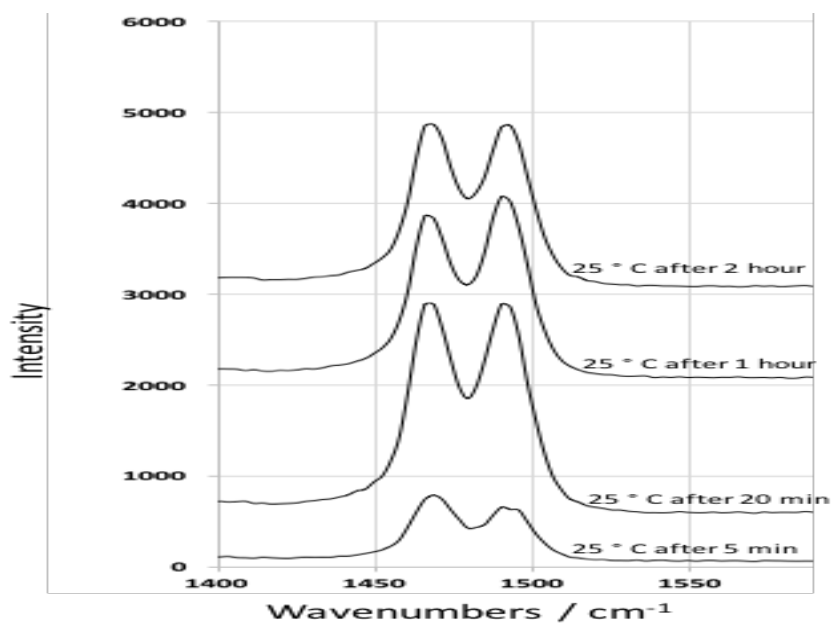


Figure 3-1-5. Raman spectrum of a COM crystal at 25 °C after 5, 20, 60 and 120 minutes.

3.1.1.2 COM dendrites Raman spectra in 1600-1800 cm^{-1} region

Changes in the 1600-1800 cm^{-1} region of the Raman spectra were used to identify the antisymmetric C-O stretch of our COM crystal. The Raman spectrum of a COM dendrite showed a single band at 1630 cm^{-1} at 25 °C (Figure 3-1-2). At 75 °C, there was no shift in the band position, which indicates no change in crystal structure (Figure 3-1-6). Between the temperatures of 75 °C and 125 °C, there was a band shift from 1630 cm^{-1} to 1646 cm^{-1} ¹. This observation indicated that COM crystal had changed to the COA phase.

The spectra of a COM crystal between 100-125 °C is presented in Figure 3-1-7. The spectra suggest that the change in band position (1649 cm^{-1}) happened between 105 and 110 °C. When the crystal was cooled, the Raman spectrum exhibited bands located at 1631 cm^{-1} which is a COM spectral feature (Figure 3-1-8). This data confirmed that the COM to COA phase transformation is a thermally reversible process. This conclusion suggests that COA absorbs water molecules from the surrounding air to convert back to the COM phase. Similar results, in this spectral region, were obtained from all five COM dendrites crystals examined.

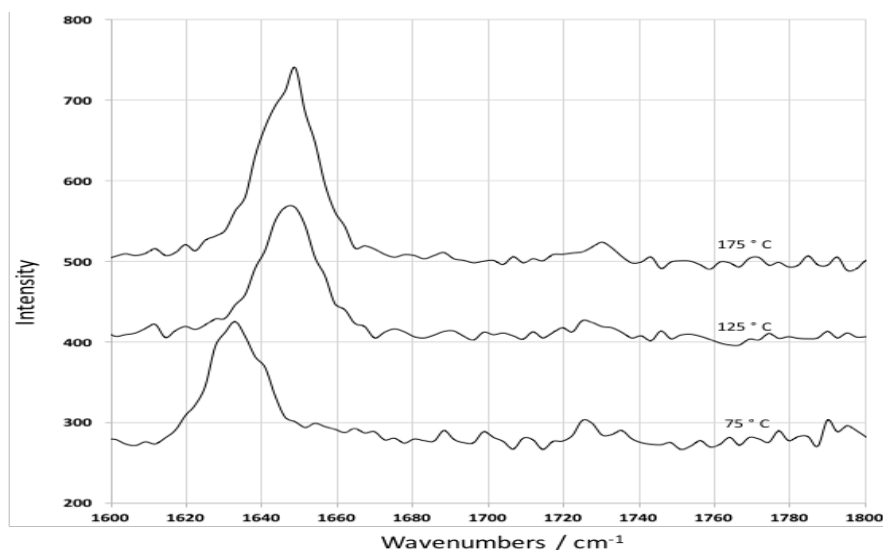


Figure 3-1-6. Raman spectrum of a COM crystal from 75-175 °C.

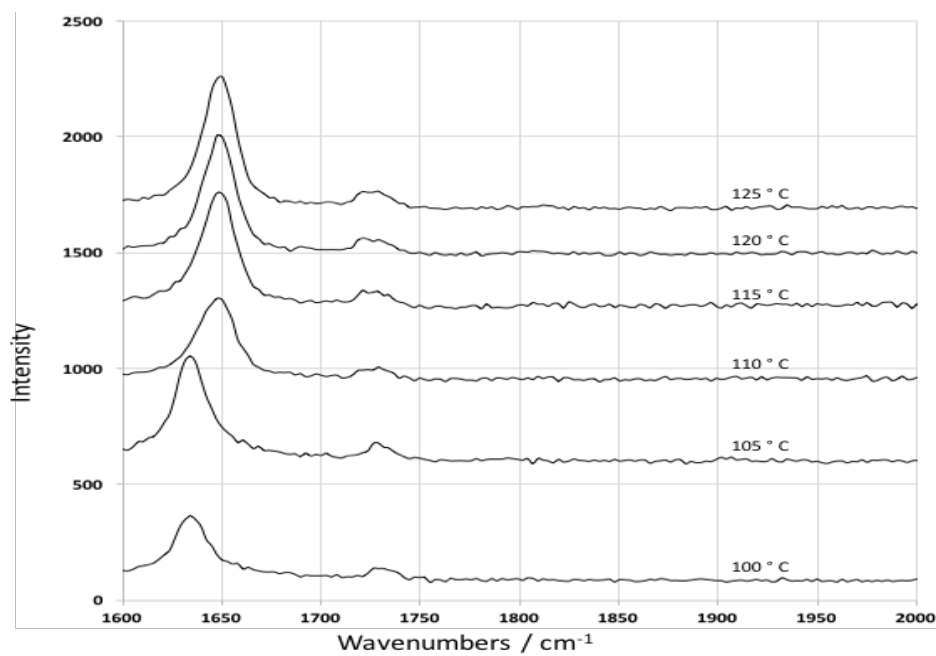


Figure 3-1-7. Raman spectrum of a COM crystal between 100-125 °C.

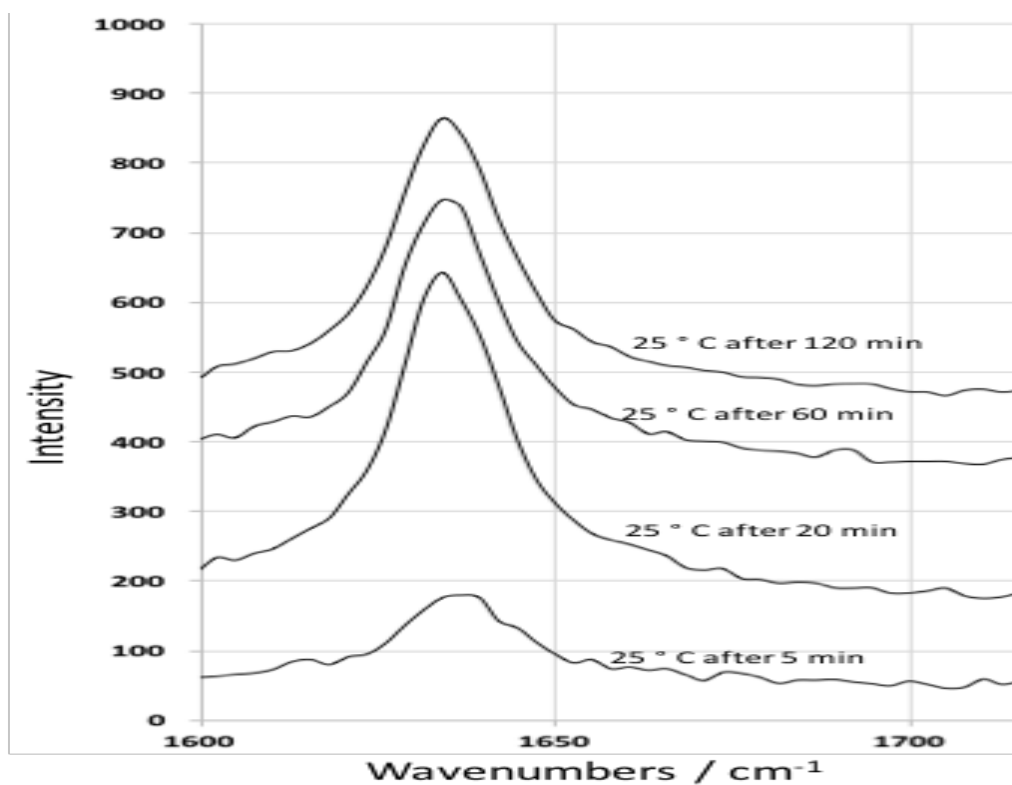


Figure 3-1-8. Raman spectrum of a COM crystal at 25 °C after 5, 20, 60 and 120 minutes.

3.1.1.3 COM dendrites Raman spectra in the 800-950 cm^{-1} region

The C-C spectral feature region was also used to obtain further evidence of crystal phase changes during thermal treatment. Previous studies observed that C-C stretching vibration was 896 cm^{-1} for COM and 904 cm^{-1} for COA.³⁴ At 25°C and 75°C , a single band was observed at 897 cm^{-1} and is assigned to this COM stretching vibration (Figure 3-1-9 and 3-1-10). As the temperature increased to 125°C , a noticeable shift of this band to 904 cm^{-1} was observed. This band is identical to a COA band position in the same stretching region. Upon further thermal treatment to 175°C , the Raman spectrum continued to show a band at 904 cm^{-1} , which matches COA stretching mode (Figure 3-1-10). It is important to note that these spectral changes occur specifically in the $105 - 110^\circ\text{C}$ range (Figure 3-1-11).

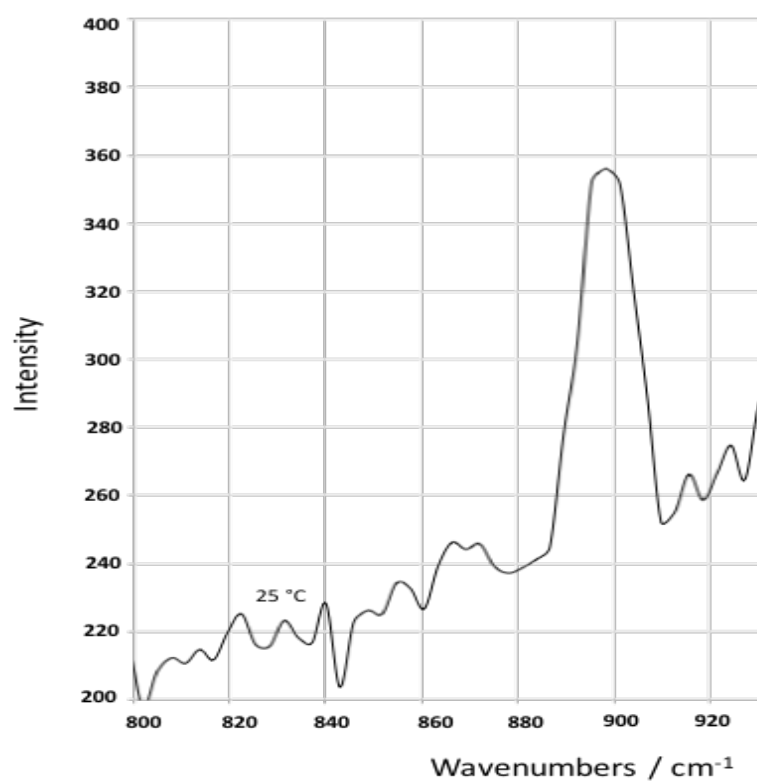


Figure 3-1-9. Raman spectrum of a COM crystal at 25°C .

After cooling the crystal back down to 25 °C, the C-C stretching vibration was again observed at 897 cm^{-1} (Figure 3-1-12). This corresponds to the C-C stretching mode of the COM phase. Initially, after cooling down the COM crystals to 25 °C, two peaks were observed; one at 902 cm^{-1} and the other at 896 cm^{-1} . This suggests that the COA is being converted to COM. Recovery of the original COM spectrum, and thus complete transformation occurred within 20 minutes (Figure 3-1-12). Similar results were obtained from all five COM dendrites crystals examined.

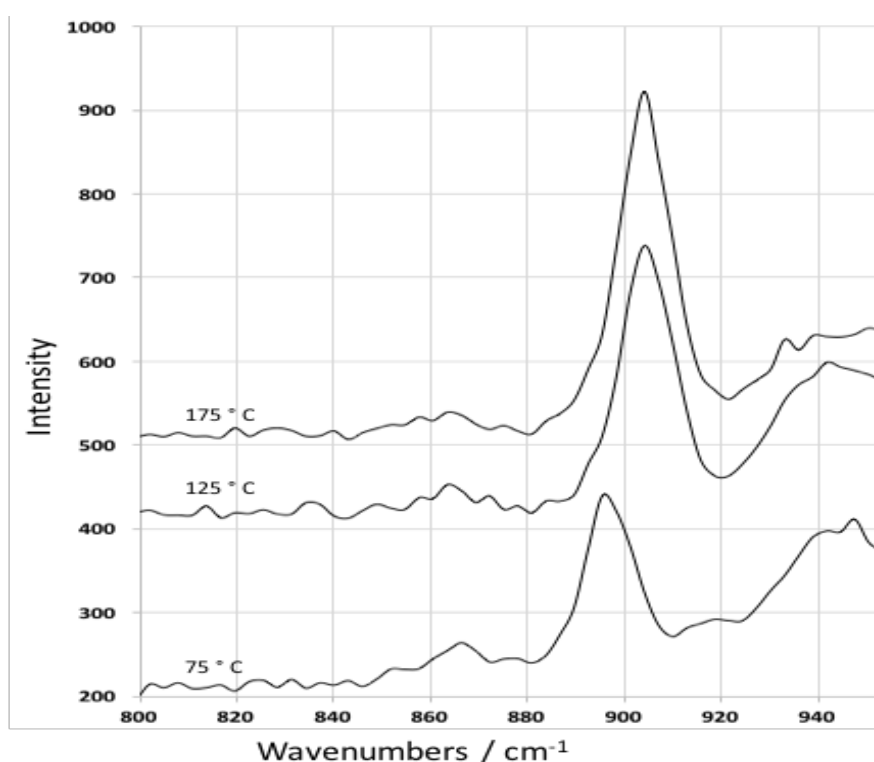


Figure 3-1-10. Raman spectrum of a COM crystal between 75-175 °C.

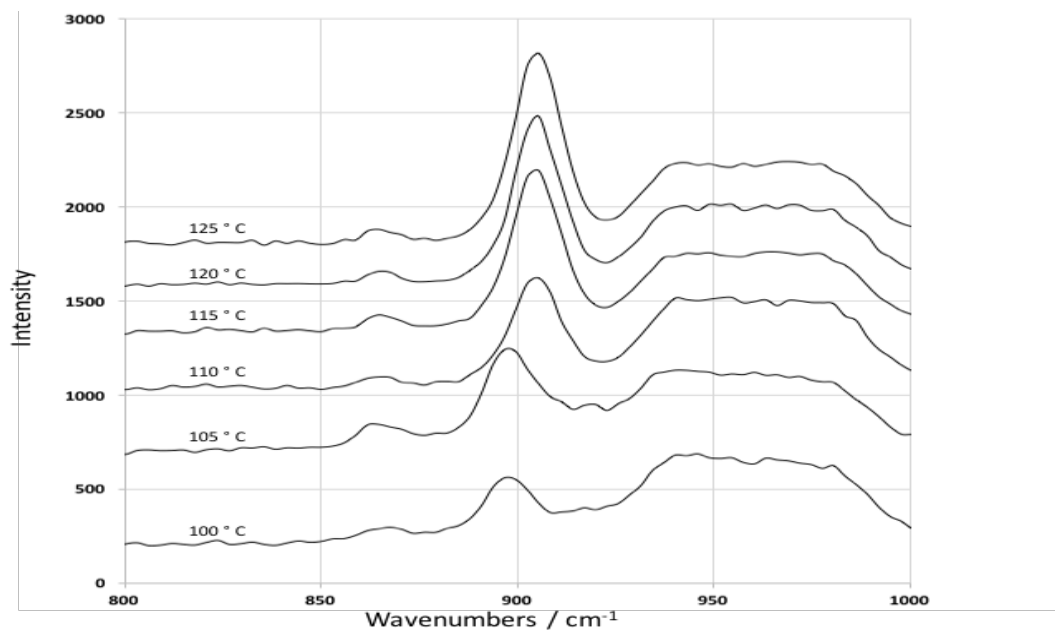


Figure 3-1-11. Raman spectrum of a COM crystal between 100 -125 °C. The broad peak at $\sim 960 \text{ cm}^{-1}$ is from the Si substrate.

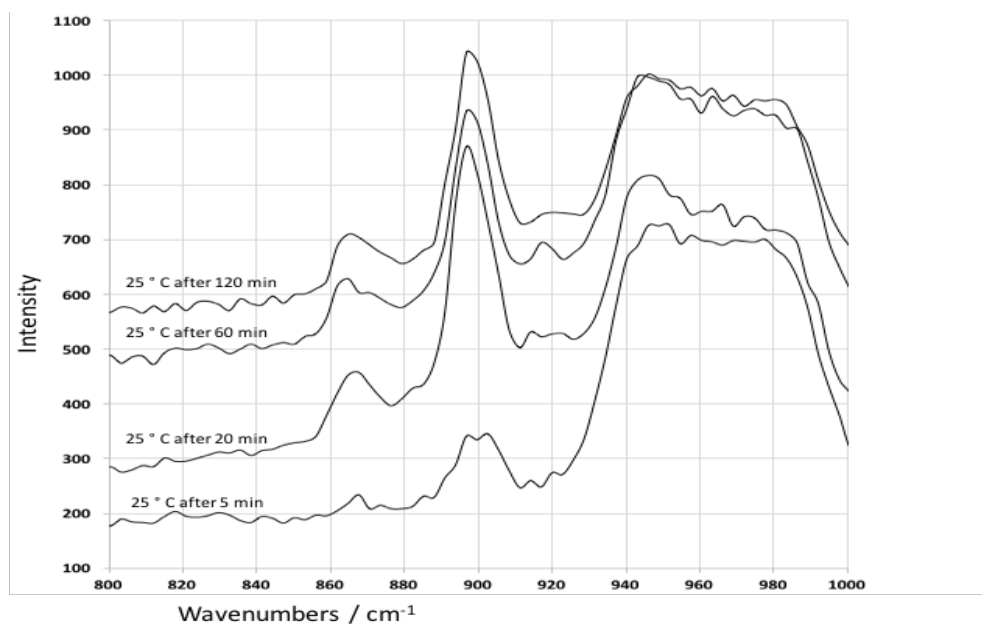


Figure 3-1-12. Raman spectrum of a COM crystal at 25 °C after 5, 20, 60 and 120 minutes.

3.1.1.4 COM dendrites overall shape

It is unclear if a single dendritic crystal of COM transforms to one single crystal of COA or if it transforms to several small COA crystals. We see no or little optical evidence

for the latter. Moreover, if the latter occurred, we would expect to create small (i.e., smaller than our original COM crystal) COA crystals that upon cooling would form small crystals of COM. This occurrence would likely cause a distinct difference in the ratios of the Raman peak intensities (not peak positions) between the original (unheated) COM crystal spectrum and the one obtained after cooling down (Figure 3-1-13). Put differently, the same polarization of light would yield different intensity ratios for the Raman bands when it is exciting an ensemble of randomly oriented small crystals than when it is exciting a single crystal. This is because it is presumed that the orientations of the unit cells in these small crystals (with respect to the polarization light) will be different for each small crystal. However, we observe very little difference in ratios, i.e., spectra look relatively identical. This suggests that either (1) small crystals form but their crystal axes orientation is not random but rather similar to the original unheated COM crystal or (2) COA transforms to a single COM crystal and vice versa.

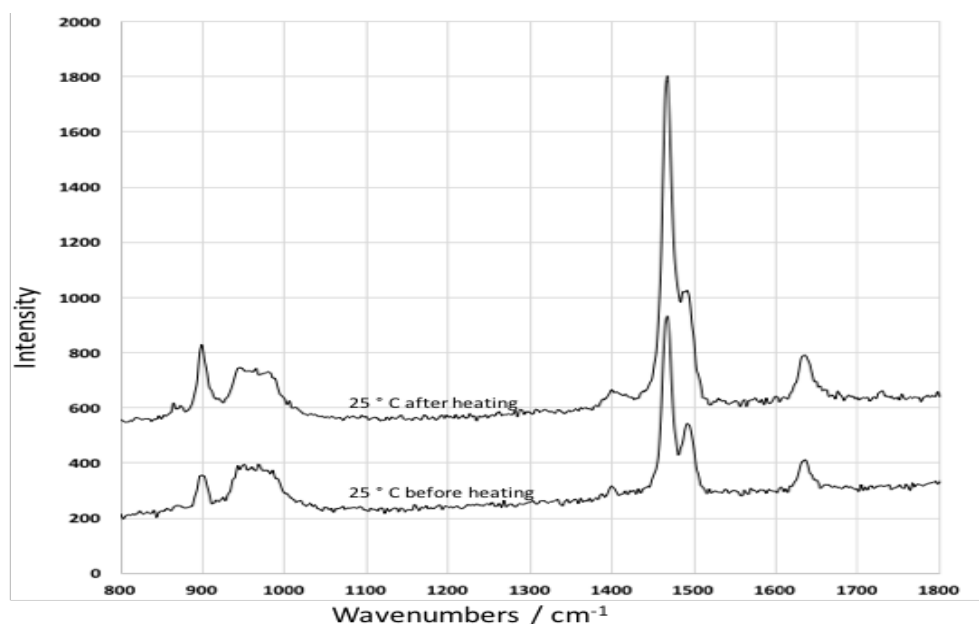


Figure 3-1-13. A COM crystal unheated and after being heated. The broad peak at $\sim 960\text{ cm}^{-1}$ is from the Si substrate.

3.1.2 COD phase transition

Like other CaOx phases, the COD phase has different habits and in order to identify COD crystals based on their habit, different names are used. For example, tetragonal bipyramid, dumbbell, and rounded crystals are different habits of COD.⁶⁹ In this study, COD crystals were obtained by using non-equimolar Ca^{2+} (40 mM) and Ox^{2-} (200 mM) side stream input concentrations (see Section 2.2.3). Using NaCit (0.01 mM) as an additive in the crystallization of COD bipyramid was necessary to promote the formation of COD. Both the images (SEM and optical) and spectra of our obtained COD crystal are consistent with previous reports in which the crystal morphology was also confirmed by SCXRD (Figure 3-1-14).^{74, 75, 76, 77}

In order to study the thermal transformation of a COD crystal, the sample was heated

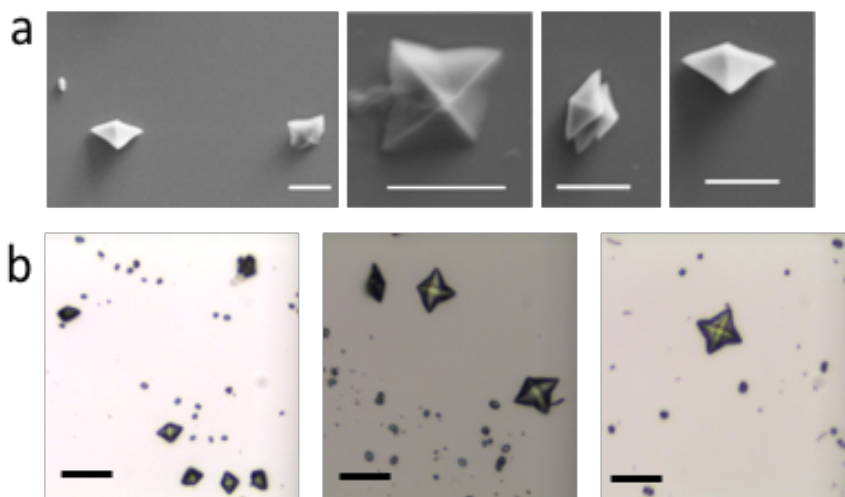


Figure 3-1-14. (a) SEM and (b) optical images of COD bipyramids. Scale bar in SEM images is 5 μm , and scale bar in optical images is 20 μm .

and examined by Raman spectroscopy as described in Chapter 2. Based on previous findings, CaOx crystals have a high intensity feature in the 1400-1800 cm^{-1} region which is attributed to the C-O stretching vibration.^{66, 67}

3.1.2.1 COD bipyramid Raman spectra in 1400-1550 cm^{-1} region

The Raman spectrum of a COD crystal that was measured at 25 °C has a single band at 1476 cm^{-1} (Figure 3-1-15). Mild heating to 75 °C showed no change in the position of this 1476 cm^{-1} peak. This suggests there was no phase transformation up to this temperature, and this result disagrees with a 2003 study, which suggests based on Raman spectra COD transforms to COM by 50 °C.⁴² There was a noticeable change in our bipyramid crystal spectral characteristic (e.g., peak shifts) upon heating to 125 °C (Figure 3-1-16). At 100 °C, a band was observed at 1476 cm^{-1} , which indicates that no change happened at this temperature. At 125 °C,

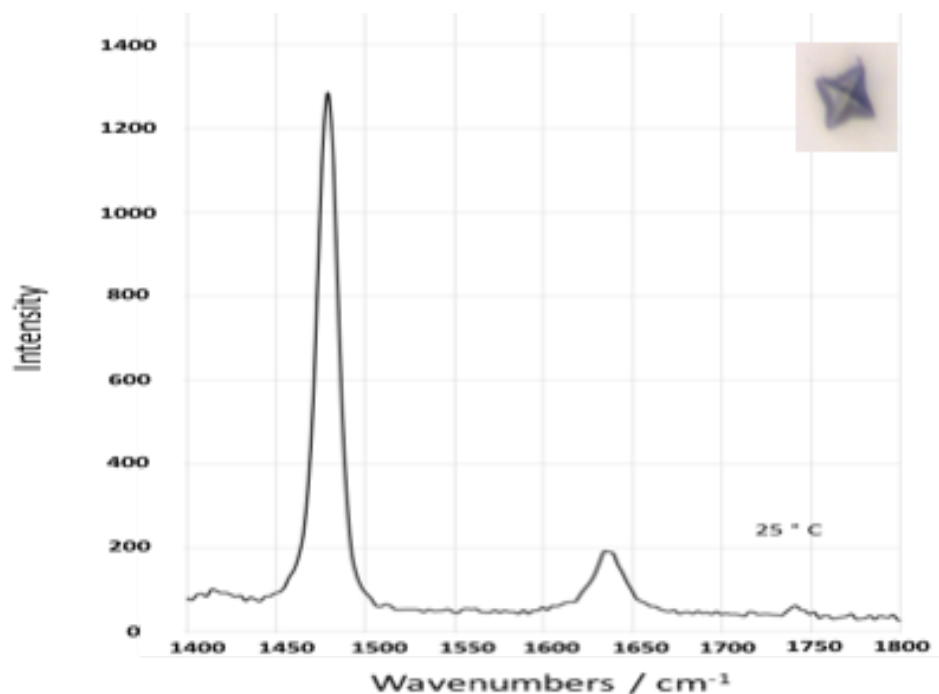


Figure 3-1-15. Raman spectrum of a COD crystal at 25 °C.

two peaks appeared at 1468 and 1479 cm^{-1} , and these are bands associated with COA. The peaks observed at 150 °C were consistent with those at 125 °C, and this suggests no phase transformation between 125-150 °C. At these high temperatures (> 125 °C), the spectra for COD look identical to the high temperature spectra for heated COM crystals (Figure 3-1-

4). These thermally-induced spectral changes that occurred by 125 °C were observed in at least fifteen other isolated COD bipyramids. No more than six crystals were examined per substrate, and thus these crystals were distributed across at least three different substrates (which were obtained in different crystallization experiments).

To be more accurate with regards to the temperature at which these spectral shifts occur, the temperature was increased in increments of 5 °C, beginning at 100 °C until 125 °C. All spectra between 100-115 °C had the same band that appeared around 1475 cm⁻¹ that indicated the COD vibration (Figure 3-1-17). However, at 120°C and 125 °C, the spectra showed a peak with a shoulder, having band positions around the 1468 and 1479 cm⁻¹. This implied a phase transformation.

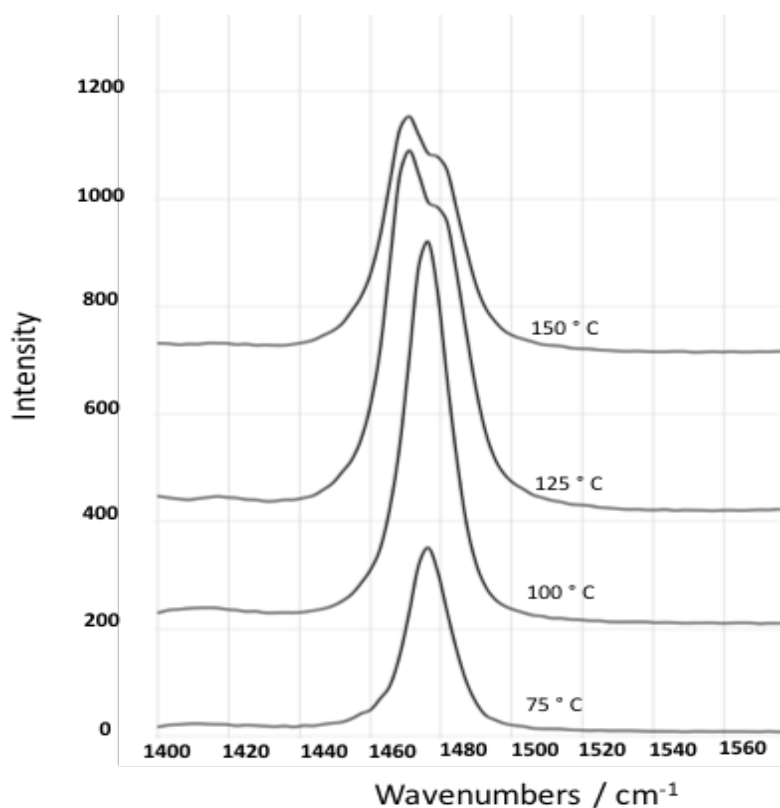


Figure 3-1-16. Raman spectrum of a COD crystal between 75-150 °C.

These band positions match the COA stretching vibration bands in this region. This spectral shift suggests that the COD crystal had transformed into COA by 125 °C (specifically between 115-125 °C).

Cooling the sample to 25 °C, did not provide a noticeable change in spectra within 20 minutes (Figure 3-1-18). It remained in the COA phase up to this point. After waiting for 180 minutes, a shoulder was observed near 1468 cm^{-1} and the peak was broader which indicated the COA had begun converting to COM the most stable phase. In contrast with COM dendrites, the phase transformation for a COD bipyramid was slow. The same

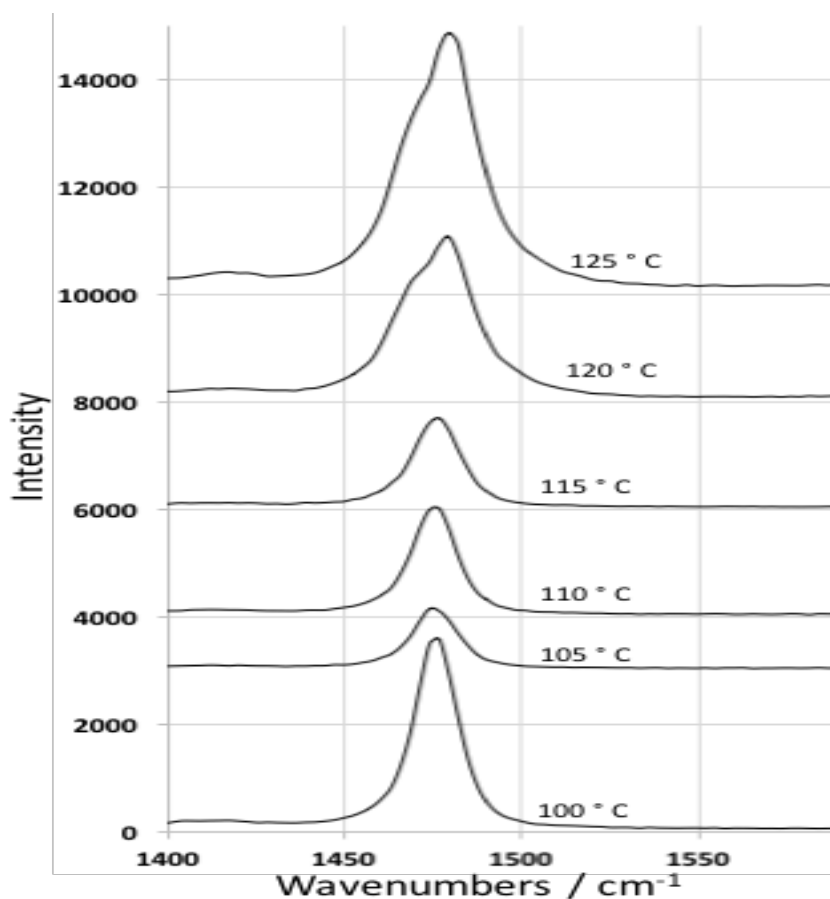


Figure 3-1-17. Raman spectrum of a COD crystal between 100-125 °C.

heating process was carried out on at least ten other crystals on different substrates. All

crystals transformed (i.e., showed thermally-induced spectral changes) by 125 °C, with most crystals transforming between 120-125 °C.

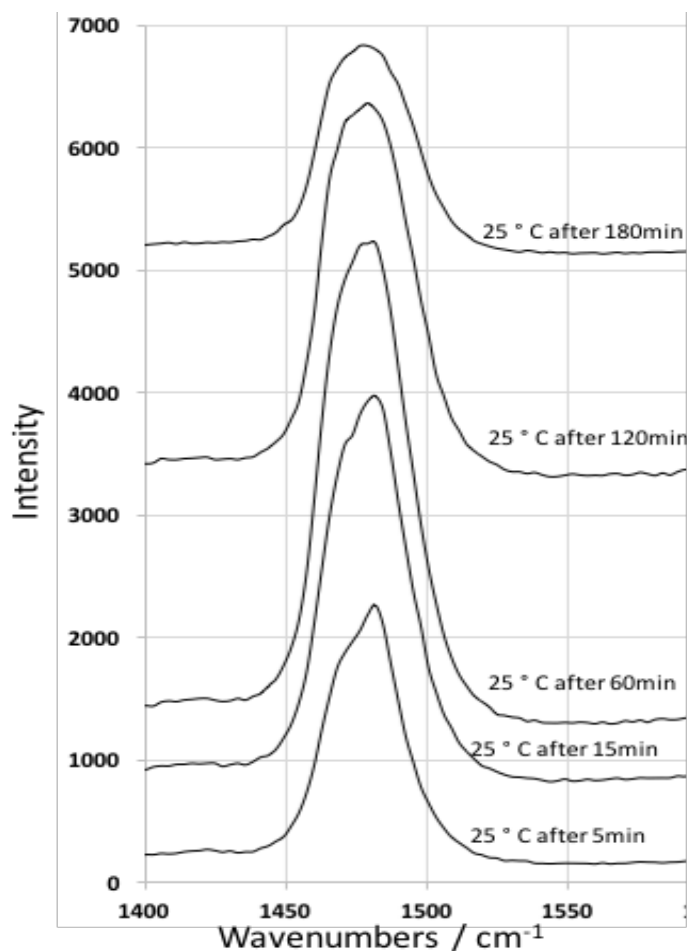


Figure 3-1-18. Raman spectrum of a COD crystal at 25 °C after 5, 15, 60, 120 and 180 minutes.

3.1.2.2 COD bipyramid Raman spectra in the 1600-1800 cm^{-1} region

Focusing on the oxalate stretching vibration in the 1600-1800 cm^{-1} region can give more evidence about CaOx crystal structure. At 75 °C, a peak was observed at 1633 cm^{-1} , which shows that no change in phase occurred (Figure 3-1-19). Increasing the temperature to 100 °C did not show any differences in band position, but when the temperature reached 125 °C the spectrum shifted to 1648 cm^{-1} . The change to a 1648 cm^{-1} position suggests that

dehydration occurred at this stage, and the COA phase was formed. Upon heating to 150 °C, no further changes occurred in the Raman spectra.

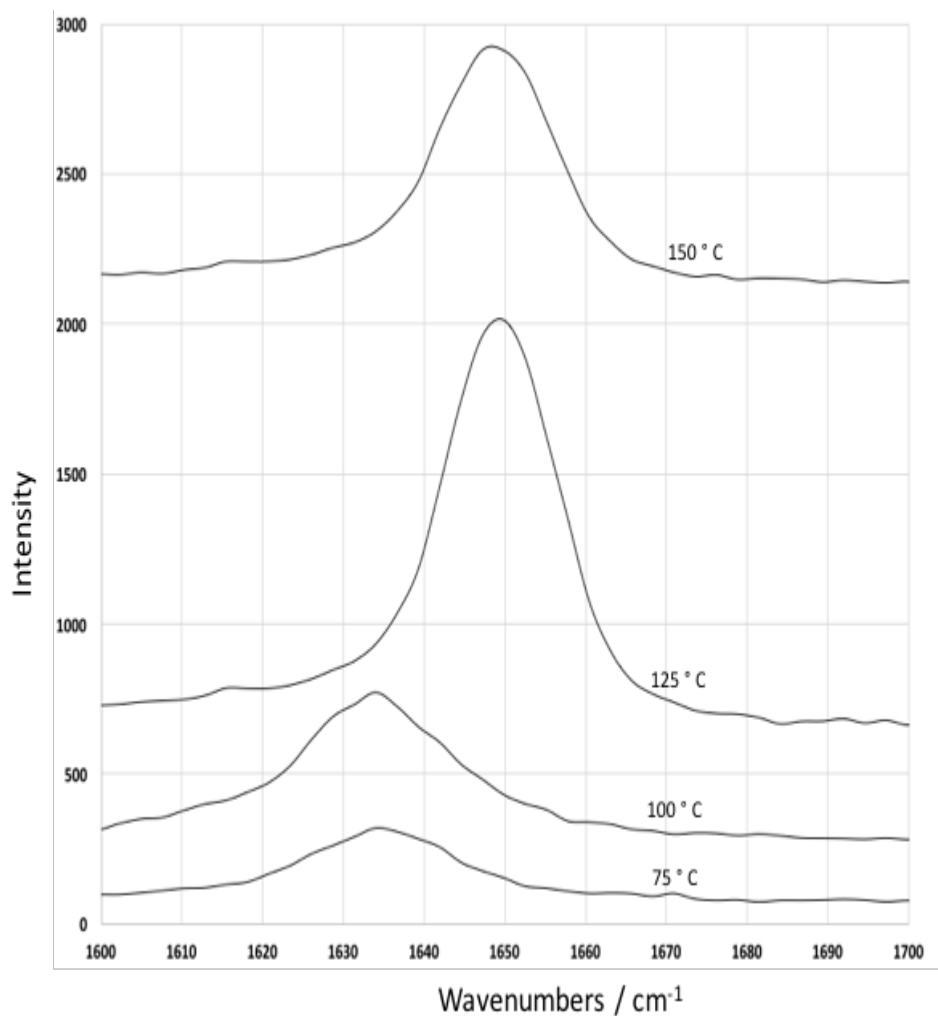


Figure 3-1-19. Raman spectrum of a COD crystal between 75-150 °C.

Spectra were collected between 100 -125 °C in order to identify at what temperature the phase transformation happened (Figure 3-1-20). There was a change in the spectrum at 120 °C, (the vibration band shifted to $\sim 1648 \text{ cm}^{-1}$), which was an evidence of a phase transformation. The COD bipyramid crystals were cooled to 25 °C and their spectra were collected over a period of 180 minutes (Figure 3-1-21). At 25 °C, the spectra were identical

to COA spectrum at 5, 15 and 60 minutes, so cooling down these COD crystals to 25 °C does not produce recovery of the original COD spectra even after 20 minutes.

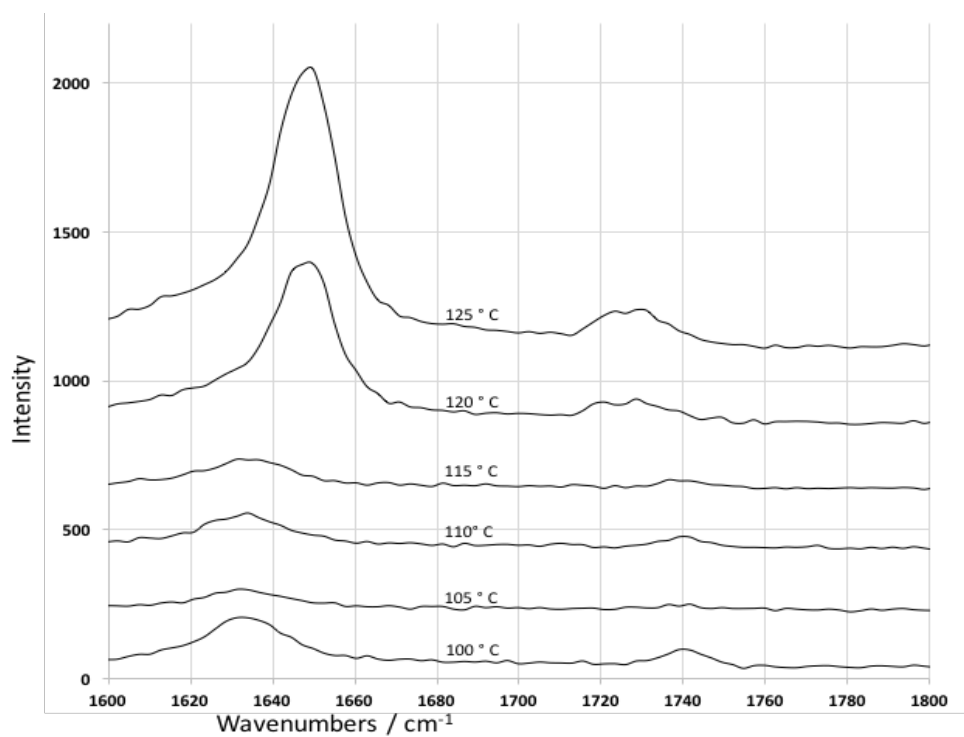


Figure 3-1-20. Raman spectrum of a COD crystal between 100-125 °C.

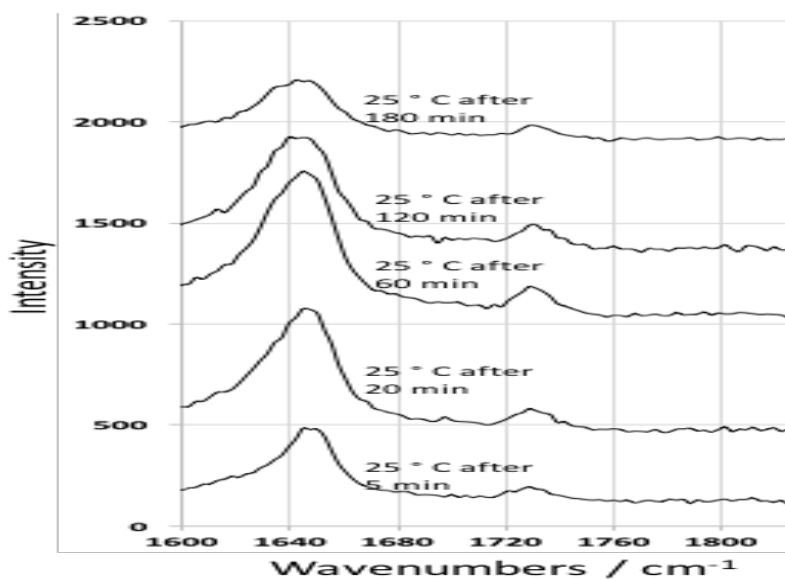


Figure 3-1-21. Raman spectrum of a COD crystal at 25 °C after 5,15, 60, 120 and 180 minutes.

The same process was followed to examine 10 other crystals, but this time the samples were heated to 100 °C, and then the Raman spectra were collected after (5 and 20 minutes) reaching this temperature to verify there was no change in spectra after 20 minutes at 100 °C. The temperature was increased in increments of 5 °C between 100 °C to 125 °C to determine the specific temperature range at which COD converts to another phase. Most crystals were transformed between 120-125 °C.

3.1.2.3 COD bipyramid Raman spectra in the 800-950 cm^{-1} region

Focusing on the C-C stretching vibration located between 800-950 cm^{-1} provides more evidence about the structure of calcium oxalate. At 25 °C, a band was observed around 911 cm^{-1} , which agrees with previously published data of COD vibrations (Figure 3-1-22).^{42, 65} Figure 3-1-23 shows the Raman spectrum of a COD crystal in this region as a function of temperature. From 75 °C to 100 °C, there were no changes in peak positions. Similar results were obtained from all

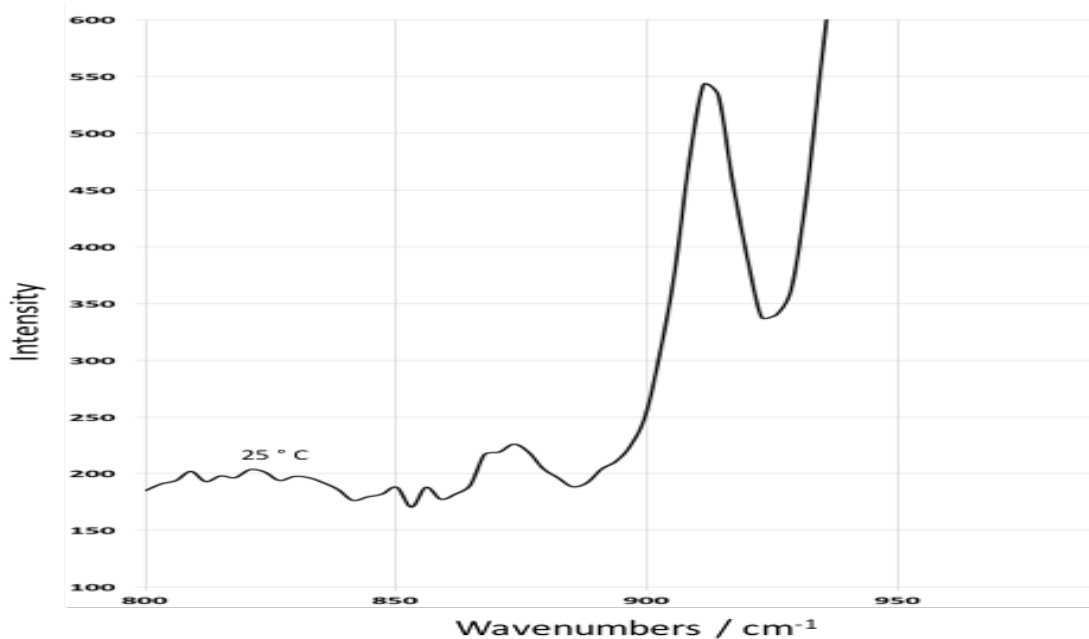


Figure 3-1-22. Raman spectrum of a COD crystal at 25 °C.

ten COD crystals that were examined. It is noted that the spectrum of C-C stretching vibration was shifted to 905 cm^{-1} when the temperature reached $125\text{ }^{\circ}\text{C}$. The same band position (905 cm^{-1}) was observed at $150\text{ }^{\circ}\text{C}$, and this is the band position of the C-C stretch of COA stretching vibration. Spectra collected between $100 - 125\text{ }^{\circ}\text{C}$ showed the change in spectrum occurred by $120\text{ }^{\circ}\text{C}$ (Figure 3-1-24). The sample was cooled back to $25\text{ }^{\circ}\text{C}$, and the peak $\sim 905\text{ cm}^{-1}$ was observed after 20 minutes (Figure 3-1-25). Within 180 minutes, there was a shoulder observed in the band at 896 cm^{-1} . This shift was identical to COM stretching vibration. Similar results were obtained from all ten COD crystals that were examined.

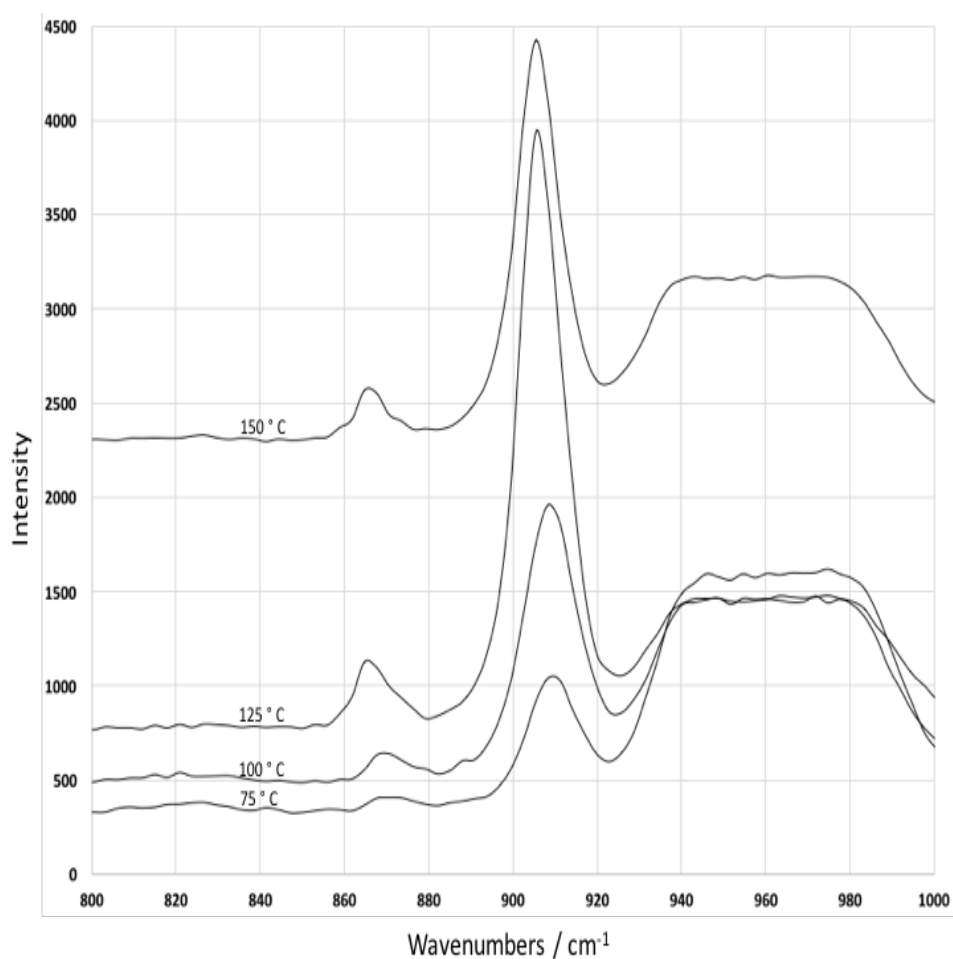


Figure 3-1-23. Raman spectrum of a COD crystal between $75\text{--}150\text{ }^{\circ}\text{C}$.

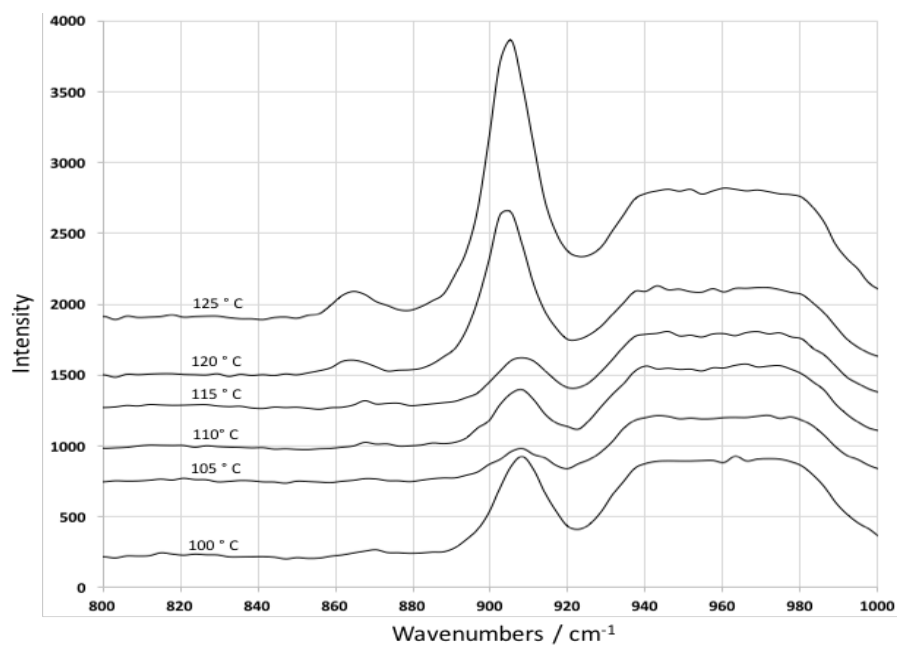


Figure 3-1-24. Raman spectrum of a COD crystal between 100-125 °C.

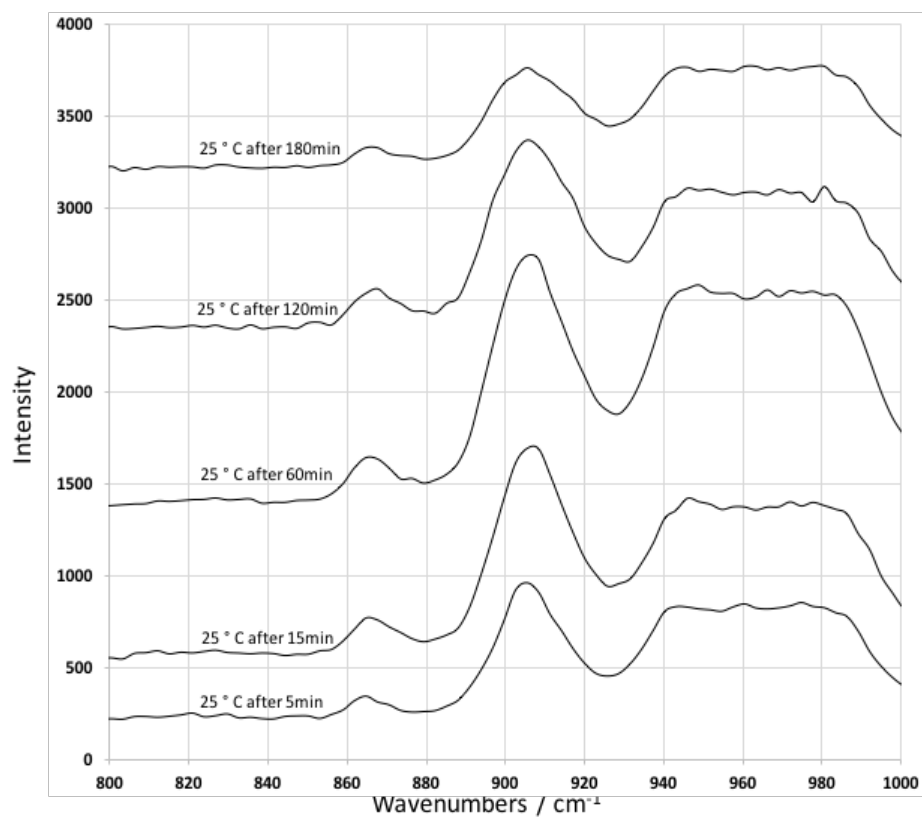


Figure 3-1-25. Raman spectrum of a COD crystal at 25 °C after 5, 15, 60, 120 and 180 minutes.

3.1.2.4 COD phase transformation temperature

Based on our results, the transition of COD-COA is: (1) indeed a one-step process (i.e., there is no change in spectral features prior to the transformation to COA) and (2) occurs at temperatures higher than the temperatures at which COM transforms. This suggests that if indeed the water molecules in COM are more tightly bound than the water molecules in COD, the relatively large difference in crystal structures between COD and COA plays a discernible role in preventing the loss of these hydrate (i.e., not the zeolitic) water molecules within the lattice.

Between 115-125 °C, the transformation of 10 hydrate COD bipyramid crystals to COA were detected. Chart 1 illustrates the range of temperatures obtained for 10 different crystals. The reason for the range in transition temperatures is not clear. It may be an intrinsic phenomenon (i.e., not all crystals transition at the same temperature). It must be noted that it seems unlikely that the temperatures of these COD transitions are being affected significantly by the contact crystals have with the surface, since preliminary work with other COD crystal habit have shown similar results. Indeed, even if dendrites have better contact with the underlying heat stage, one would expect that waiting for suitably long times would allow even crystals with more limited contact to transform. Also, considering that for some samples both COM and COD crystals were examined on the same substrate and in the same general vicinity (within 100 μm), it is not likely that these differences are due to different substrate temperatures.

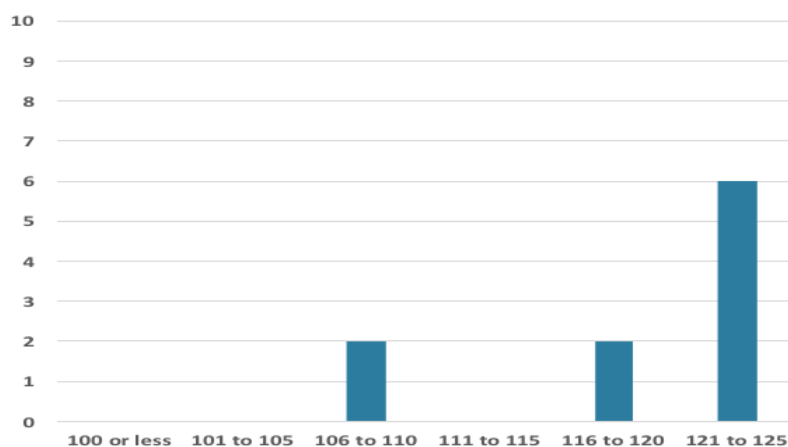


Chart 3-1-1. Comparing ten COD crystals with temperature.

Moreover, the cooling down of our heated COD crystals does not result in the recovery of the original unheated COM crystal spectrum. Thus, it can be concluded (as expected) that unlike the COM-to-COA transition, the COD-to-COA transformation is not reversible. Furthermore, COA crystals derived from heating COD crystals transition to COM structures over longer time scales (180 min) than COA structures derived from COM crystals. Possible reasons for this COA stability may be due to the similar unit cell structure of COM and COA, while COD has a very different unit cell structure than COM and COA.

3.1.2.5 COD and COM overall shape

The overall shape of our COD crystals also changes when the phase transformation to COA occurs (Figure 3-1-26). Specifically, cracks form and some crystals break apart (Figure 3-1-27). While the overall shape of the heated COD crystals changes during the transition, it is still not clear if each COD transforms to one COA crystal or to several small COA crystals. In contrast, the overall shape of our COM dendrites showed no changes when these crystals transform to COA (Figure 3-1-28).

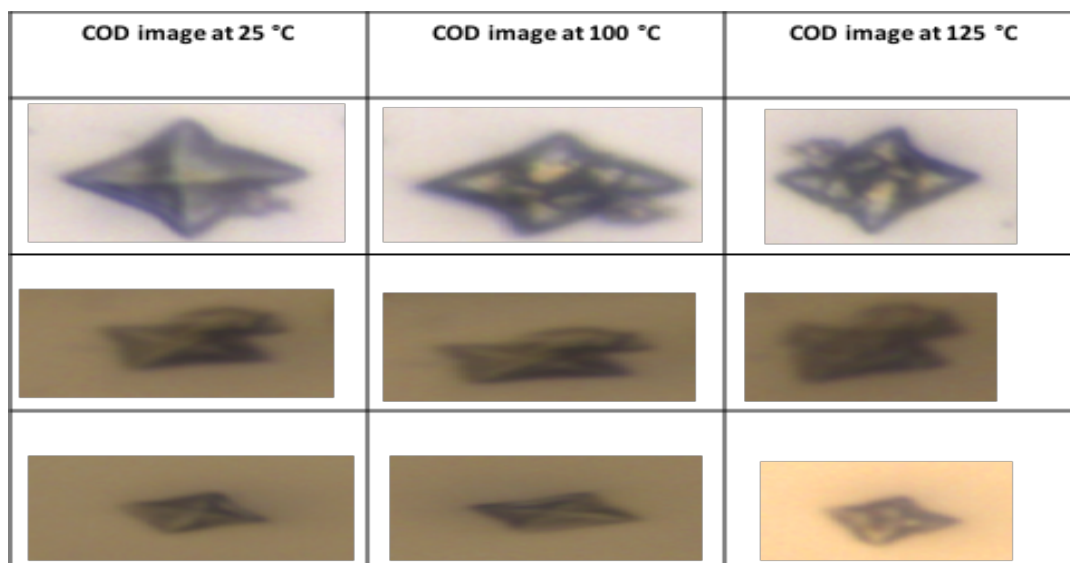


Figure 3-1-26. Different COD crystals after being heated.

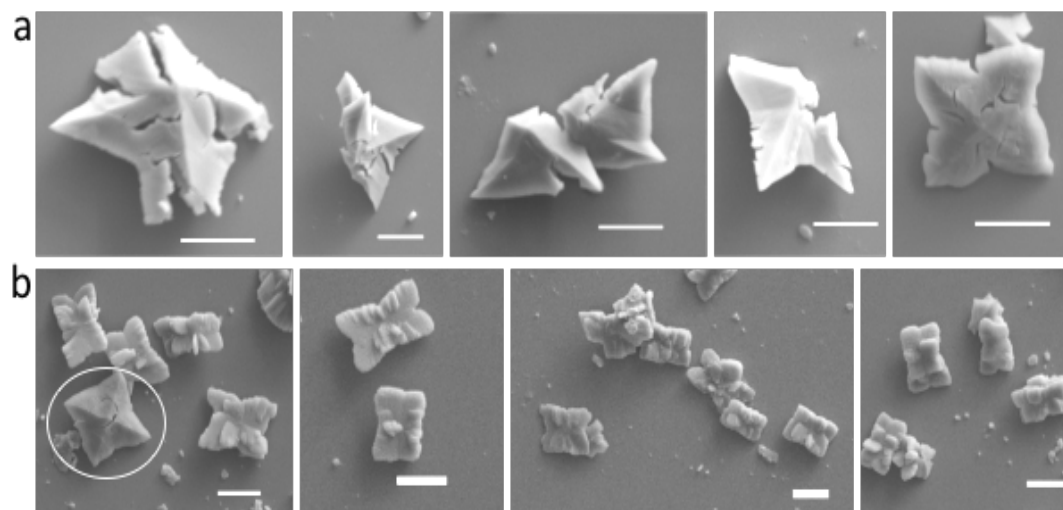


Figure 3-1-27. SEM images of CaOx crystals after being heated to 125°C. Prior to heating, the phase for these various crystals was (a) COD (i.e., COD bipyramids) and (b) COM (i.e., COM dendrites); the only bipyramid in panel (b) is encircled. SEM images were taken at room temperature (i.e., after cooling samples and then sputter-coating with a metal film). Scale bar in SEM images is 5 μm.

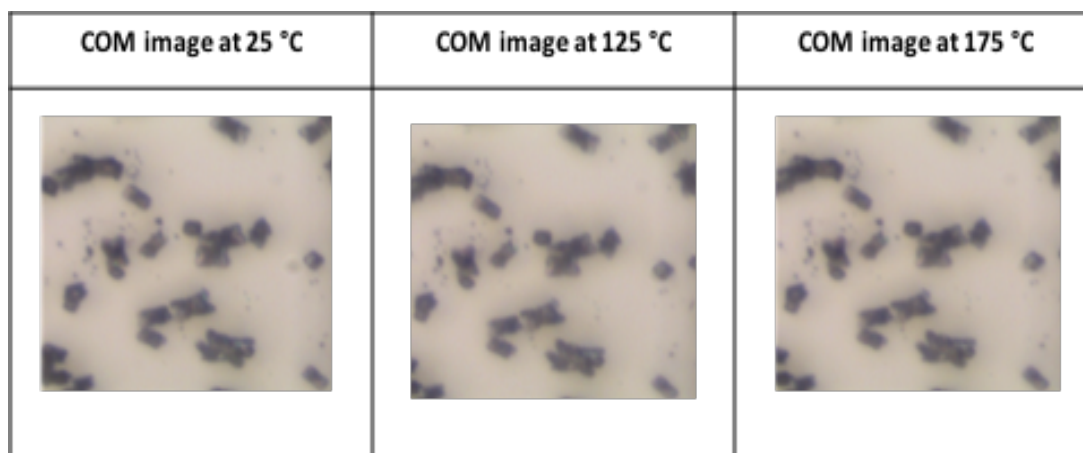


Figure 3-1-28. Different COM crystals after being heated.

Summary

We provide evidence that the COM-to-COA phase transition occurs at a slightly lower temperature than the COM-to-COD transformation. Unlike previous results supporting this conclusion that used CaOx agglomerations or powders,^{34, 42} our experiments were performed using single crystals that by our optical and vibrational characterizations were morphologically pure. Our results also indicate that at room temperature COD-derived COA crystals transform to COM more slowly than COM-derived COA.

3.2 Dissolution results and discussion

Dissolution therapy has been explored as an effective method to treat kidney stone disease,⁷⁸ and dissolution strategies are also useful for removing scale from industrial pipes.⁷⁹ Ideally, dissolution agents could be utilized as a method to dissolve CaOx crystals. A number of studies have been done to understand the effect of various solutions on CaOx crystal structure.^{55, 71, 80, 81}

In this work, the kinetics of dissolution of CaOx crystals, which were mainly COM, was examined in the presence of 5 mM concentrations of four different carboxylic acid solutions. Specifically, the effect of the monocarboxylate acetate ion (Acet), dicarboxylate

malonate ion (Malo), tricarboxylate citrate ion (Cit), and tetra-carboxylate EDTA ion on dissolving COM crystals was investigated (Table 3-2-1). These CaOx crystals were synthesized by using equimolar side stream input concentrations of Ca^{2+} (80 mM) and Ox^{2-} (80 mM) solutions with distilled water in the middle stream (see Section 2.2.3). This synthesis results in a variety of COM crystals, such as prismatic, X-shaped, and dendrites, and a few COD crystals (bipyramids) (Figure 3-2-1). Based on previous findings in our laboratory, COM crystals made using this procedure have differences in habit and size due to two main causes: position of crystal formation and velocity. If a crystal is formed near the exit of the middle stream it will be smaller than a crystal formed near the entrance of the middle stream. The difference in velocity between the middle stream (where the velocity is high) and the two side streams (where the velocity is low) can also contribute to crystal size differences in the middle stream. Larger crystals form near the low velocity side-streams because these crystals have a greater residence time than crystals in the center of the middle stream (Figure 3-2-2).

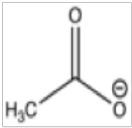
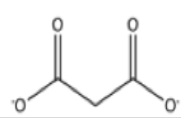
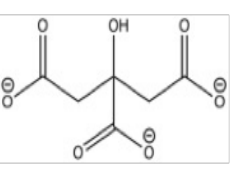
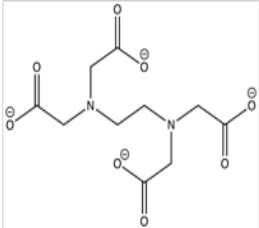
Fully deprotonated acetate ion	Fully deprotonated malonate ion	Fully deprotonated citrate ion	Fully deprotonated EDTA ion
			

Table 3-2-1. Illustration the fully deprotonated structures of acetate, malonate, citrate, and EDTA ions.

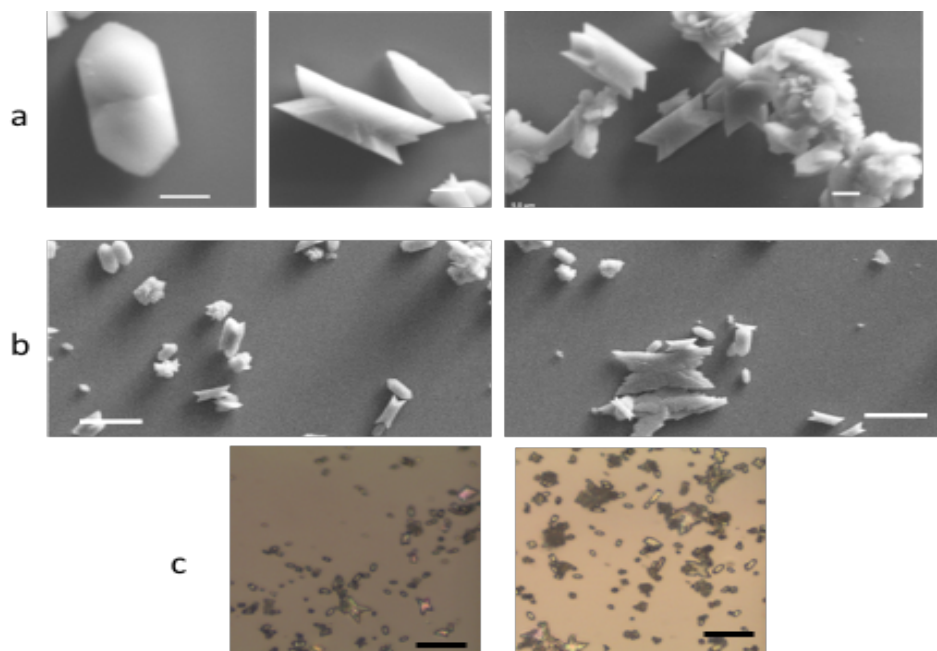


Figure 3-2-1. (a, b) SEM images of COM crystals (prismatic and dendritic) and (c) optical images of COM crystals (prismatic and dendritic). Scale bar of a = 1 μm , b = 5 μm , and c = 20 μm .

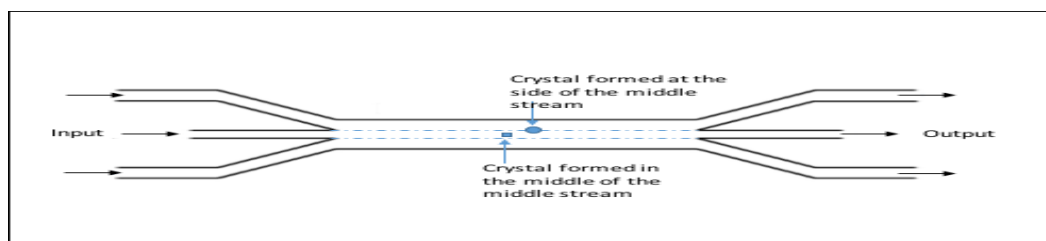


Figure 3-2-2. Illustration of different size of crystals due to the different velocity in the middle stream (the square travels faster).

After synthesizing CaOx crystals, a microfluidic dissolution device was used to optically observe the crystal size changes as a function of time. The flow rate for the dissolution solutions was 200 $\mu\text{L}/\text{min}$. Several different flow rates (ranging from 50-500 $\mu\text{L}/\text{min}$) were tried for the EDTA and citrate solutions. The low flow rates (~ 50 $\mu\text{L}/\text{min}$) did not show any significant dissolution activity within an hour. At high flow rates (~ 500 $\mu\text{L}/\text{min}$), crystals were easily dislodged.

Two sets of experiments were conducted. These experiments were designed to obtain insight into the role of COO^- concentration on the Ca^{2+} complexation process. In one set,

the formal concentration (5 mM) of each solution was kept constant. In the other set, the pH \approx 10 and the formal concentration were kept constant. Three or more repeated dissolution experiments were carried out for each solution (i.e., for each type of COO⁻ ion). The formal concentration was chosen based on a previous study which had shown that EDTA and citrate ion solutions of this concentration dissolve CaOx crystals within an hour.⁵⁹

3.2.1 5 mM Experiments (varying pH)

Passing a solution of 5 mM sodium EDTA (pH = 4.92) over a collection of CaOx crystals lead to removal (either dissolving or dislodging) of all crystals in 20 minutes (Figure 3-2-3a). This “dissolution time” was the shortest for any of the solutions examined, and this was not surprising since EDTA is one of the most effective Ca²⁺ complexing agents. The binding of EDTA with Ca²⁺ ion in solution decreases the concentration of free Ca²⁺ ion in solution, thereby shifting the equilibrium of the system such that more crystals dissolve. This result fits well with other investigations that confirm the strong dissolution effect of EDTA on COM crystals.⁵⁹

Passing a solution of 5 mM Na-Cit (pH= 7.53) over several CaOx crystals had a significant impact on CaOx crystal size and number. All crystals on the substrate, which was placed in the dissolution device, dissolved after \sim 30 minutes of treatment with the citrate solution (Figure 3-2-3b). This results also fit well with other published papers that suggest citrate may be very useful in stone treatment.^{71, 82}

In contrast, 5 mM of Na-Malo (pH=7.40) exhibited less CaOx dissolution ability than the EDTA and citrate solution. CaOx crystals dissolved within \sim 40 minutes after contact with this 5 mM solution (Figure 3-2-4a). While the 5 mM Na-Acet solution (pH= 6.87)

slightly reduced CaOx crystals size, this solution had a weak affect compared to citrate and EDTA (Figure 3-2-4b).

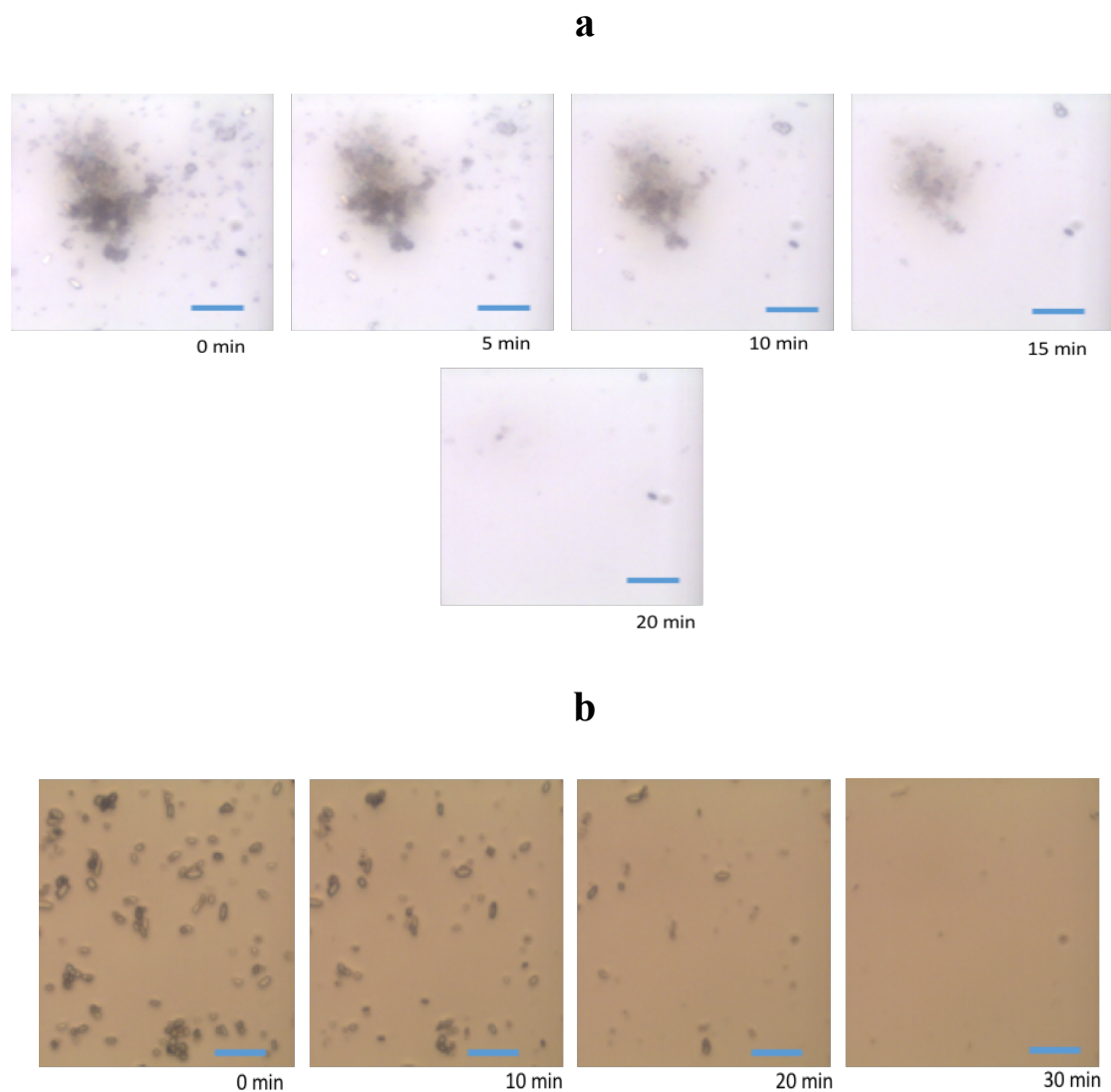


Figure 3-2-3. (a) Optical images of the dissolution action of EDTA and (b) optical images of the dissolution action of citrate. The scale bar is 20 μm .

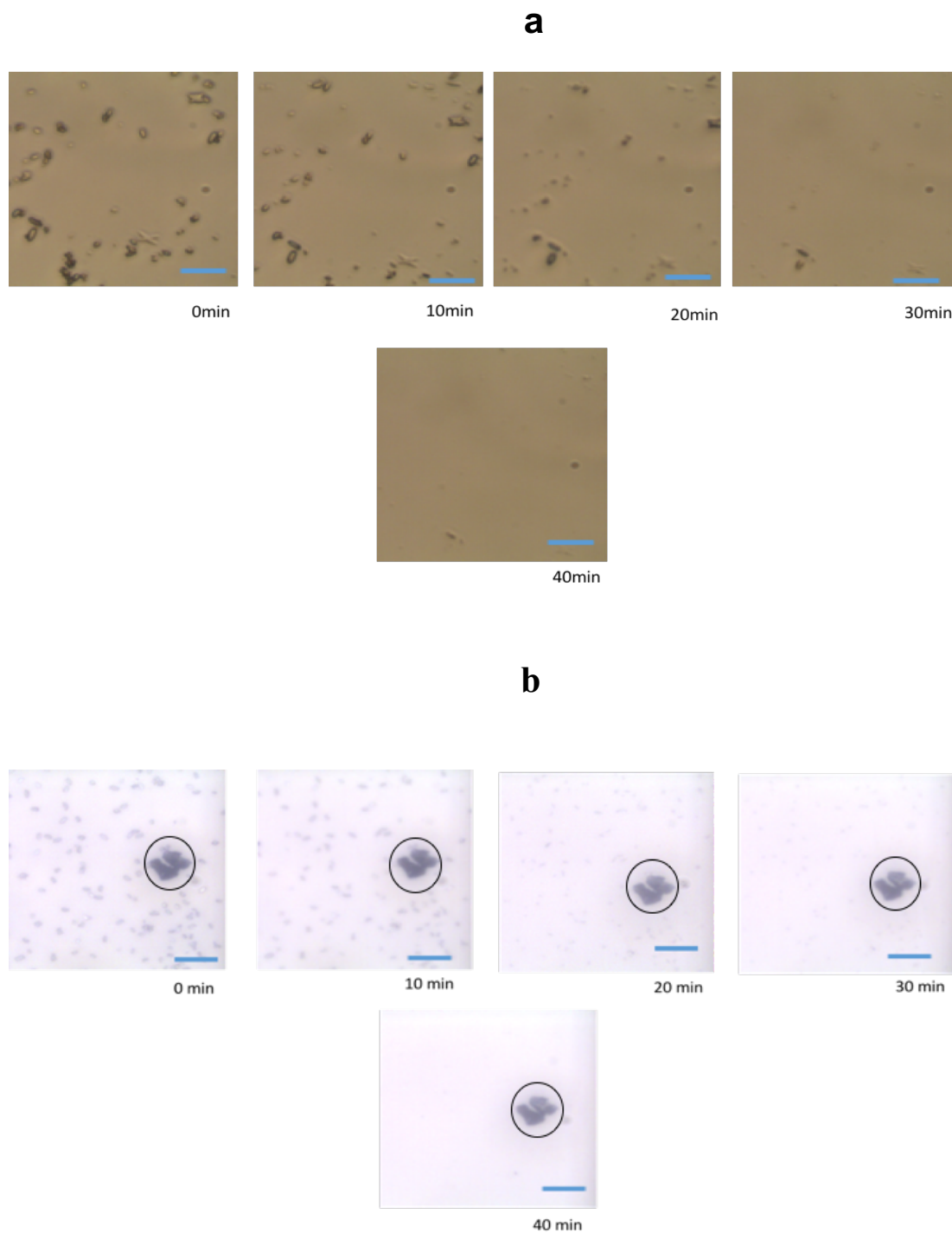


Figure 3-2-4. (a) Optical images of the dissolution action of malonate and (b) optical images of the dissolution action of acetate. The scale bar is 20 μm . The encircled object is most likely a piece of silicon.

The dissolution rate of a single CaOx crystal is expected to be different based on different solutions that are used because of the differing number of COO^- in the solution.

All solutions used in this study were sodium salts (EDTA, citrate, malonate, acetate) so as to eliminate the cation effect in this study. Moreover, Chutipongtanate and coworkers reported that sodium chloride did not show any effect on COM dissolution.⁵⁹ As a result, any dissolving action in our study would be the result of the anions (EDTA, citrate, malonate, or acetate). Our result seems to suggest that at the same formal concentration (but different solution acidities), ions with more COO^- groups are better dissolution agents (Table 3-2-2).

COO^-	Formal concentration	pKa value or values	pH	predominate COO^- form in solution at this pH	Time
EDTA	5mM	0.0, 1.5, 2.00, 2.69, 6.13, 10.37.	4.92	$[\text{EDTA}^{2-}]$	~20 min
Citrate	5mM	3.13, 4.76, 6.40	7.53	$[\text{cit}^{3-}]$	~30min
Malonate	5mM	2.83 and 5.69	7.40	$[\text{Mal}^{2-}]$	~40min
Acetate	5mM	4.76	6.87	$[\text{Acet}^-]$	~40min

Table 3-2-2. Illustration of 5 mM Experiments of EDTA, citrate, malonate and acetate ions (varying pH). pKa values obtained from Quantitative Chemical Analysis.⁸³

Carboxylate ions have the ability to form complexes with calcium ions, and this promotes dissolution. This dissolution may be a result of competition for Ca^{2+} between the oxalate ions and the carboxylate ion in the solution. The carboxylate ion in di and tri carboxylic acids has the ability to inhibit the nucleation of, or may dissolve, the COM.^{19, 84, 85} Previous studies found that the solutions that contain more carboxylic groups are the most active growth inhibitors for CaOx crystals.^{72, 84}

EDTA has been explored as a therapy treatment to remove heavy metals such as mercury from the blood and treat atherosclerosis. However, there is no current approval for its use in dissolving kidney stones.^{86, 87} Citrate is a candidate that provides a promising advantage in dissolving CaOx crystals, and should offer insight into the treatment of kidney

stone disease. This advantage may be attributed to the strong competition between oxalate groups and citrate anion.

3.2.2 5 mM experiment with constant pH

In order to examine the pH effect on the dissolution activity, the pH for all solutions was increased to 10 by using a buffer solution (see section 2 for buffer materials). This step can determine whether pH has an effect on CaOx crystal dissolution.

Passing a 5 mM Na-EDTA solution over the CaOx sample, after increasing the pH of this solution to 10, had a significant effect on a CaOx crystal dissolution. The time of dissolution activity decreased from ~20 minutes to ~10 minutes (Figure 3-2-5a). The EDTA solution at pH \approx 10 showed a greater dissolution rate relative to the rate when the pH was 4.92. This is due to the full deprotonation (specifically deprotonation of the nitrogen atoms) of EDTA at pH \approx 10, and because of the strong ability of the COO⁻ ions and nitrogen atoms (specifically the lone pairs of electrons) to form complexes with Ca²⁺ ions. This result was in agreement with other studies that showed EDTA at high pH had the best dissolution activity of COM crystal.⁵⁹ Other studies have demonstrated that EDTA causes reduction in CaOx crystal growth rates, and it is the best CaOx crystal growth inhibitor.⁸⁸

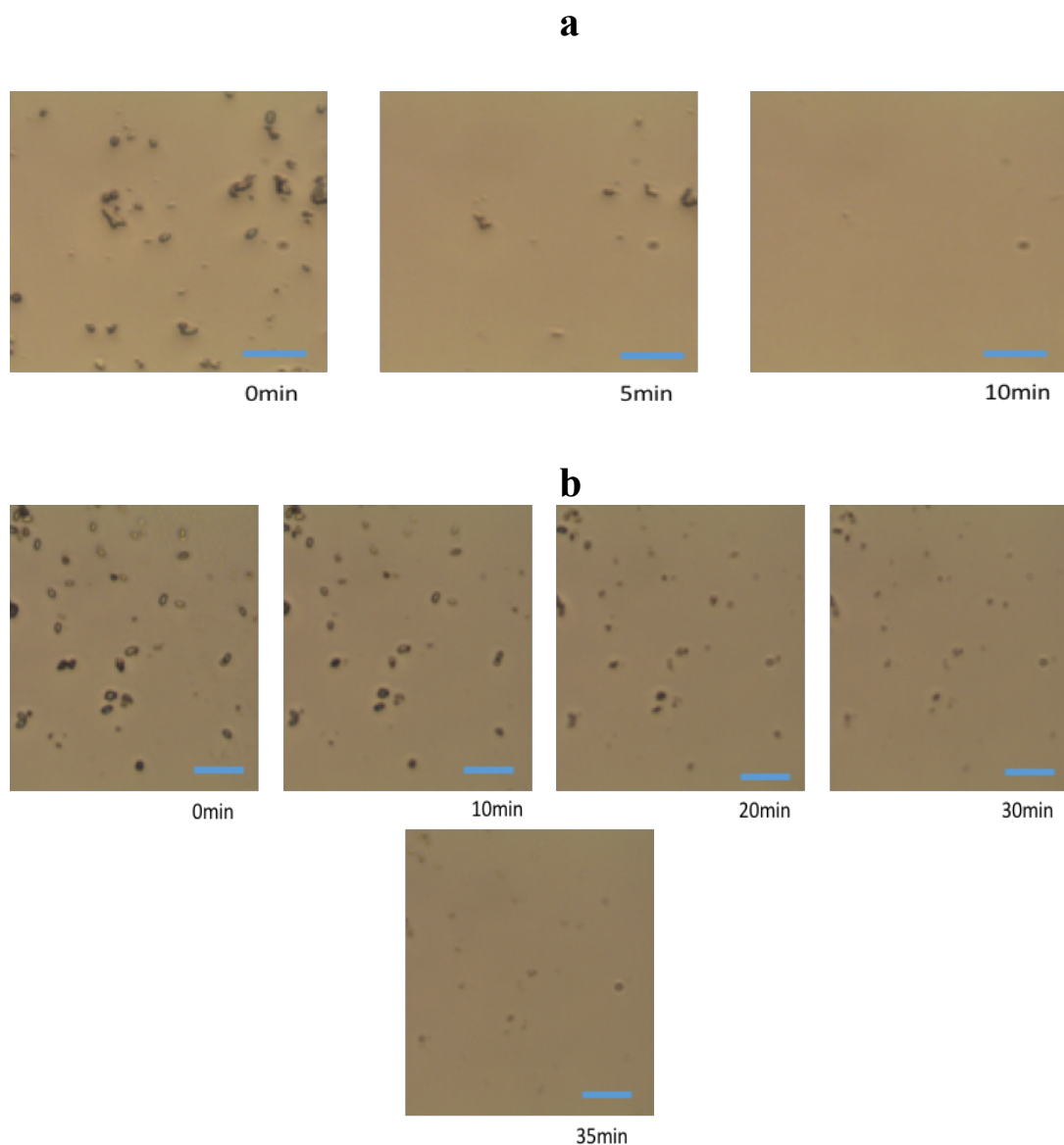


Figure 3-2-5. (a) Optical images of EDTA the dissolution action at $\text{pH} \approx 10$ and (b) optical images of the dissolution action of citrate at $\text{pH} \approx 10$. The scale bar is $20\ \mu\text{m}$.

At $\text{pH} \approx 10$, the citrate agent data revealed that increasing the pH from 7.53 to 10 had no effect on crystal dissolution. The CaOx crystal in this experiment had approximately the same dissolution time when the $\text{pH} = 7.53$ (Figure 3-2-5b). At $\text{pH} = 7.53$, all citrate ions were fully deprotonated, so increasing the pH does not further promote dissolving of the CaOx crystals as this study showed. However, citrate may be the best agent to be used in

dissolution therapy when compared to malonate and acetate since citrate showed better CaOx dissolution than malonate and acetate.

The crystal size of CaOx crystals was affected by the diprotic carboxylate ions (Na-Malo ion). The result obtained when the $\text{pH} \approx 10.00$ was nearly the same as when the $\text{pH} = 7.40$ before increasing the pH of malonate. This means there was no significant effect of increasing the pH on CaOx dissolution activity.

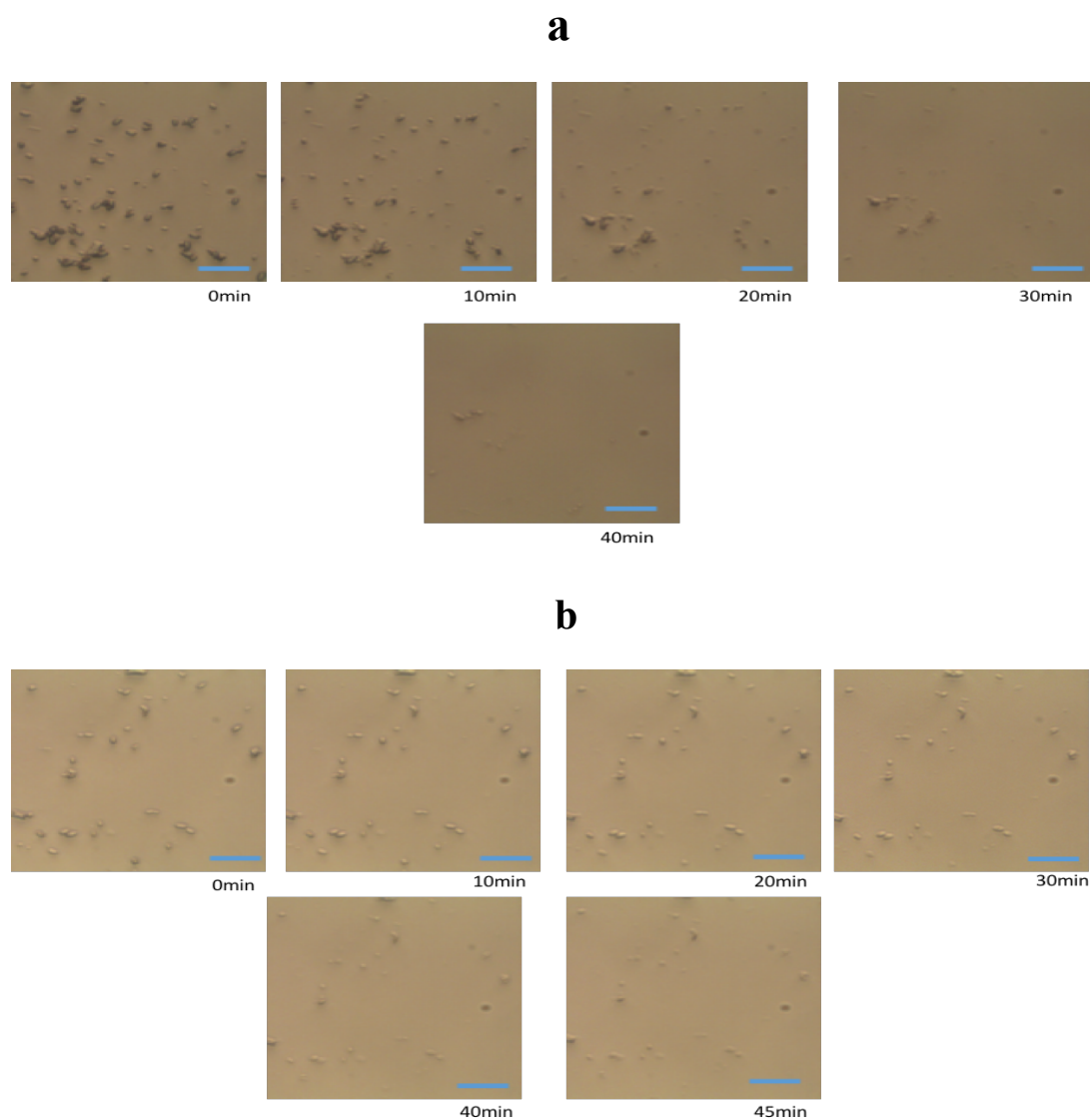


Figure 3-2-6. (a) Optical images of the dissolution action of malonate at $\text{pH} \approx 10$ and (b) optical images of the dissolution action of acetate at $\text{pH} \approx 10$. The scale bar is $20\ \mu\text{m}$.

The malonate agent was able to dissolve CaOx crystals within ~40 minutes (Figure 3-2-6a). In agreement with a previous study that observed that pH does not have a significant impact on the CaOx crystals dissolution action in the pH range from 5 to 10,⁵⁹ our result showed that Na-Acet had a similar dissolution rate when the pH was increased from ~6 to ~10 (Figure 3-2-6b). This similarity in dissolution rate because of all acetate ions were fully deprotonated at pH =6.87, so increasing the pH does not further promote dissolving of the CaOx crystals. Na-Acet showed the weakest dissolution effect amongst the dissolution agents examined; it had the fewest COO⁻ ions per molecule (Table 3-2-3). In fact, one study reported that one COO⁻ ion per molecule for a particular agent is not enough to suppress COM formation, so acetic acid is a poor inhibitor of CaOx formation.⁸⁹ This study may explain the slow dissolution rate of our CaOx crystals; the single COO⁻ ion of an acetate ion probably does not form a tightly bound complex with Ca²⁺. This is because each acetate ion (monodentate) can only coordinate weakly to one Ca²⁺ ion.

Overall, CaOx exhibited different kinetic dissolution behavior as compared to EDTA at pH= 4.92 and pH≈10. EDTA was the better candidate in dissolving CaOx crystals in this study, and it is used widely in dissolving this kind of crystal.

COO ⁻	Formal concentration	pKa value or values	pH	predominate COO ⁻ form in solution	Time
EDTA	5mM	0.0, 1.5, 2.00, 2.69, 6.13 and 10.37	10	[EDTA ⁴⁻]	~10 min
Citrate	5mM	3.13,4.76,6.40	10	[cit ³⁻]	~35min
Malonate	5mM	2.83 and 5.69	10	[Mal ²⁻]	~40min
Acetate	5mM	4.76	10	[Acet ⁻]	~45min

Table 3-2-3. Illustration of 5 mM Experiments of EDTA, citrate, malonate and acetate (constant pH). pKa values obtained from Quantitative Chemical Analysis.⁸³

Summary

In summary, the dissolution of CaOx was determined in the presence of four different types of carboxylate anions, i.e., the acetate ion, the malonate ion, the citrate ion, and EDTA ion. Our present study indicated that the dissolution rate greatly increased when the dissolution agent can interact with Ca^{2+} in a manner that creates several ligand bonds. EDTA and citrate at 5 mM were found to be the best solutions to dissolve CaOx due to their ability to form complexes with Ca^{2+} . Most likely, this is because EDTA is a hexadentate ligand and citrate is a tridentate ligand, which means that each of these molecule can form more than one coordinate covalent bonds with Ca^{2+} . Carboxylic groups may play an important role in improving the dissolution activity of CaOx crystals because the COO^- ions can easily coordinate to the Ca^{2+} . The solutions differed in their ability to promote CaOx dissolution: EDTA > citrate > malonate > acetate acid. Increasing the pH to 10 enhanced the dissolution of CaOx crystals in the presence of EDTA, but no significant changes in dissolution occurred with the other carboxylate anions.

Chapter 4: Future Directions

The details concerning CaOx transformations from one phase to another are relatively poorly understood. The experiments described in this work provide insight into the thermally-induced phase transitions of COM dendrites and COD bipyramids. However, there are various habits of COD and COM crystals, and it is unclear if all COM and COD crystals will exhibit the same thermal stability characteristics because there is no study directly comparing these thermally-induced transformations for various habits. The transformation of all COM habits at the same temperature would suggest that either (1) all COM habits have the same metastability with respect to the COM-to-COA transition or (2) no COM habit is noticeably metastable with respect to this transition. In contrast, it is possible that the shape of certain habits may make these habits less inclined (kinetically) to dehydrate, thus allowing them to exist as COM at temperatures slightly higher than the thermodynamically-defined transition temperature. Furthermore, the thermal Raman studies presented here examined isolated single crystals, and determining if agglomerations of COM or COD display the same traits observed with single crystals is important since such clusters often spontaneously form in various environments.

The several (>5) COM and COD crystals used in our Raman studies provided a measure of the range of temperatures over which the thermally-induced transformations occur in these crystals. However, the inclusion of a larger (~50) number of crystals would provide a more representative distribution for these temperatures. Also, reducing the heating rate (5 °C/min) and temperature intervals (5 °C) used in the 100 – 125 °C range will yield a more precise transition temperature for each crystal.

The ever-increasing discovery of polymorphic materials continues to drive research of the details about polymorphic phase transitions.⁹⁰ In such studies, the determination whether a particular transformation is either a single-crystal-to-single-crystal or a single-crystal-to-multiple crystal transition is often of prime importance.^{91, 92, 93} All image (optical and vibrational) and vibrational data in the work presented in the preceding chapters suggest that all the transitions discussed are most likely single-crystal-to-single-crystal. However, more convincing experimental evidence must be collected for this to be a trusted conclusion. Ideally, XRD characterizations of room temperature (~25 °C) CaOx single crystals after heating to temperatures above 150 °C (to convert to COA) would provide more compelling data about the nature of the transitions described here.

The metastable nature of COD crystals is also an area of interest with respect to CaOx research. A recent study examined the impact of humidity on the stability of such crystals, and it was reported that COD crystals transformed to COM at room temperature in high humidity environments. To obtain a better temporal comprehension of this transformation, a COD single crystal Raman microscopy study could be conducted in a microfluidic device, much like the dissolution device described in Section 2.2.4. Raman spectra and optical images collected at regular time intervals should provide data about the kinetics of this transformation. Because this transformation is believed to be solvent-mediated, it would also be interesting to determine the effect of various solution additives on this transformation.

The direct synthesis of COA, e.g., in solution, has yet to be reported. Indeed, the structure of COA was determined by heating a COM crystal to high temperatures (>200 °C) and maintaining the crystal in an inert atmosphere during and after cooling to prevent

its conversion to the COM phase.³³ As part of these studies, we attempted to extend the 'lifetime' of our COA crystals by flowing nitrogen (industrial grade) through our Raman heating stage. However, these attempts were not successful most likely because gaseous water molecules were not sufficiently removed from our system. Similar experiments could be carried out using a higher grade of nitrogen or argon gas. Raman spectra of cooled COM crystals (after heating to >200 °C) would confirm that without water vapor present, COA crystals can be maintained at room temperature indefinitely.

In this research, a microfluidic dissolution device was used to examine the effect of mono, di, tri, and poly carboxylate ions on CaOx dissolution. Effective CaOx dissolving solutions are few due to the unclear understanding of crystallization and dissolution mechanisms. Future studies could be designed to explore more CaOx dissolving solutions so as to provide a good comparison of the best dissolving agent at different pH values and to create a library of dissolving solutions that may demonstrate the specific properties of ideal agent or mixture of agents. One of the obstacles encountered with dissolution device used in this study was the dislodging, i.e., washing away, of some crystals as the solution passed over the sample. While the flow rate was kept constant and relatively low to limit this problem, a better solution would be to design a microfluidic dissolution system with traps that hold the crystals in place. Prototypical microfluidic systems that accomplish this task have already been reported.⁹⁴

References

1. Franceschi, V. R.; Nakata, P. A., Calcium oxalate in plants: formation and function. *Annual Review of Plant Biology* **2005**, (56), 41-71.
2. Brečević, L.; Škrtić, D.; Garside, J., Transformation of Calcium Oxalate Hydrates. *Journal of Crystal Growth* **1986**, 74 (2) 399-408.
3. Lin, T. J.; Hung, D. Z.; Hu, W. H.; Yang, D. Y.; Wu, T. C.; Deng, J. F., Calcium oxalate is the main toxic component in clinical presentations of alopecia macrorrhiza (L) Schott and Endl poisonings. *Veterinary and Human Toxicology* **1998**, 40(2), 93-95.
4. Franceschi, V. R.; Nakata, P. A., Calcium oxalate crystals in plants. *The Botanical Review* **1980**, 46(4), 361-427.
5. Baldwin, H., An experimental study of oxaluria, with special reference to its fermentative origin. *The Journal of Experimental Medicine* **1900**, 5 (1).
6. Gorostiza, P.; Isacoff, E. Y., Optical switches for remote and noninvasive control of cell signaling. *Science* **2008**, 322, (5900), 395-399.
7. Konya, E.; Umekawa, T.; Iguchi, M.; Kurita, T., The role of osteopontin on calcium oxalate crystal formation. *European Urology* **2003**, 43(5), 564-571.
8. Coe, F. L.; Evan, A.; Worcester, E., Kidney stone disease. *The Journal of Clinical Investigation* **2005**, 115, (10), 2598-2608.
9. Sakhaee, K., Recent advances in the pathophysiology of nephrolithiasis. *Kidney International* **2009**, 75, (6), 585-595.
10. Worcester, E. M.; Coe, F. L., Nephrolithiasis. *Primary Care: Clinics in Office Practice* **2008**, 35, (2) 369-391.
11. Sheng, X.; Ward, M. D.; Wesson, J. A., Adhesion between molecules and calcium oxalate crystals: critical interactions in kidney stone formation. *Journal of the American Chemical Society* **2003**, 125(10), 2854-2855.
12. Wesson, J. A.; Ward, M. D., Pathological Biomineralization of Kidney Stones. *Elements* **2007**, 3 (6), 415-421.
13. Sabbioni, C.; Zappia, G., Oxalate patinas on ancient monuments: the biological hypothesis. *Aerobiologia* **1991**, 7 (1), 31-37.
14. Yu, H.; Sheikholeslami, R.; Doherty, W. O. S., Mechanisms, thermodynamics and kinetics of composite fouling of calcium oxalate and amorphous silica in sugar

- mill evaporators-A preliminary study. *Chemical Engineering Science* **2002**, 57 (11), 1969-1978.
15. Health, U., Types of kidney stones. *University of Wisconsin Hospital and Clinics Authority* **2010**. at <<http://www.uwhealth.org/urology/types-of-kidney-stones/11206>>
 16. Frey-Wyssling, A., Crystallography of the two hydrates of crystalline calcium oxalate in plants. *American Journal of Botany* **1981**, 130-141.
 17. Thomas, A., Biomimetic growth and morphology control of calcium oxalates. *PhD thesis, Max-Planck Institute in Dresden*. **2009**.
 18. Deganello, S.; Kampf, A. R.; Moore, P. B., The crystal structure of calcium oxalate trihydrate; $\text{Ca}(\text{H}_2\text{O})_3(\text{C}_2\text{O}_4)$. *American Mineralogist* **1981**, 66 (7-8), 859-865.
 19. Wierzbicki, A.; Sikes, C. S.; Sallis, J. D.; Madura, J. D.; Stevens, E. D.; Martin, K. L., Scanning electron microscopy and molecular modeling of inhibition of calcium oxalate monohydrate crystal growth by citrate and phosphocitrate. *Calcified Tissue International* **1995**, 56(4), 297-304.
 20. Datta, S. a.; Grant, D. J. W., Crystal structures of drugs: Advances in determination, prediction and engineering. *Nature Reviews Drug Discovery*. **2004**, 3 (1), 42-57.
 21. West A, R., Basic solid state chemistry. *John Wiley & Sons* **1999**.
 22. MJ, B., Crystal-structure analysis. *Krieger Pub Co* **1980**.
 23. Hammond, C., The basics of crystallography and diffraction. *Oxford University Press* **2009**, 12.
 24. Senechal, M., Structures beyond superspace. *Acta Crystallographica B: Structural Science, Crystal Engineering and Materials* **2015**, 71 (3), 250-1.
 25. Vippagunta, S. R.; Brittain, H. G.; Grant, D. J., Crystalline solids. *Advanced Drug Delivery Reviews*. **2000**, 48(1), 3-26.
 26. Thakur, K.; Velumurgan, A., Phase properties and type of earth's water ice and space ices. *Science of Solar System Ices* **2008**, 9014.
 27. Tazzoli, V.; Domeneghetti, C., The crystal structures of whewellite and weddellite: re-examination and comparison. *American Mineralogist* **1980**, 65, 327-334.
 28. Echigo, T.; Kimata, M.; Kyono, A.; Shimizu, M., Re-investigation of the crystal structure of whewellite [$\text{Ca}(\text{C}_2\text{O}_4) \cdot \text{H}_2\text{O}$] and the dehydration mechanism of caoxite [$\text{Ca}(\text{C}_2\text{O}_4) \cdot 3\text{H}_2\text{O}$]. *Mineralogical Magazine* **2005**, 69(1), 77-88.

29. Bannister, F. A.; Hey, M. H., Report on some crystalline components of the Weddell Sea deposits. *Discovery Reports* **1936**, *13*, 60-69.
30. Schubert, G.; Ziemer, B., A new calcium oxalate monohydrate produced by thermal dehydration of weddellite. *Crystal Research and Technology* **1981**, *16*(9), 1025-1031.
31. Gardner, G. L., Nucleation and crystal growth of calcium oxalate trihydrate. *Journal of Crystal Growth* **1975**, *30*(2), 158-168.
32. Perez-Rodriguez, J. L.; Duran, A.; Centeno, M. A.; Martinez-Blanes, J. M.; Robador, M. D., Thermal analysis of monument patina containing hydrated calcium oxalates. *Thermochimica Acta* **2011**, *512* (1-2), 5-12.
33. Hochrein, O.; Thomas, A.; Kniep, R., Revealing the crystal structure of anhydrous calcium oxalate, Ca [C₂O₄], by a combination of atomistic simulation and Rietveld refinement *Zeitschrift für anorganische und allgemeine Chemie*. **2008**, *634* (11), 1826-1829.
34. Frost, R. L.; Weier, M. L., Thermal treatment of whewellite-a thermal analysis and Raman spectroscopic study. *Thermochimica Acta* **2004**, *409* (1), 79-85.
35. Kirkpatrick, S., Optimization by simulated annealing: Quantitative studies *Journal of Statistical Physics* **1984**, *34* (5-6), 975-986.
36. Bond, A. D.; Jones, W., Structure prediction as a tool for solution of the crystal structures of metallo-organic complexes using powder X-ray diffraction data. *Acta Crystallographica Section B: Structural Science* **2002**, *58* (2), 233-243.
37. Housecroft, C.; Alan, G., Inorganic chemistry. *Prentice Hall* **2012**.
38. Klug, H.; Leroy, E., X-ray diffraction procedures. *New York: Wiley* **1954**, *2*.
39. Freeman, E. S.; Carroll, B., The application of thermoanalytical techniques to reaction kinetics: the thermogravimetric evaluation of the kinetics of the decomposition of calcium oxalate monohydrate. *The Journal of Physical Chemistry* **1958**, *62* (4), 394-397.
40. Gabbott, P., ed, Principles and applications of thermal analysis. *John Wiley & Sons* **2008**.
41. Kutaish, N.; Aggarwal, P.; Dollimore, D., Thermal analysis of calcium oxalate samples obtained by various preparative routes. *Thermochimica Acta* **1997**, *297* (1), 131-137.

42. Frost, R. L.; Weier, M. L., Thermal treatment of weddellite—a Raman and infrared emission spectroscopic study. *Thermochimica Acta* **2003**, *406* (1-2), 221-232.
43. Wendlandt, W. W.; Simmons, E. L., The thermal decomposition of metal complexes—XVI: Potassium tris (oxalato) cobaltate (III) trihydrate. *Journal of Inorganic and Nuclear Chemistry* **1965**, *27*(11), 2317-2323.
44. Wendlandt, W. W.; George, T. D.; Krishnamurty, K. V., The thermal decomposition of metal complexes—I: thermogravimetric and differential thermal analysis studies. *Journal of Inorganic and Nuclear Chemistry* **1961**, *21*(1), 69-76.
45. Lepage, L.; R, T., Growth and characterization of calcium oxalate dihydrate crystals (weddellite). *Journal of Pharmaceutical Sciences* **1982**, *71* (9), 1059-1062.
46. Lozano, R.; Roman, J.; Jesus, F.; Jerez, A.; Gaitan, M.; Ramos, E., Kinetic studies by DSC on the thermal decomposition of calcium oxalate. *Thermochimica Acta* **1989**, *143*, 93-100.
47. Ngo, T. C.; Assimos, D. G., Uric acid nephrolithiasis: recent progress and future directions. *Reviews in Urology* **2007**, *9* (1), 17.
48. Tiselius, H. G., New horizons in the management of patients with cystinuria. *Current Opinion in Urology* **2010**, *20* (2), 169-173.
49. Xiang-bo, Z.; Zhi-ping, W.; Jian-min, D.; Jian-zhong, L.; Bao-liang, M., New chemolysis for urological calcium phosphate calculi—a study in vitro. *Boston Medical Urology* **2005**, *5*(1), 9.
50. Crowell, A., Cystine nephrolithiasis. *Surgery Gynecology Obstet* **1924**, *38*, 87-91.
51. Albright, F.; Sulkowitch, H. W.; Chute, R., Nonsurgical aspects of the kidney stone problem. *Journal of the American Medical Association* **1939**, *113* (23), 2049–2053.
52. Jianming, O., Chemical basis in the investigation of calcium oxalate stones. *Chemistry* **2002**, *65* (5), 326-332.
53. Cody, A. M.; Cody, R. D., Calcium oxalate trihydrate phase control by structurally-specific carboxylic acids. *Journal of Crystal Growth* **1994**, *135* (1-2), 235-245.
54. Bouropoulos, K.; Bouropoulos, N.; Melekos, M.; Koutsoukos, P. G.; Chitanu, G. C.; Anghelescu-Dogaru, A. G.; Carpov, A. A., The inhibition of calcium oxalate monohydrate crystal growth by maleic acid copolymers. *The Journal of Urology* **1998**, *159* (5), 1755-1761.

55. Ouyang, J. M.; Deng, S. P.; Zhou, N.; Tieke, B., Effect of tartrates with various counterions on the precipitation of calcium oxalate in vesicle solutions. *Colloids and Surfaces A: Physicochemical and Engineering Aspects* **2005**, 256 (1), 21-27.
56. Aras, B.; Kalfazade, N.; Tuğcu, V.; Kemahlı, E.; Özbay, B.; Polat, H.; Taşçı, A. İ., Can lemon juice be an alternative to potassium citrate in the treatment of urinary calcium stones in patients with hypocitraturia? A prospective randomized study. *Urological Research* **2008**, 36, (6), 313-317.
57. Zuckerman, J.; Dean, G. A., Hypocitraturia: pathophysiology and medical management. *Review Urology* **2009**, 11, (3), 134-144.
58. Oussama, A.; Touhami, M., In vitro and in vivo study of effect of lemon juice on urinary lithogenesis. *Archivos Españoles de Urología* **2005**, 58 (10), 1087-92.
59. Chutipongtanate, S.; Chaiyarit, S.; Thongboonkerd, V., Citrate, not phosphate, can dissolve calcium oxalate monohydrate crystals and detach these crystals from renal tubular cells. *European journal of pharmacology* **2012**, 689 (1), 219-225.
60. Aslier, S. A.; Munro, C. H.; Chi, Z., UV Lasers Revolutionize Raman Spectroscopy. *Laser Focus World* **1997**, 33(7), 99-109.
61. Edwards, H. G. M.; Farwell, D. W.; Jenkins, R.; Seaward, M. R. D., Vibrational Raman spectroscopic studies of calcium oxalate monohydrate and dihydrate in lichen encrustations on Renaissance frescoes. *Journal of Raman Spectroscopy* **1992**, 23(3), 185-189.
62. Frost, R. L.; Bahfenne, S., Thermal analysis and Hot-stage Raman spectroscopy of the basic copper arsenate mineral. *Journal of Thermal Analysis and Calorimetry* **2010**, 100(1), 89-94.
63. Joy, D. C., Scanning electron microscopy. *Wiley-VCH Verlag GmbH & Co. KGaA* **2006**.
64. Lametschwandtnr, A.; Lametschwandtnr, U.; Weiger, T., Scanning electron microscopy of vascular corrosion casts--technique and applications: updated review. *Scanning Microscopy* **1990**, 4(4), 889-940.
65. Frost, R. L., Raman spectroscopy of natural oxalates. *Analytica Chimica Acta* **2004**, 517(1), 207-214.
66. Shippey, T. A., Vibrational studies of calcium oxalate monohydrate (whewellite) and an anhydrous phase of calcium oxalate. *Journal of Molecular Structure* **1980**, 63(2), 157-166.

67. Duval, D.; Condrate, R. A., A Raman spectral study of the dehydration of calcium oxalate monohydrate. *Applied Spectroscopy* **1988**, 42(4), 701-703.
68. Conti, C.; Casati, M.; Colombo, C.; Possenti, E.; Realini, M.; Gatta, G. D.; Merlini, M.; Brambilla, L.; Zerbi, G., Synthesis of calcium oxalate trihydrate: New data by vibrational spectroscopy and synchrotron X-ray diffraction. *Spectrochimica Acta Part A: Molecular and Biomolecular Spectroscopy* **2015**, 150, 721-730.
69. Yu, H.; Sheikholeslami, R.; Doherty, W. O. S., The effects of silica and sugar on the crystallographic and morphological properties of calcium oxalate. *Journal of Crystal Growth* **2004**, 265(3), 592-603.
70. Thongboonkerd, V.; Semangoen, T.; Chutipongtanate, S., Factors determining types and morphologies of calcium oxalate crystals: molar concentrations, buffering, pH, stirring and temperature. *Clinica Chimica Acta* **2006**, 367 (1-2), 120-31.
71. Ouyang, J. M.; Duan, L.; Tieke, B., Effects of Carboxylic Acids on the Crystal Growth of Calcium Oxalate Nanoparticles in Lecithin-Water Liposome Systems. *Langmuir* **2003**, 19(21), 8980-8985.
72. Ouyang, J. M.; Deng, S. P., Controlled and uncontrolled crystallization of calcium oxalate monohydrate in the presence of citric acid. *Dalton Transactions* **2003**, (14), 2846-2851.
73. Person, W. B. a. Z., G, Vibrational intensities in infrared and Raman spectroscopy *Elsevier Science Ltd* **1982**, 20.
74. Jung, T.; Kim, W. S.; Choi, C. K., Crystal structure and morphology control of calcium oxalate using biopolymeric additives in crystallization. *Journal of Crystal Growth* **2005**, 279(1), 154-162.
75. Zhang, D.; Qi, L.; Ma, J.; Cheng, H., Morphological control of calcium oxalate dihydrate by a double-hydrophilic block copolymer. *Chemistry of Materials* **2002**, 14(6), 2450-2457.
76. Yu, H.; Sheikholeslami, R.; Doherty, W. O. S., Calcium oxalate crystallization in silica and sugar solutions-characterization of crystal phases and habits. *Powder Technology* **2005**, 160(1), 2-6.
77. Jung, T.; Kim, W. S.; Choi, C. K., Biomineralization of calcium oxalate for controlling crystal structure and morphology. *Materials Science and Engineering* **2004**, 24(1), 31-33.
78. Tomazic, B. B.; Nancollas, G. H., The dissolution of calcium oxalate kidney stones. A kinetic study. *The Journal of Urology* **1982**, 128(1), 205-208.

79. Kotake, M.; Mori, T.; Hayakawa, K.; Ltd., N. C. I., Process for removing calcium oxalate scale. *U.S. Patent* **1981**, 4, 264,463.
80. Guo, S.; Ward, M. D.; Wesson, J. A., Direct visualization of calcium oxalate monohydrate crystallization and dissolution with atomic force microscopy and the role of polymeric additives. *Langmuir* **2002**, 18(11), 4284-4291.
81. Yu, J.; Tang, H.; Cheng, B., Influence of PSSS additive and temperature on morphology and phase structures of calcium oxalate. *Journal of Colloid and Interface Science* **2005**, 288 (2), 407-411.
82. Miller, G. H.; Vermeullen, C. W.; Moore, J. D., Calcium oxalate solubility in urine; experimental urolithiasis. *The Journal of Urology* **1958**, 79(3), 607.
83. Harris, D. C., Quantitative chemical analysis. *W.H. Freeman and company* **2010**.
84. Wang, L.; Zhang, W.; Qiu, S. R.; Zachowicz, W. J.; Guan, X.; Tang, R.; Hoyer, J. R.; De Yoreo, J. J.; Nancollas, G. H., Inhibition of calcium oxalate monohydrate crystallization by the combination of citrate and osteopontin. *Journal of Crystal Growth* **2006**, 291(1), 160-165.
85. Sayan, P.; Sargut, S. T.; Kiran, B., Calcium oxalate crystallization in the presence of amino acids, proteins and carboxylic acids. *Crystal Research and Technology* **2009**, 44(8), 807-817.
86. Flora, S. J. S.; Mittal, M.; Mehta, A., Heavy metal induced oxidative stress & its possible reversal by chelation therapy. *Indian Journal of Medical Research* **2008**, 128(4), 501.
87. Lamas, G. A.; Goertz, C.; Boineau, R.; Mark, D. B.; Rozema, T.; Nahin, R. L.; Lindblad, L.; Lewis, E. F.; Drisko, J.; Lee, K. L.; Investigators., T., Effect of disodium EDTA chelation regimen on cardiovascular events in patients with previous myocardial infarction: the TACT randomized trial. *Journal of the American Medical Association* **2013**, 309(12), 1241-1250.
88. Grases, F.; Millan, A.; Garcia-Raso, A., Polyhydroxycarboxylic acids as inhibitors of calcium oxalate crystal growth; relation between inhibitory capacity and chemical structure. *Journal of Crystal Growth* **1988**, 89(4), 496-500.
89. East, C. P.; Doherty, W. O.; Fellows, C. M.; Yu, H., Formation of thermodynamically unstable calcium oxalate dihydrate in sugar mill evaporators. *In Proceeding of 32nd Australian Society of Sugar Cane Technologists (ASSCT) Conference* **2010**, 32, 522-533.

90. Reddy, J. P.; Swain, D.; Pedireddi, V. R., Polymorphism and phase transformation behavior of solid forms of 4-amino-3, 5-dinitrobenzamide. *Crystal Growth & Design* **2014**, *14*(10), 5064-5071.
91. Naumov, P.; Bharadwaj, P. K., Single-crystal-to-single-crystal transformations. *Crystal Engineering Communications* **2015**, *17*(46), 8775-8775.
92. Liu, G.; Liu, J.; Liu, Y.; Tao, X., Oriented single-crystal-to-single-crystal phase transition with dramatic changes in the dimensions of crystals. *Journal of the American Chemical Society* **2013**, *136*(2), 590-593.
93. Kariuki, B. M.; El-Hiti, G. A., A Reversible Single-Crystal to Single-Crystal Thermal Phase Transformation of 3-(2-Bromo-4-(1-methylethyl) phenyl)-1, 1-dimethyl urea. *Crystals* **2017**, *7*(3), 75.
94. Windbergs, M.; Weitz, D. A., Microfluidics: Drug Dissolution Chip (DDC): A Microfluidic Approach for Drug Release. *Small* **2011**, *7*(21), 2958-2958.